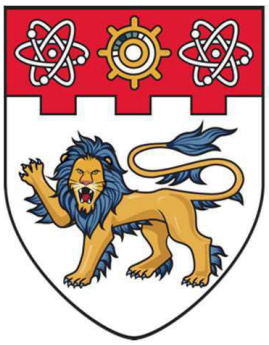

NANYANG TECHNOLOGICAL UNIVERSITY
SINGAPORE

STUDIES ON AGGRESSIVE MASS FINISHING FOR METAL COMPONENT REMANUFACTURING

JEREMY HO WENG KEONG

SCHOOL OF MECHANICAL AND AEROSPACE ENGINEERING

2024

STUDIES ON AGGRESSIVE MASS FINISHING FOR METAL COMPONENT REMANUFACTURING

JEREMY HO WENG KEONG

School of Mechanical and Aerospace Engineering

A thesis submitted to the Nanyang Technological University

in partial fulfilment of the requirement for the degree of

Master's Degree of Engineering

2024

Statement of Originality

I hereby certify that the work embodied in this thesis is the result of original research, is free of plagiarised materials, and has not been submitted for a higher degree to any other University or Institution.

03/08/2023

. . . . . .

Date

. . . . . .

JEREMY HO WENG KEONG

Supervisor Declaration Statement

I have reviewed the content and presentation style of this thesis and declare it is free of plagiarism and of sufficient grammatical clarity to be examined. To the best of my knowledge, the research and writing are those of the candidate except as acknowledged in the Author Attribution Statement. I confirm that the investigations were conducted in accord with the ethics policies and integrity standards of Nanyang Technological University and that the research data are presented honestly and without prejudice.

03/08/2023

. . . . . .

Date

. . . . . .

Associate Professor Yeo Swee Hock

Authorship Attribution Statement

This thesis **does not** contain any materials from papers published in peer-reviewed journals or from papers accepted at conferences in which I am listed as an author.

03/08/2023

. . . . . .

Date

. . . . . .

JEREMY HO WENG KEONG

Acknowledgements

First, I would like to acknowledge my ARTC family and friends for the opportunity to support me both financially and spiritually in my studies, since my Undergraduate at NTU and now my master's while I stay committed to the A*STAR family since 2016. This is an extension to my work and the grateful opportunity to work at Spire Pte Ltd under the T-Up programme not once but twice, which allowed me to be exposed to the real world of mass finishing and how it really contributes to the local aerospace industry. Many thanks to Mr. Alan Lim, Managing Director of Spire for supporting my study in the supply of equipment, consumable, and most importantly, tutelage.

I would also like to give my acknowledgement to my NTU supervisor, Associate Professor Yeo Swee Hock for being very patient and understanding as I venture a vertical uphill to further my studies while taking on the multitude of projects and responsibility at work.

I would like to extend my heartfelt gratitude to my ARTC co-supervisor Dr. Tan Kai Liang for his unwavering support and guidance for my thesis, especially with my transition out from my technical role at ARTC. Without him, this thesis would have never come to fruition.

I would like to give my dearest and most profound gratefulness to my family and girlfriend and now (finally) my wife, for the many days and nights in rendering support to my already hectic schedule.

Finally, my final thank you is to my dear firstborn who has given me joy like no other.

Table of Contents

Abstract

This thesis introduces a novel vibratory finishing machine designed for the aerospace industry, featuring a domeless, circular vibratory finishing bowl. The study aims to explore the machine's advantages over conventional dome vibrators, particularly for annular components, with limited existing literature in this area.

The investigation focuses on the domeless-type vibrofinishing process, analysing its performance based on varying component-machine sizing and orientation. Results indicate that airfoil orientation relative to the media flow has the greatest impact on material removal. The optimal position for surface finishing is at a 45-degree angle, resulting in the highest surface roughness improvement and material removal. Certain airfoil positions lead to reduced media flow and stagnation, negatively affecting the finishing process. The study also explores indirect media interaction, where media particles interact with surfaces not directly exposed to the primary media flow, contributing to material removal and surface finishing with approximately half the effectiveness of direct contact.

Furthermore, the thesis three vibrofinishing techniques - domeless, dome, and trough – theoretically, experimentally, and economically. Theoretical analysis demonstrates the potential for more efficient processing with the domeless design, with an 80.5% increase in excitation force and up to 144.6% increase in excitation moment compared to the dome design. Experimental results confirm higher material removal in domeless vibrofinishing, while the trough process fails to meet surface roughness requirements. Cost analysis reveals significant differences in capital and operational expenses, with potential cost savings of 70.3% and 60.3% by adopting the domeless bowl to replace the trough and dome bowl, respectively.

In conclusion, this thesis provides strong evidence for a domeless vibratory finishing machine's advantages in material removal and surface roughness improvement. The experimental and theoretical analysis conducted demonstrates the potential for more efficient processing, higher material removal rate, and cost benefits when compared to the conventional designs.

Acronyms

OEM	Original Equipment Manufacturer
MRO	Maintenance, Repair and Overhaul
PU	Polyurethane
PCD	Pitch Circle Diameter
KPV	Key Parameter Variable
QC	Quality Control
RPM	Revolution Per Minute
PGI	Phase Grating Interferometer
OD	Outer Diameter
ID	Inner Diameter
DoE	Design Of Experiment
CapEx	Capital Expenditure
OpEx	Operating Expense

List of Symbols

φ	Alignment (Phase) angle
Ω	Angular velocity
k_v	Spring constant - vertical
k_h	Spring constant - horizontal
c_v	Damping constant - vertical
c_h	Damping constant - horizontal
ζ_v	Damping factors - vertical
ζ_h	Damping factors - horizontal
ζ_θ	Damping factors - angular
ω_{nv}	Natural frequency - vertical
ω_{nh}	Natural frequency - horizontal
$\omega_{n\theta}$	Natural frequency – angular
ω_{dv}	Damping frequency - horizontal
ω_{dh}	Damping frequency - vertical
$\omega_{d\theta}$	Damping frequency - Angular
L	Horizontal length of vertical springs to mass M centroid
L_t	Vertical length of top eccentric plate to mass M centroid
L_b	Vertical length of bottom eccentric plate to mass M centroid
r	Horizontal length of eccentric plate to mass M centroid
M	Total mass of bowl, media, component(s), compound, water, and fixture(s)
m_t	Top eccentric plate and flyweight mass
m_b	Bottom eccentric plate and flyweight mass

List of Figures

List of Tables

This page is intentionally left blank.

Chapter 1 **Introduction**

This chapter presents a brief introduction of the research work. Background on the research field is first provided. Following which, the research problem is defined and the motivation to delve into this research project is presented. Research objectives are established next. The novelty and significance of this research work are then highlighted. Finally, an overview of the thesis structure is outlined at the end of this chapter.

1.1 Mass Finishing

Mass finishing is a general term to describe a series of industrial processes that utilise a mass of loose abrasive or non-abrasive particles, known as media, to impart energy onto component surfaces through physical contact via a variety of vibratory-cyclic motions. The motion and level of energy or aggressiveness is highly depending on the type of mass finishing process. The basic mass finishing processes include:

- Vibratory finishing
- Barrel finishing
- Spindle finishing
- Drag finishing
- Centrifugal barrel finishing
- Centrifugal disc finishing

The effectiveness of mass finishing is influenced by several key process variables (KPVs) that are interconnected and work together to produce the desired surface finish on components. These KPVs include the selection of media, machine geometry, component characteristics, and compound solutions. With a right process parameter combination through in-depth understanding, mass finishing is a versatile process that can achieve a range of surface improvements, including deburring, polishing,

cleaning, brightening, descaling, and surface hardening and is used across many industries globally. One of which is the aerospace industry, especially in maintenance, repair, and overhaul (MRO).

1.2 Remanufacturing in Aerospace MRO Industry

Remanufacturing plays a vital role in the aerospace maintenance, repair, and overhaul (MRO) industry, as it allows high-value components to be restored and given extended value and warranty. The aerospace sector has the largest remanufacturing market size globally [1]. It is important to differentiate between recycling, reusing, and remanufacturing, as they involve distinct processes. Recycling involves disassembling or dissolving end-of-life components to obtain raw materials for repurposing, while reusing refers to cleaning, repairing, or restoring used components for repurposing, including aesthetic purposes. Remanufacturing utilizes advanced manufacturing processes to restore or enhance the mechanical and/or chemical properties of components, resulting in increased value and an extended service life [2].

Table 1.1 Summary of remanufacturing activities between different sectors [1]

Sectors	Turnover (€bn)	Firms	Employment ('000)	Core ('000)	Intensity
Aerospace	12.4	1,000	71	5,160	11.5%
Automotive	7.4	2,363	43	27,286	1.1%
Electronics	3.1	2,502	28	87,925	1.1%
Furniture	0.3	147	4	2,173	0.4%
Heavy-Duty & Off-Road	4.1	581	31	7,390	2.9%
Machinery	1.0	513	6	1,010	0.7%
Marine	0.1	7	1	83	0.3%
Medical equipment	1.0	60	7	1,005	2.8%
Rail	0.3	30	3	374	1.1%
Total	29.8	7,204	192	132,405	1.9%

In aerospace remanufacturing, various factors must be considered, such as design for disassembly, cleaning processes, and suitable repairing/reconditioning methods to address the complex damages observed in incoming components with the steps illustrated in Figure 1.1. Surface integrity, including both surface and sub-surface properties, is crucial for aerodynamic efficiency and safety in air transportation.

Components requiring remanufacturing in the aerospace industry include turbine blades, fans, vanes, stator rings, impellers, and blisks (Blade-Integrated-Disk), which are functional surfaces used for power transmission. Edge finishing, such as burr removal and edge rounding, is also important to prevent stress concentration and maintain joint fastening tolerances [3], [4].

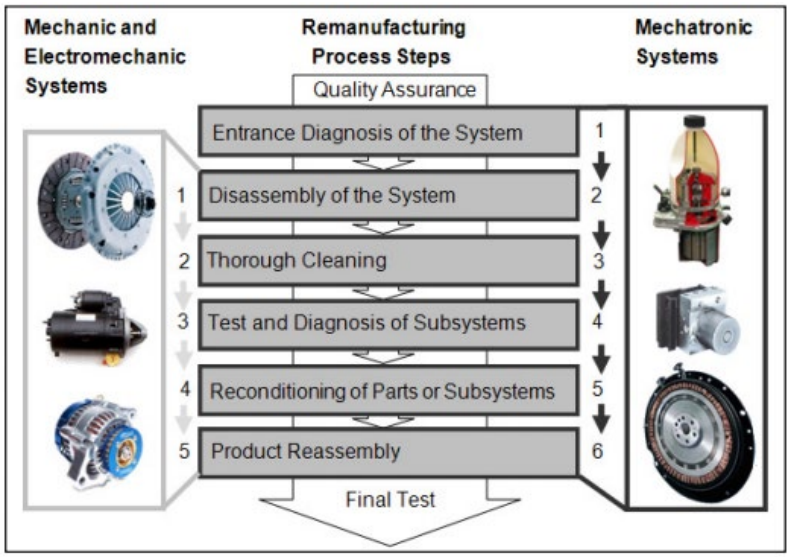

Figure 1.1 Aerospace Remanufacturing steps [5]

The reconditioning step within the full remanufacturing process primarily focus on surface enhancement methods that target both surface and sub-surface. Sub-surface enhancement includes shot peening and deep cold rolling to increase the fatigue strength of aerospace components [6]. After these sub-surface enhancement processes, mass finishing is widely used to meet the final surface finish requirements.

Vibrofinishing, a variant of mass finishing, is a widely used process in aerospace remanufacturing. It is chosen for its versatility in handling components of various sizes and meeting production schedules. The two main shapes of vibrofinishing machines used in the aerospace industry are bowl and trough designs as shown in Figure 1.2. Additionally, variations in size, elevation, dome removal (for bowl type), and fixture methods are employed to accommodate different industrial needs.

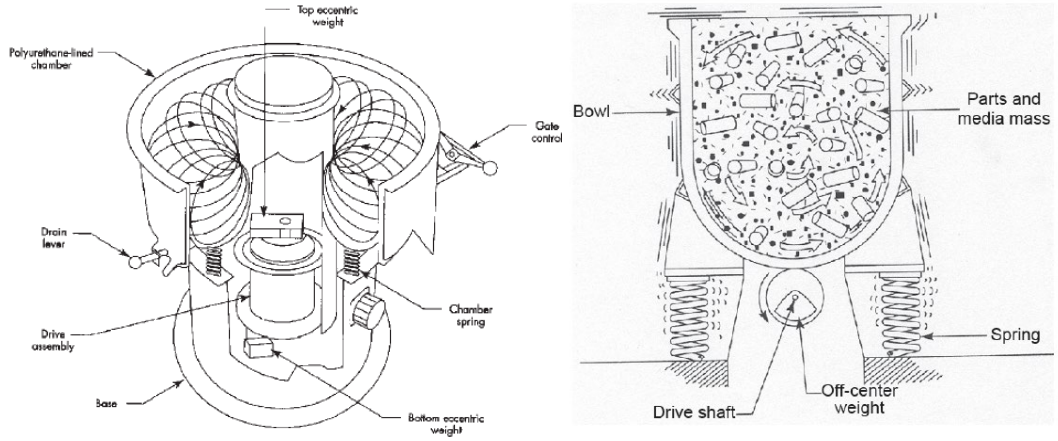

Figure 1.2 Vibrofinisher types such as (left) Bowl and (right) trough [3]

A summary in Table 1.2 shows a compiled list of aerospace components that undergoes vibrofinishing and their methodology such as machine type, fixture, and processing quantity [7], [8].

Table 1.2 Aerospace components that use vibrofinishing and their methodologies

Component	**Machine Type**	**Process Type ****	**Fixture method(s)**	**Quantity per cycle***
Small Turbine Blade	Dome Bowl	Wet compound with ceramic/plastic abrasive media	a) Free b) Free (compartments)	a) > 50 pcs b) 8 – 12 pcs
Fan Blades	Trough	Wet compound with plastic media	a) Free b) External Fixture	a) Single b) 4 pcs
Large Aircraft structures	Trough	Wet compound with metallic media	Free	Single
Small Blisk	a) Dome Bowl b) Trough	Grinding polishing paste with ceramic media	a) Free (compartments) b) Internal Fixture	a) 2 – 4 pcs b) 4 – 6 pcs
sectioned vanes	Dome Bowl	Wet compound with ceramic/plastic abrasive media	a) Free b) Free (compartments)	c) > 50 pcs 8 – 12 pcs
Large Blisk Drums	Domeless Bowl	Wet compound with ceramic/plastic abrasive media	a) Internal fixture	1 pc
Complete Stator Rings	Domeless Bowl	Wet compound with ceramic/plastic abrasive media	a) Internal fixture	1 pc

** Quantity per cycle highly dependent on machine capacity and compartment setup.*
*** Some components undergo multi-step vibrofinishing of different media-compound recipes to get better results.*

As the aerospace MRO industry embraces advanced manufacturing technologies, there is a trend towards producing components as single integrated units, such as blisks. To cater to these developments, specialized domeless vibrofinishers have been introduced by mass finishing OEMs. These domeless bowls are particularly effective for processing disks and complete stator rings, as they provide better accessibility to the annular geometries of aerofoils for the vibrofinishing media. [9]

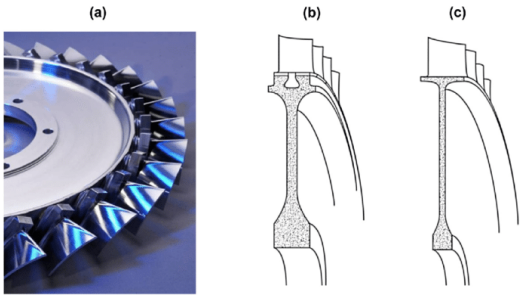

Figure 1.3 (a) a typical blisk component (b) schematic diagram of blade attachments via fir tree on disk and (c) blisk [10]

As compiled in Table 1.2, full drum blisks and complete stator rings have utilised this vibrofinishing variant. There are opportunities to extend the domeless vibratory bowl to other annular-shaped aerospace components. In addition, there is limited in-depth understanding of the domeless bowl's fundamental principles and efficiency. Both of these provide strong justification to pursue the study of annular aerospace components to be processed by domeless round vibrofinishing.

1.3 Research Motivation

Vibrofinishing has been established for decades in the aerospace industry. The various vibrofinishing processes are usually limited by the different sized aerospace components. An example would be the use of a trough-shaped vibrofinisher for a long turbine. Smaller, non-elongated components are usually processed by round-shaped vibrofinishers. With the rise of complex geometrical manufacturing such as the blisk (BLade–Integrated–dISK), some mass-finishing OEMs devised a domeless round-shaped equipment. Based on the author's knowledge and experiences, the aerospace industry in Singapore has not adopted this type of machine and a validation through

a thorough theoretical, technical, and economic analyses may enable a potentially more efficient and effective process for the industry.

Therefore, the research motivation of the author is to validate the effectiveness of a domeless circular-shaped vibrofinishing process as compared to the conventional variants (round dome and trough), through theoretical, experimental, and economic analyses. The results and research outcome would provide useful guidelines for local aerospace companies to consider adoption of this technology. Improved process understanding also allows processed owners to look out for other feasible components from both technical and economical perspectives.

1.4 Objectives and Scope

This project aims to conduct an independent study to validate the effectiveness of a domeless round vibrofinisher on annular aerospace components made of aerospace stainless steel grade 304 (SUS304). A systematic approach was devised as follows:

1. Conduct a fundamental study to improve process understanding on the domeless round vibrofinisher, both qualitatively and quantitatively
2. Conduct a theoretical, experimental, and economical comparative study to establish the efficiency and effectiveness of the domeless round vibrofinisher with respect to conventional methods (dome round or trough vibrofinishers)

The work conducted in this thesis was part of an industrial project undertaken by the author through the in-kind support from Spire Pte Ltd, Singapore. Their provision of a domeless round vibrofinisher equipment, consumables, and decades of expertise in mass finishing are an extension of several on-going engagements with the local aerospace manufacturing and MROs. The objectives of these engagements were to improve their surface finishing processes, such as surface roughness improvements, cycle time and cost improvement, as part of their Kaizen exercises. Due to the commercial sensitivity of these engagements, parts of the data will be omitted from this thesis.

Chapter 2 **Literature Review**

This chapter presents a literature review of the key parametric variables of mass finishing, the use of vibrofinishing in the aerospace industry and the various machine designs to meet the industry's demands, followed by an empirical and theoretical review of the vibrofinishing process.

2.1 Mass Finishing

Mass finishing processes are broadly based on four key process variables (KPVs) as shown in Figure 2.1 below, with an additional subcategory of each KPV. Though selection for each KPV is individualised, they are very much interlinked to enable the desired finishing output.

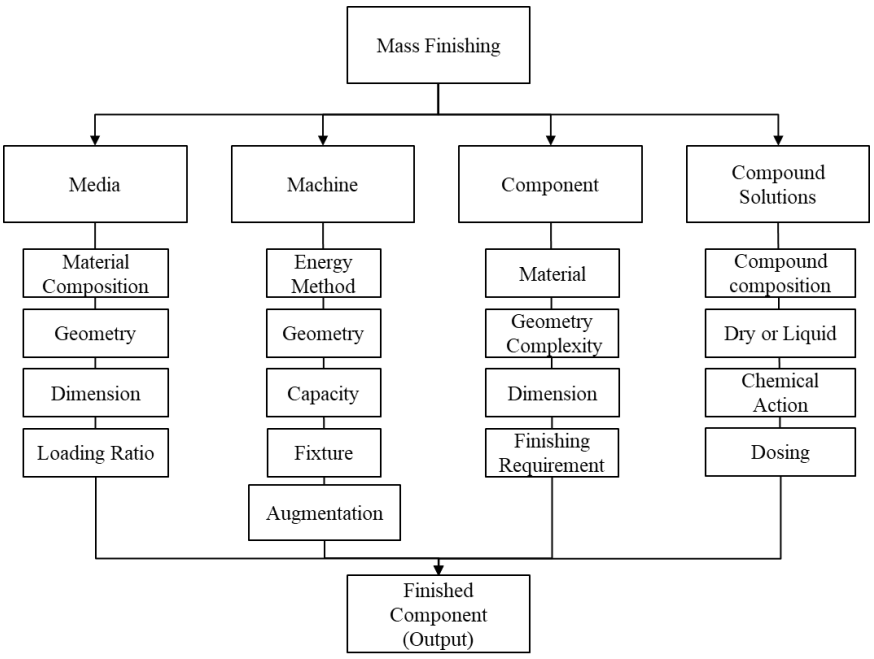

Figure 2.1 Key Process Variables of Mass Finishing

The functions of each KPV are briefly described below [3] [11], with an in-depth review on the machine KPV and its subcategories:

1. Media: Media comes in various shapes, sizes, and materials to meet various surface finishing requirements. Media selection is based on the component material and the degree of process aggressiveness required, such as cutting or finishing. Generally, there are four types of materials: Ceramic, Plastic, Metallic and Natural Media. Typically, ceramics are preformed and ladened with abrasive particles to increase cutting rates. Shape and size selection are crucial to enable the right cutting action onto the component. If the size is too fitting or the shape is too wide, media might get lodge into component features such as grooves or slots, thus preventing finishing or even damaging these features as seen in Figure 2.2. Media is the key medium to impart energy from machine to component surface, with three types of contacts methods: Free impact, Rolling and Adjacent media rolling over a stationary media. [12] Finally, the amount of media-to-component ratio inside a machine is crucial to maximise processing output via media-to-component contact. Conversely, the ratio is critical to reduce the chances of component-to-component contact. To which too little media will cause surface damages to the components and cause scrap.

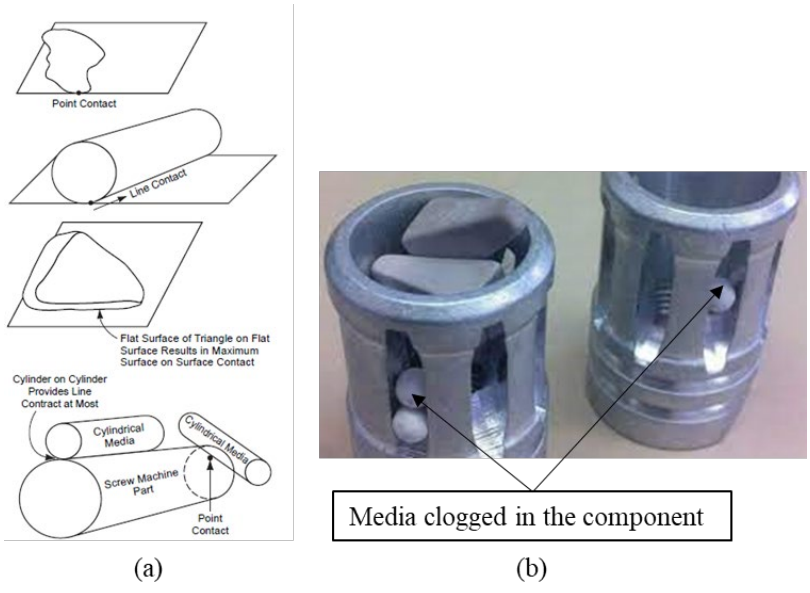

Figure 2.2 (a) Media contact methods onto component surface and (b) Media clogged in component feature [3], [5]

2. Component: Before the downselection of a suitable mass finishing process, an analysis of the component is critical. Based on the surface requirements, a downselection of process can be established. Mass finishing is capable of deburring, polishing, radiusing, brightening, cleaning, degreasing, descaling, de-rusting, and surface hardening. In addition, a component material would need to be known beforehand. An example would be whether the component is ferrous or non-ferrous that could affect the pH within the process and cause oxidation. The complexities of a component's geometry and features would further affect the choice of media size and shape. Occasionally, there are requirements for targeted finishing on specific, necessitating pre-processing. An example would be the deburring of specific edges while maintaining the overall surface finish of a casted component. Potential solutions include masking the surfaces while exposing the burrs, or to use a robotic arm to hold onto components and orientate the burrs towards the media flow in a spindle-type mass finishing machine.
3. Compound Solution: As described in the Mass Finishing Handbook [3] , a common misconception on compounds is that it is different from compound solutions as compounds are the base or ingredients used to make compound solutions. This is critical to note, as compound selection for mixing should not be based on the effectiveness of the solution but a proper understanding of the functionality. There are seven types of solution functions: Abrasive, descaling, cleaning, deburring/polishing/radiusing, burnishing and colouring. For example, in abrasive finishing requirement, a compound solution is used to increase imparting energy through surface activation (Isotropic Superfinishing). Conversely, media wear rates could be reduced through dampening the energy onto the surface (wet-type mass finishing processes). At the same time, it could produce lustre or colour, or be used to prevent flat surfaces from sticking to one other while maintaining the pH value within the working area.

4. Machine:

- Energy Method: The energy method refers to the type of energy imparted to the components and media in the mass finishing machine. The variation in mass finishing processes is fundamentally differentiated by the methodology of imparting energy, such as vibration, tumbling, rotation, or centrifugal forces which all have varying effects on the surface finish. Comparatively, vibration motion (vibrofinishing) provides the lowest energy and aggressiveness, followed by tumbling motion (Barrel Tumbling), rotation (drag, spindle finishing) and high-speed rotation or centrifugal (centrifugal barrel, centrifugal disk). Some of which, like centrifugal, could go up to 40-50 times the aggressiveness in comparison to vibrofinishing [13]. Generally, energy method selected should align with the desired finishing objectives and component requirements to achieve the desired process result.
- Machine Geometry: The geometry of the mass finishing machine itself can have a significant impact on the process result. The shape, size, and design of the machine can influence the distribution of energy (from machine to media to component), media movement, and contact with the components. For example, different machine geometries, such as round vibratory bowls, troughs, or barrel drums, can provide different motion patterns and energy transfer characteristics to the components and media. The machine geometry also determines the available working space and media-to-component ratio, which can affect the efficiency and effectiveness of the finishing process. Additionally, the machine geometry should be compatible with the size and shape of the components to ensure proper media flow and contact. An example would be that long components like shafts and turbine blades are not able to fit in round shaped machines must be processed by trough-shaped machines. Choosing the appropriate machine geometry based on the specific component requirements and finishing objectives is essential to achieve the desired process result.

- Fixture: High values parts that risk surface-to-surface impingement between components could use a fixture or a divider to be used with the machine and is subjected to the machine type. An example is the use of a fixture in a vibrofinisher as opposed to conventional means of free tumbling with the vibrating media. Some form of fixtures would be clamping samples onto the base of the machine using nut and bolt or magnetism, or having an external fixture that will dip the component into the machine. Apart from solving the surface-to-surface impingement, as analysed by Kunal et al. [14], a fixtured component may improve the surface roughness reduction efficiency due to relatively faster media flow with respect to the component surface that is now static.

5. Augmentation: Some processes augment energy impartations via magnetism (Magnetic-abrasive finishing), electricity, chemical (chemical loose abrasive finishing), a combination of electricity and chemistry (electrochemical mass finishing) or even a combination of all three (magnetic electrochemical abrasive finishing) [3].

2.2 Vibrofinishing in Aerospace industry

Prior to the advent of mass finishing techniques, aerospace components were manually finished by skilled laborers using hand tools like grinding disks or buffing machines. However, this manual approach had its limitations as the human factor introduced variations in the final finish of each component. Furthermore, with the onset of the third Industrial Revolution, there was a growing demand for increased productivity through automation, while simultaneously facing a decline in the availability of skilled labour and manpower. As a result, there arose a need for a more efficient and rapid method of finishing aerospace components.

Mass finishing has gained significant traction in the aerospace industry, encompassing both new manufacturing and maintenance, repair, and overhaul (MRO) operations. This is primarily attributed to the enhanced efficiency and precision

offered by mass finishing compared to manual processes for polishing. As discussed in Chapter 1 vibrofinishing is widely employed for the mass finishing of aerospace engine components, which exhibit diverse surface integrity requirements in terms of size, shape, and production specifications. Examples of such components include aerofoils ranging from large fan blades measuring several meters in length to small high-pressure compressor aerofoils measuring a few centimetres [15].

It is important to note that surface finishing plays a critical role in the aerospace industry. By achieving the appropriate surface finish, the lifespan of engine components can be significantly extended while also enhancing their resistance to stress corrosion cracking. Smooth turbine blades, for instance, improve laminar flow characteristics and minimize frictional and turbulence losses in airflow. Furthermore, planarisation of airfoil surfaces in a multistage turbine engine contributes to overall turbine efficiency.

2.2.1 Types of Vibrofinishing

As explained in Chapter 1.2, the two generic vibrofinishing shapes are the bowl and trough. For a bowl shape, there are further bowl shape variants to meet various requirements such as ‘dome’ and ‘domeless’ options. The ‘dome’ in the bowl shape vibrofinishing refers to the protrusion from the base of the machine’s work area, and holds the motor and flyweights that cause the vibration. ‘Domeless’, on the other hand, means that the motor is positioned below the work area such that there is no protrusion. In the examples in Figure 2.3, a series of dome and domeless options are shown. More detail between dome and domeless is explained in section 2.3.1.

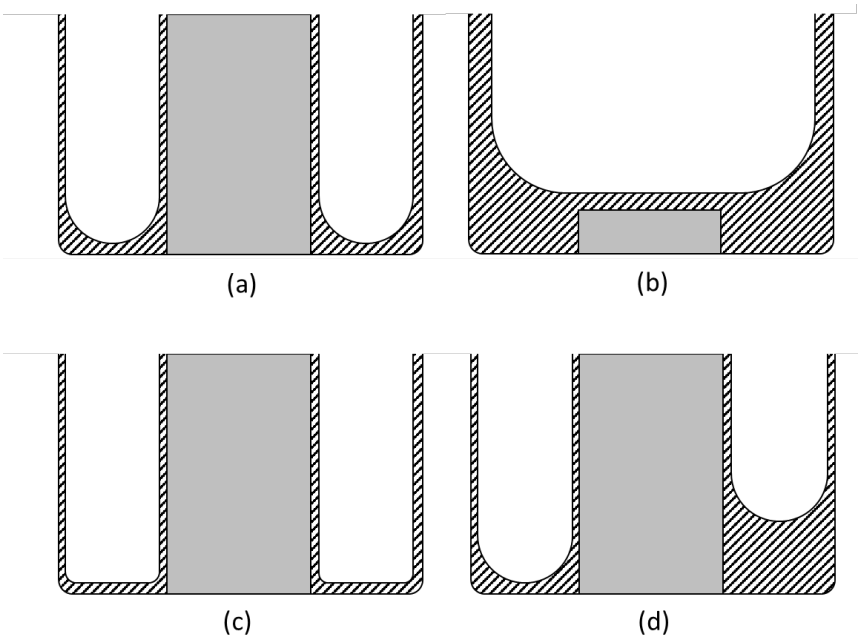

Figure 2.3 Cross-section schematic of bowl-shaped vibrofinishers variants. (a) Dome, Round base, non-elevated (b) Domeless, Round base, non-elevated (c) Dome, Flat base, non-elevated (d) Dome, Round base, elevated

The elevation option is selected for small components that risk sticking to each other which prevents media contact. The elevation forces components to 'drop' and thereby rotate. Flat or round bottom utilisation are based on the type of component. A flat bottom enables wider components such as a fan blade to be placed lower to the bowl, usually through a fixture, without hitting the curvature of the bowl, while a round bottom is more generically used as it reduces components from being trapped at the corner of the bottom due to the 'rolling' nature of media flow.

For components that are processed in batches within the vibrofinisher, a likely risk of part impingement might occur due to contact-to-contact between these components, causing high valued scrap. The solution for this is compartmentalising through

addition of dividers outfitted into the machines as seen in Figure 2.4.

Figure 2.4 Compartmentalised Vibratory (left) bowl and (right) trough [16]

Apart from compartments, another alternative is the use of external fixture to hold components in place during vibrofinishing as shown in Figure 2.5. Generally, heavier components utilise external fixture to avoid damaging to the Polyurethane (PU) coating on the machine surface [3].

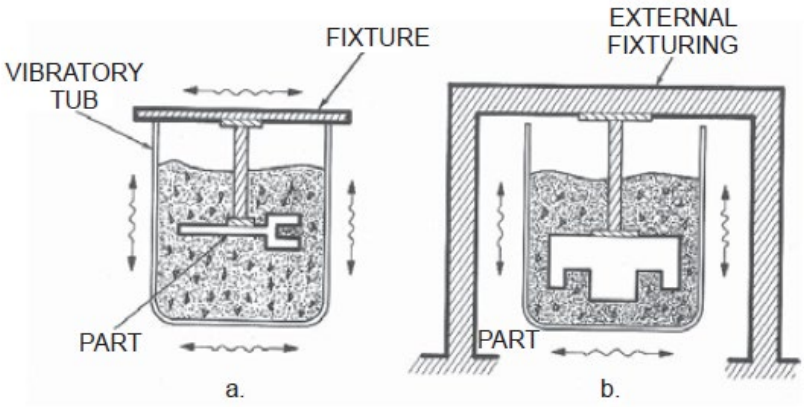

Figure 2.5 Fixture methods for vibrofinishing (left) internal and (right) external [3]

For example, turbine blades are fixtured a robotic holder such as in Figure 2.6 after fatigue enhancing processing. The robot dips the blades into a large and deep trough vibrofinisher and holds them in place.

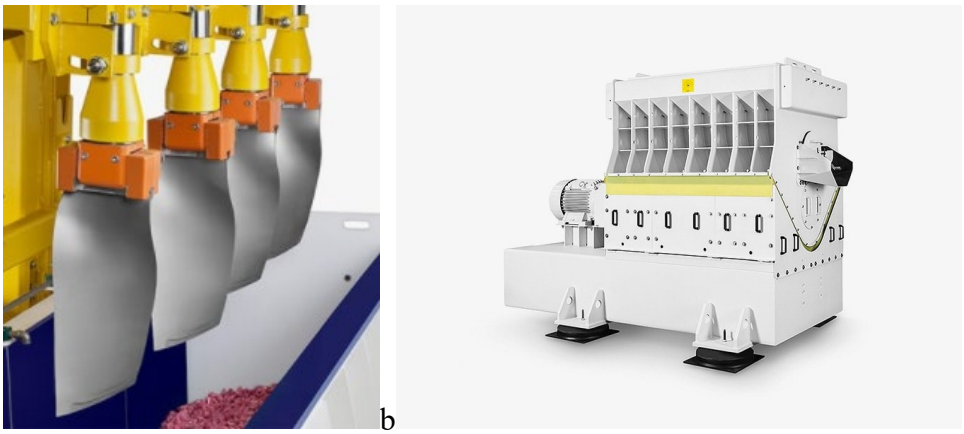

b

Figure 2.6 (left) four robotic arms for holding turbine blades for vibrofinishing process and (right) trough vibrofinishing machine [9]

Internal fixture such that fix components in place via mechanical assembly or magnetism at the base of the bowl. Figure 2.7 shows an example of a blisk-drum fastened to the base of a vibrofinisher via a fixture.

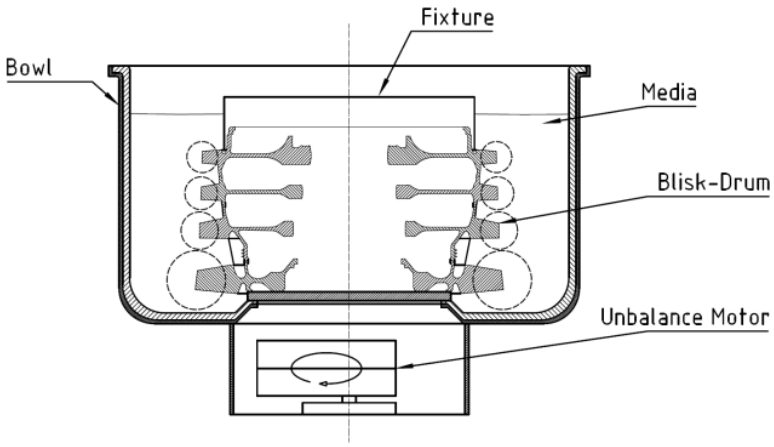

Figure 2.7 Schematic view of a blisk-drum fixtured onto a domeless round vibrofinisher [15]

Based on the mass finishing handbook [3], the benefits of fixture can be classified below:

- Faster processing (almost 33% increase [1])
- More pieces per load
- Finer finishes

- Prevents part-on-part impingement (damage)
- Better accessibility or internal work in narrow passages and openings
- Allows smaller media to be more effective
- Allows higher machine frequencies to be used
- Prevents damage to the machine liner from sharp edged parts.

There is increasing developments of fixtured vibrofinishing for both internal and external types with the capability to induce effective surface hardening. [15] Due to this additional processing capability, it has been dubbed as a variant of vibrofinishing called vibrostrengthening, coined by Sangid et al. or another term called vibropeening process. [14], [17] Fundamentally, the relative motion between media with respect to component increases and thus able to produce sub-surface compressive residual stress to improve fatigue life. This potentially replaces fatigue enhancement processes like shot peening by combining both polishing and fatigue enhancement into one.

2.2.2 Post-Vibrofinishing Quality Control

Before the vibrofinishing process, for both new-make and MRO, certain components would require sub-surface enhancements. For example, fatigue enhancement through processes like shot peening, would undergo polishing processing, such as vibrofinishing, thereafter, to get a glossy finish for aesthetics purposes, and some situation for mechanical purpose such as pre-coating preparation. There are also instances that after vibrofinishing the components will be soaked in chemicals for cleaning, coating, surface treatment, or even to conduct additional surface finishing. As such, a key component to ensure the component is fit for the next process is the measurement of the surface quality such as roughness, material removal or sub-surface inspections.

There are multiple quality control (QC) measurements to ensure components functions correctly and are safe to use. Generally, the remanufacturing shop floor conducts QC based on sampling, which more complicated ones done at a lower

sampling rate. The most common sampling measurement is the surface roughness which typically range between 1.0 μm < R_a < 0.20 μm depending on component [15] [18] [7]. The general requirements from Spire Pte Ltd's aerospace customers are R_a 0.625 μm. Such surface roughness measurement is mostly done by a contact-type surface profilometer.

Another surface requirement is the check for the material removal or stock loss after processing. Usually, as vibrofinishing is either provide a net or near-net shape, such measurements could be as simple as ensuring less than 0.01mm change or 'no changes in value' by using a Vernier calliper to measure. Another more stringent, and expensive, sampling could involve a Coordinate Measurement Machine (CMM) that can measure up to a precision of 1 μm.

2.3 Vibrofinishing modelling

There is much research on vibrofinishing modelling for simulation purpose. As this thesis focuses on the use of domeless round, non-elevating vibrofinishing process, this review aims to do three things:

1. To briefly explain the mechanics of a vibrofinishing process
2. The industrial practice used in the aerospace industry as advised by Spire Pte Ltd
3. Review modelling papers of a dome, round vibratory finishing.

The review here will be used as a basis for theoretical analysis of a domeless, round and non-elevating vibrofinishing process.

2.3.1 Mechanics of vibrofinishing

The media flow in vibrofinishing process is induced by the agitation of vibration motion. The vibration motion is generated by a motor with eccentric flyweights that are mounted at two different heights and alignment (as illustrated in Figure 2.8 (c) along a motor drive shaft. The misalignment between the top and bottom flyweights

induces eccentric motion which generates the agitation necessary for the media flow in the vibrofinishing process. In the case of a domeless vibrofinisher, the top and bottom flyweights are placed under the base of the working area instead. A series of spring are mounted between the bowl and the base to isolate the vibration to its working area. Another use of the spring is as it compresses, the vibratory bowl falls. Inversely, spring expansion results in bowl rise. As seen in Figure 2.8 (a) and (b), a schematic drawing of both dome and domeless bowls are shown in front view. Figure 2.8 (c) shows a schematic drawing both dome and domeless bowls' top view due to similarity in setup in this view, and the alignment angle between the two eccentric weights.

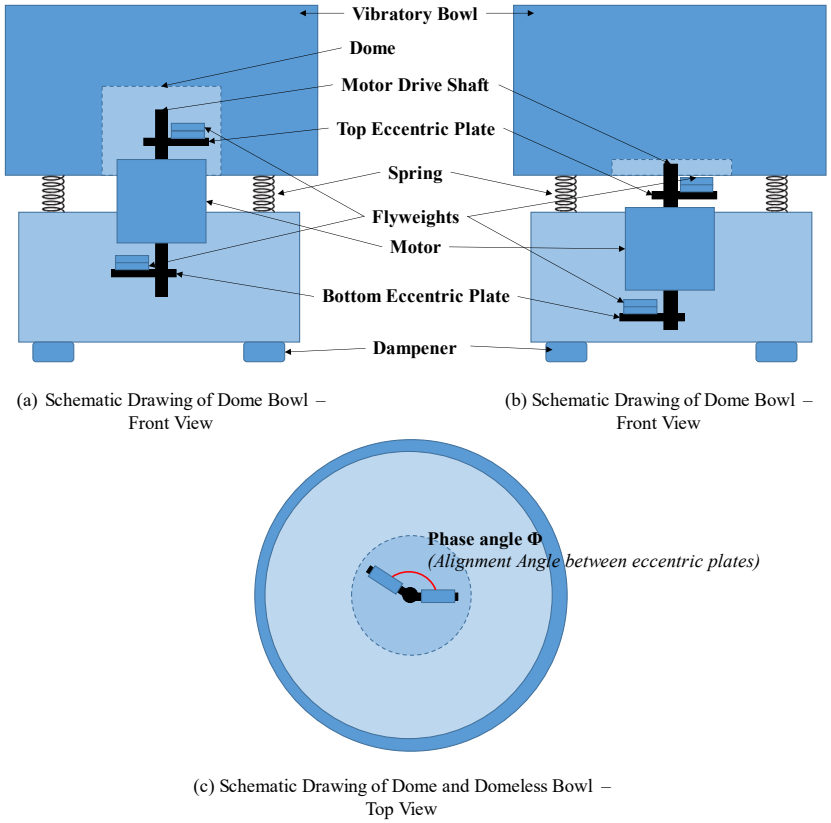

Figure 2.8 Schematics of vibrofinishing machine at top view (a) dome and (b) domeless

This vibration motion causes a helix motion along the peripherals of the bowl. By observing from two planes, the motion is split into two forms instead– Roll and Feed.

(See Figure 2.9) A roll is explained as the motion of media rising outwards to the machine wall and falling downwards at the centre. Feed is explained as the clockwise or anti-clockwise lapping path around the circumference of the machine, to which the direction is determined by the motor rotation. Direction of bowl's vibration is always opposite of the motor's rotational direction. As seen in Figure 2.9, both dome and domeless configurations follow the described vibratory motions, with the key difference of the domeless configuration having larger radial roll due to the absence of blockage by the dome.

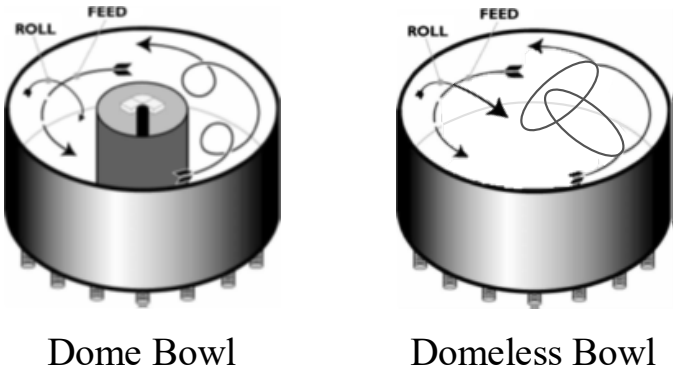

Figure 2.9 Forms of vibrofinishing motions by (left) dome [19] and (right) domeless configurations

A study on the dome bowl by Hashimoto and Johnson [20] explained that when motion was observed in two planes of the bowl, there were two forms of helical motions at play each. An experimental trial was conducted by using a fishing line glued to a medium to observe the trajectory of the medium at different starting positions. The results showed that in the top view of the bowl or the *x*-*y* plane, media had a circular trajectory at constant radius with a counterclockwise rotation. The circular trajectory had a constant radius which was accounted as the amplitude. Figure 2.10 showed the observation of the motion results attained of the dome bowl by Hashimoto and Johnson [20].

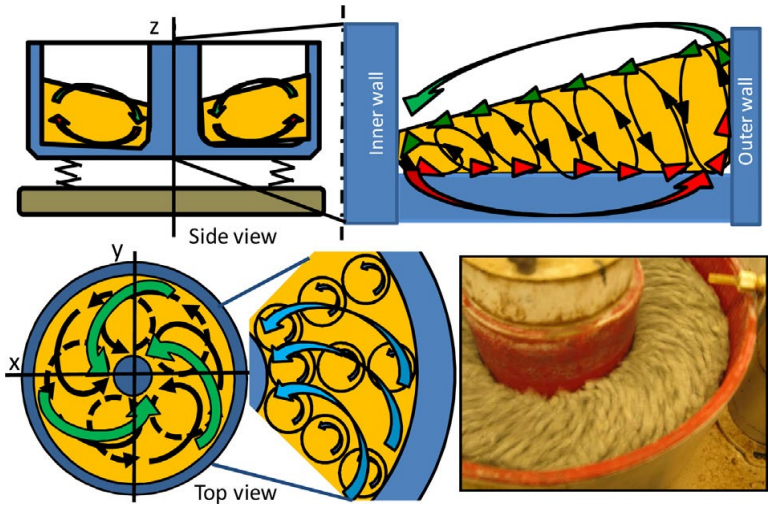

Figure 2.10 Two forms of spiral motion observed at two planes [20]

2.3.2 Industrial Practice of Vibrofinishing

The practice for controlling the roll and feed is determined by three factors – Rotational speed of the vibratory drive system, the mass of the eccentric weights and the alignment (phase) angle between these eccentric weights that are positioned at the top and bottom of the vibratory drive system respectively. These factors are quantified by the amplitude and frequency of vibration, enabling precise control over the roll and feed motions.

Fundamentally, amplitude and frequency can be represented as a spring-mass diagram as seen in Figure 2.11. A mass moving from point A to B, in the units of mm, represents amplitude while frequency refers to the total number of oscillations from point A to B and back to A, per unit time. Frequency is represented in Hz which is the number of cycles per second.

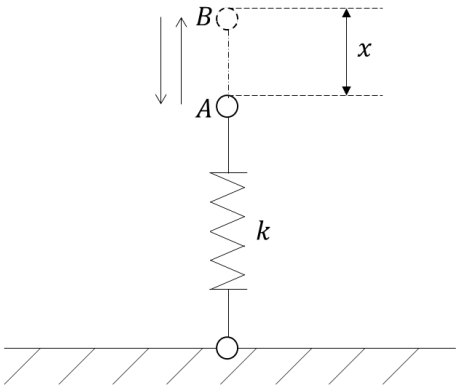

Figure 2.11 A spring-mass diagram to explain amplitude and frequency of vibrofinishing

The selection criteria of the amplitude and frequency may vary according to different use cases. In the context of domeless vibrofinishing, there is no known operating guidelines. Therefore, a summary of known operating guidelines for amplitude and frequency selection will be explored in this section that would set a baseline for the domeless vibrofinishing.

Vibration in a vibrofinisher is created through a motor drive shaft that rotates eccentric flyweights. An off-balanced spinning of the flyweights creates an unbalanced momentum to the containment in a shape of a bowl or trough, resulting in an exaggerated, aggressive rolling action [3], which is measured in amplitude. Essentially, the amplitude is controlled by the flyweights' mass and relative angles between them. First, an increase in the relative mass between the bottom and top flyweight will increase the imbalance during rotation of the motor. Additionally, adding mass to the flyweight that is positioned further away to the bowl or trough may increase the imbalance of the system and therefore the unbalance momentum. For a dome vibrofinisher, it may be either the top or bottom flyweight depending on the machine maker. In the context of domeless bowl, the bottom flyweight is always the furthest from the centroid of mass. A schematic diagram of both dome and domeless and each of their flyweight placement is shown in Figure 2.12.

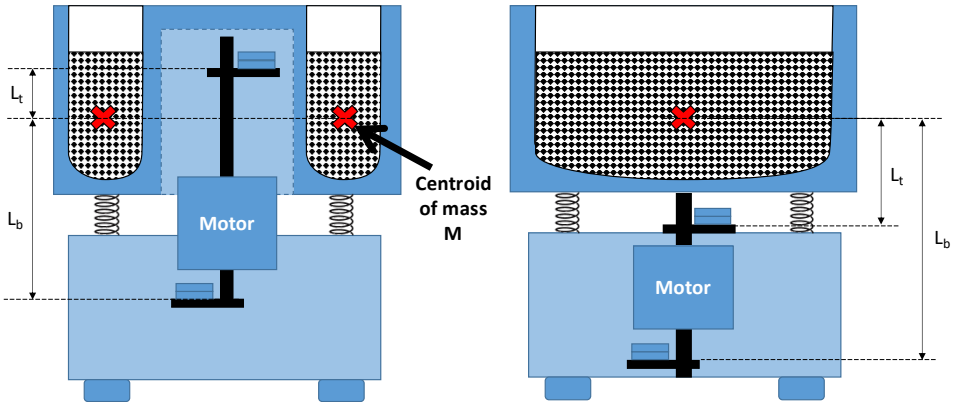

Figure 2.12 Position of top and bottom flyweights relative to the centroid of mass of (left) Dome and (left) Domeless

Based on the above point, a quick trial on the domeless vibrofinisher provided by Spire Pte Ltd validated this claim. To which more weight had to be added to the bottom eccentric flyweight to achieve a similar amplitude value relative to a dome vibrofinisher. A further exploration will be done in Chapter 4.

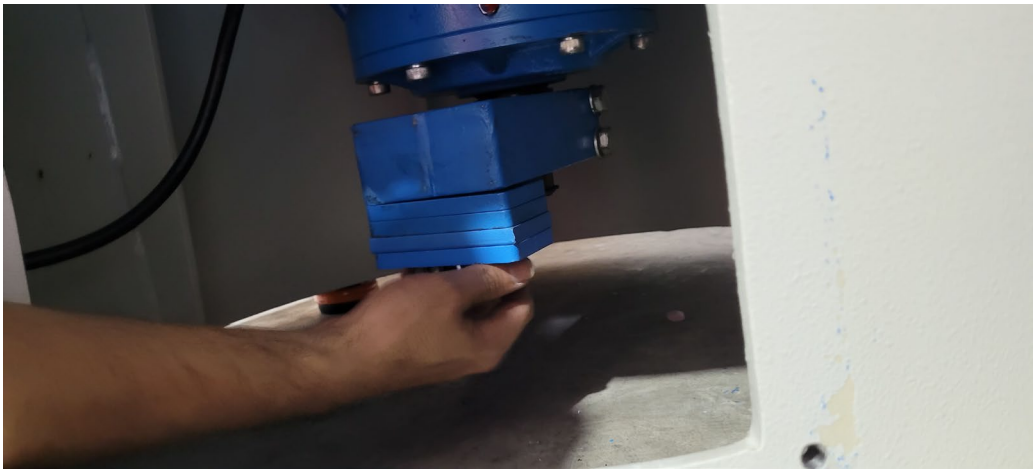

Figure 2.13 Setup of bottom flyweight on Spire Pte Ltd Domeless bowl

Next, the alignment (phase) angle between the top and bottom flyweights may be set as well. Generally, a smaller angle produces higher amplitude. The highest intensity is produced at zero degrees as seen in Figure 2.14 (a), while the lowest, which generates no vibration, is produced at 180 degrees as seen in Figure 2.14 (b).

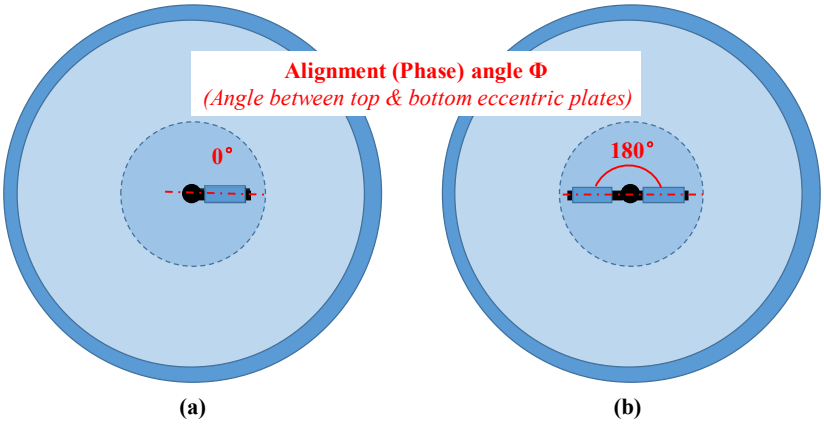

Figure 2.14 (a) 0° and (b) 180° Alignment (Phase) angle between top and bottom flyweight

For free moving components processing, higher rolling will allow heavier components to be 'lifted' by the vibrating media. This is important to note, as components with heavier materials such as Inconel or larger sizes might lead to damage to both the component and the Polyurethane (PU) layer on the machine wall if they are unable to be lifted by the media. In instances like this, more flyweights at the bottom eccentric plate must be mounted to increase the amplitude, similar to the quick trial mentioned earlier.

As per ASM Surface Engineering handbook [11], carbon steels are typically refined in this amplitude range. Softer metals, such as aluminium and zinc, would be refined better at a lower amplitude range of 2.5 to 3.5 mm. This can be achieved by removing all the bottom flyweights. Very soft metals, such as brass, may be damaged by amplitudes greater than 2.5 mm, and are usually finished with no weights on the bottom eccentric plate. On the other hand, exceptionally rough components, or components where it is not at a final stage of processing, can be run at higher amplitude of 5.5 to 7.0 mm. Exceptionally heavy components may require higher amplitudes of 6.5 to 7.0 mm to simply generate enough inertia to lift the part and roll it in the bowl channel to which an alternate approach is to employ a fixture to avoid damages to the wall lining.

Another way to select the amplitude may be through an RPM-Amplitude selection

table, as seen in Figure 2.15. Red and yellow zones provide a safety guideline to prevent users from exceeding the safe operatable acceleration of a vibrofinishing machine.

RÖSLER finding a better way...	Acceleration values depending on speed and amplitude																		
	Result in multiples of g (gravity 1g = 9.81 m/s²)										Accelerations higher than 6g must be avoided!								
Speed	Amplitude in mm as read of the amplitude sticker attached to the outermost part of the machine																		
(rpm)	1	1.5	2	2.5	3	3.5	4	4.5	5	5.5	6	6.5	7	7.5	8	8.5	9	9.5	10
950	0.5	0.8	1.0	1.3	1.5	1.8	2.0	2.3	2.5	2.8	3.0	3.3	3.5	3.8	4.0	4.3	4.5	4.8	5.0
1000	0.6	0.8	1.1	1.4	1.7	2.0	2.2	2.5	2.8	3.1	3.4	3.6	3.9	4.2	4.5	4.8	5.0	5.3	5.6
1100	0.7	1.0	1.4	1.7	2.0	2.4	2.7	3.0	3.4	3.7	4.1	4.4	4.7	5.1	5.4	5.7	6.1	6.4	6.8
1150	0.7	1.1	1.5	1.8	2.2	2.6	3.0	3.3	3.7	4.1	4.4	4.8	5.2	5.5	5.9	6.3	6.7	7.0	7.4
1200	0.8	1.2	1.6	2.0	2.4	2.8	3.2	3.6	4.0	4.4	4.8	5.2	5.6	6.0	6.4	6.8	7.2	7.6	8.0
1300	0.9	1.4	1.9	2.4	2.8	3.3	3.8	4.3	4.7	5.2	5.7	6.1	6.6	7.1	7.6	8.0	8.5	9.0	9.4
1400	1.1	1.6	2.2	2.7	3.3	3.8	4.4	4.9	5.5	6.0	6.6	7.1	7.7	8.2	8.8	9.3	9.9	10.4	11.0
1450	1.2	1.8	2.4	2.9	3.5	4.1	4.7	5.3	5.9	6.5	7.1	7.6	8.2	8.8	9.4	10.0	10.6	11.2	11.8
1500	1.3	1.9	2.5	3.1	3.8	4.4	5.0	5.7	6.3	6.9	7.5	8.2	8.8	9.4	10.1	10.7	11.3	11.9	12.6
1600	1.4	2.1	2.9	3.6	4.3	5.0	5.7	6.4	7.2	7.9	8.6	9.3	10.0	10.7	11.4	12.2	12.9	13.6	14.3
1700	1.6	2.4	3.2	4.0	4.8	5.7	6.5	7.3	8.1	8.9	9.7	10.5	11.3	12.1	12.9	13.7	14.5	15.3	16.2
1750	1.7	2.6	3.4	4.3	5.1	6.0	6.8	7.7	8.6	9.4	10.3	11.1	12.0	12.8	13.7	14.6	15.4	16.3	17.1
1800	1.8	2.7	3.6	4.5	5.4	6.3	7.2	8.2	9.1	10.0	10.9	11.8	12.7	13.6	14.5	15.4	16.3	17.2	18.1
1900	2.0	3.0	4.0	5.0	6.1	7.1	8.1	9.1	10.1	11.1	12.1	13.1	14.1	15.1	16.1	17.2	18.2	19.2	20.2
2000	2.2	3.4	4.5	5.6	6.7	7.8	8.9	10.1	11.2	12.3	13.4	14.5	15.7	16.8	17.9	19.0	20.1	21.2	22.4
2100	2.5	3.7	4.9	6.2	7.4	8.6	9.9	11.1	12.3	13.6	14.8	16.0	17.3	18.5	19.7	21.0	22.2	23.4	24.7
2200	2.7	4.1	5.4	6.8	8.1	9.5	10.8	12.2	13.5	14.9	16.2	17.6	18.9	20.3	21.6	23.0	24.4	25.7	27.1
2300	3.0	4.4	5.9	7.4	8.9	10.3	11.8	13.3	14.8	16.3	17.7	19.2	20.7	22.2	23.7	25.1	26.6	28.1	29.6
2400	3.2	4.8	6.4	8.0	9.7	11.3	12.9	14.5	16.1	17.7	19.3	20.9	22.5	24.1	25.8	27.4	29.0	30.6	32.2
2500	3.5	5.2	7.0	8.7	10.5	12.2	14.0	15.7	17.5	19.2	21.0	22.7	24.5	26.2	28.0	29.7	31.4	33.2	34.9
2600	3.8	5.7	7.6	9.4	11.3	13.2	15.1	17.0	18.9	20.8	22.7	24.6	26.5	28.3	30.2	32.1	34.0	35.9	37.8
2700	4.1	6.1	8.2	10.2	12.2	14.3	16.3	18.3	20.4	22.4	24.5	26.5	28.5	30.6	32.6	34.6	36.7	38.7	40.8
2800	4.4	6.6	8.8	11.0	13.1	15.3	17.5	19.7	21.9	24.1	26.3	28.5	30.7	32.9	35.1	37.3	39.4	41.6	43.8
2900	4.7	7.1	9.4	11.8	14.1	16.5	18.8	21.2	23.5	25.9	28.2	30.6	32.9	35.3	37.6	40.0	42.3	44.7	47.0
3000	5.0	7.5	10.1	12.6	15.1	17.6	20.1	22.6	25.2	27.7	30.2	32.7	35.2	37.7	40.2	42.8	45.3	47.8	50.3
3100	5.4	8.1	10.7	13.4	16.1	18.8	21.5	24.2	26.9	29.5	32.2	34.9	37.6	40.3	43.0	45.7	48.3	51.0	53.7
3200	5.7	8.6	11.4	14.3	17.2	20.0	22.9	25.8	28.6	31.5	34.3	37.2	40.1	42.9	45.8	48.7	51.5	54.4	57.2
3300	6.1	9.1	12.2	15.2	18.3	21.3	24.4	27.4	30.4	33.5	36.5	39.6	42.6	45.7	48.7	51.7	54.8	57.8	60.9
3400	6.5	9.7	12.9	16.2	19.4	22.6	25.8	29.1	32.3	35.5	38.8	42.0	45.2	48.5	51.7	54.9	58.2	61.4	64.6
3450	6.7	10.0	13.3	16.6	20.0	23.3	26.6	29.9	33.3	36.6	39.9	43.2	46.6	49.9	53.2	56.6	59.9	63.2	66.5
3500	6.8	10.3	13.7	17.1	20.5	24.0	27.4	30.8	34.2	37.7	41.1	44.5	47.9	51.4	54.8	58.2	61.6	65.1	68.5
3600	7.2	10.9	14.5	18.1	21.7	25.4	29.0	32.6	36.2	39.8	43.5	47.1	50.7	54.3	58.0	61.6	65.2	68.8	72.4

Figure 2.15 RPM vs Amplitude setting table by Rösler [21]

It is noteworthy that above mentioned amplitude values were validated from Spire Pte Ltd's experiences. Example is a double roll as shown in Figure 2.16(b) for the precision engineering industry on soft and small metal pieces for high volume production in a dome bowl. A typical media flow employed by aerospace customers would be as shown in Figure 2.16(a).

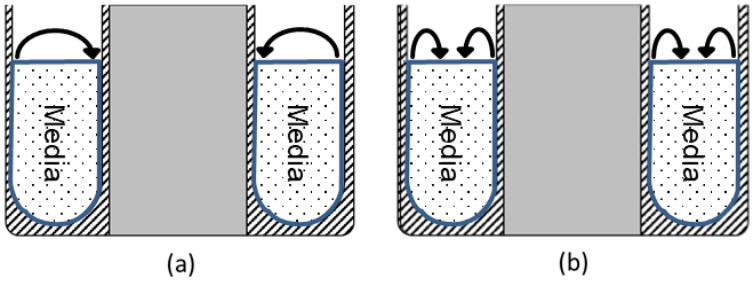

Figure 2.16 (a) Typical flow with max Amplitude (b) Double roll with lower Amplitude

Secondly, frequency fundamentally controls the feed rate. Feed rate is usually adjusted for two operational reasons – To enable quicker unloading process and to control the overall processing time.

To finish components quicker, a tighter helical motion such as left drawing of Figure 2.17, having a high number of helixes per circumferential lap, would be desirable. Especially for components that can tolerate part-on-part damage or surface requirements are not a big criterion are good choices. In practice, the helix count is increased by decreasing the number of flyweights on the top eccentric plate. Opposingly, very delicate components that cannot afford any part-on-part impingement damage may reduce the number of flyweights at the top eccentric plate.

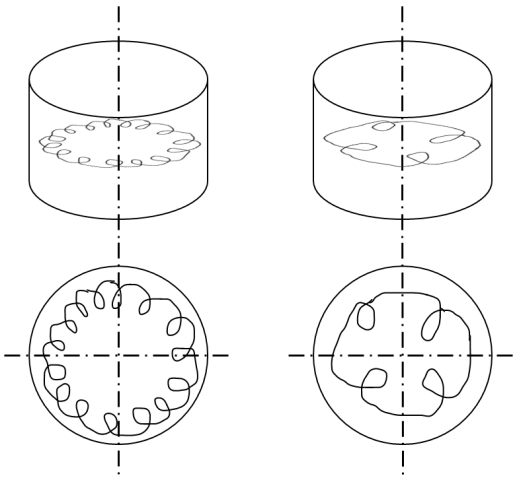

Figure 2.17 Drawing to explain the number of helical motions a component might travel in one circumferential lap (bi-directional) - (left) closer helical motion of 16 cycles/lap compared to (right) wider helical motion of 4 cycles/lap

One key difference between a domeless to a dome type is the feed rate of a similar

bowl diameter as due to the increase in roll of a domeless type from a wider circular motion towards the centre axis of the bowl due to the absence of the dome. Operationally, increasing the flyweights at the top eccentric plate for a domeless bowl may increase the feed rate.

The inspection is through a visual inspection of a Vibrascope that is attached onto the vibrating bowl, as seem in Figure 2.18a. Figure 2.18b illustrates how the plate looks like in actual operations. Firstly, the observation of the lead angle is seen as the line with the least deviation from its 'double image', in the scenario of Figure 2.18b, the lead angle is seen closest to 60°. As for the amplitude, the observation is to see which circle has the closest to tangent with its 'double image'. The example in Figure 2.18b shows that the closest value is 4.5mm.

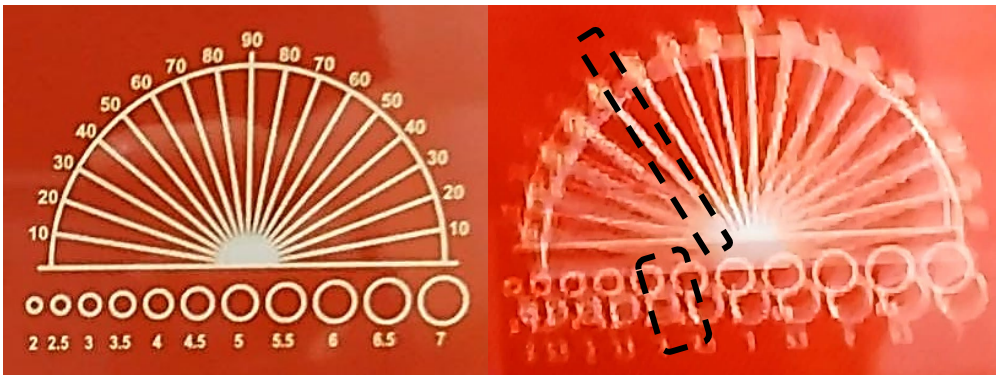

(a) (b)

Figure 2.18 Vibroscope attached to vibrofinisher at two instance (a) not in motion (b) in motion will cause 'double image' to appear for analysis

2.3.3 Modelling of vibratory finishing machine

With the lack of literature on a domeless-type vibratory finishing machine, an inference to various modelling methods of the dynamics of a dome, round and non-elevating vibrofinishing process will enable a good modelling comparison. This section will focus only on the aspects of modelling of the machine and process. Since the flow compared to domeless type is also helical in nature, kinematics will be excluded in this review. Additionally, material removal and roughness models are

excluded as well since the focus is on the dynamical changes due to the removal of the dome.

As mentioned by Hashimoto and Johnson [20] [20], a bowl type vibratory finishing machine is much more complicated as compared to a tub type due to its complex 3-D vibration modes. Their method of modelling of a bowl type machine is by assuming the bowl as an equivalent cubic body of mass *M* that refers to the total mass that includes the bowl, media, component, liquid compound, water, and any additional fixtures. The springs supporting the bowl are converted to a spring/damper at the 4 corners of the body both horizontal and vertical directions, amounting to 8 spring/damper setup.

The coefficients used for spring and damping are split between horizontal (*x*-*y* axes) and vertical (*z* axis) directions are k_h, k_v, c_h, c_v, respectively. The model rightfully assumes a 5 degree of freedom due to the inability for the bowl to rotate around the *z* axis. It is also noted that the centroid of the model or pivot point was not mentioned, to which could be assumed as the middle point of the media height. The model can be seen in Figure 2.19.

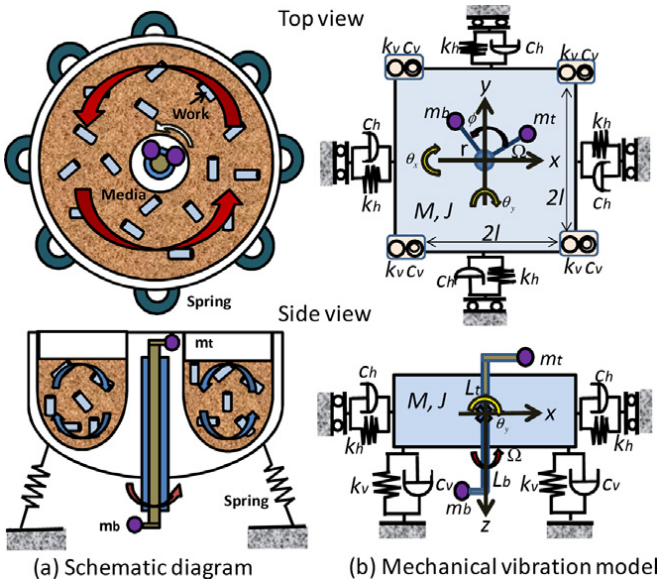

Figure 2.19 Modelling of bowl type vibratory machine by Hashimoto and Johnson [20]

This paper uses Newton's Second Law and free body diagram along the *x*-*y*-*z*

coordinate system to form a parametric representation. By solving the displacements of each axis into free and forced vibration equations, these theoretical equations were compared to their experimental results.

A dynamical analysis of a non-elevating, dome bowl vibrofinisher by Zhang et al. [22] show a dynamic model of it as seen in Figure 2.21. Interestingly, this dome-type vibrofinishing machine does not have top eccentric plate at the middle of the bowl which in comparison is similar to a domeless shape to that extend as the motor, eccentric weight, and spring are under the bowl.

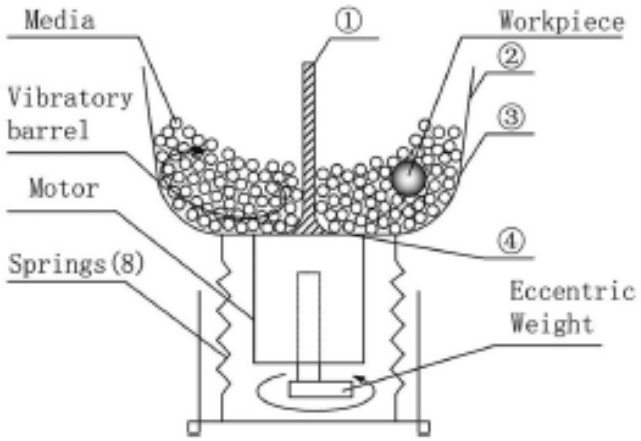

Figure 2.20 Schematic diagram of dome vibrofinishing machine by Zhang et al. [22]

This model explains the system as a mechanical vibration system. The vibrating body comprises of the bowl, media, component, and any additional accessories such fixtures or liquid compound and water. The body is represented as an equivalent cubic body of the bowl. Figure 2.21(a) shows 4 springs and dampers at 4 perpendicular points of the body to represent the *z*-axial support of the body while Figure 2.21 (b) shows 4 springs and dampeners to represent the *x*-*y*-axial support of the body.

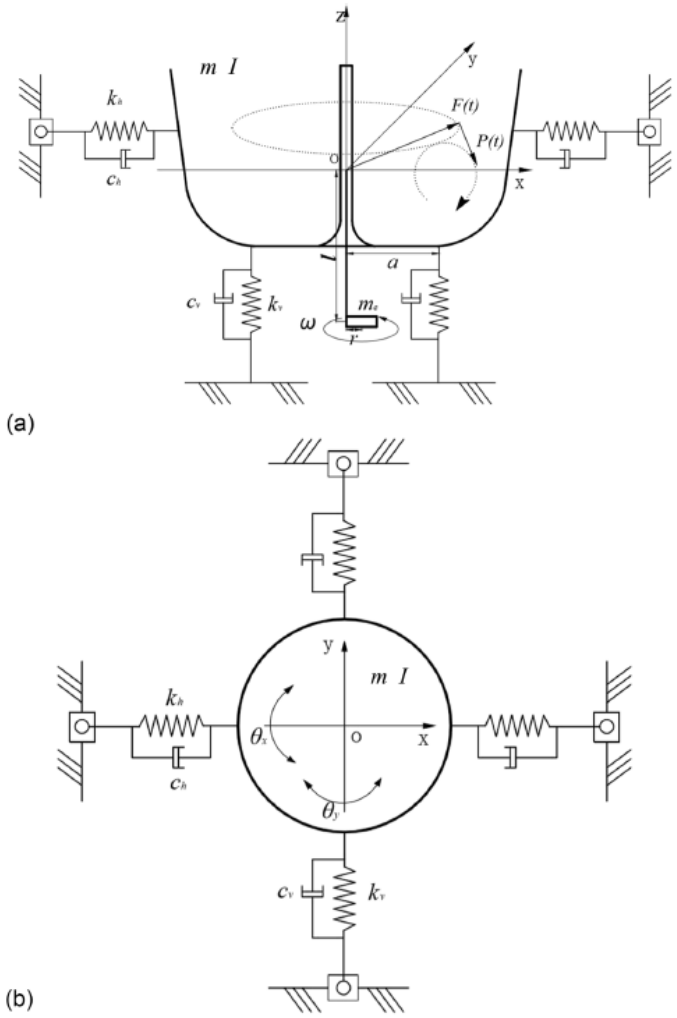

Figure 2.21 Dynamic model of vibrofinisher. (a) Front view of the model and (b) Top view of the model [22]

Zhang uses Newton's Second Law in a *x*-*y*-*z* coordinate system to similarly form a parametric representation, with the difference of establishing them in a matrix format [22]. As seen in Figure 2.21(a), the machine springs were represented in a spring/dampener setup in the *z*-axis, along with virtual spring/dampeners along the *x*- and *y*-axes as seen in Figure 2.21(b). Nevertheless, the authors [22] validated their model through experimental measurements of the frequency and amplitude and showed favourable validation.

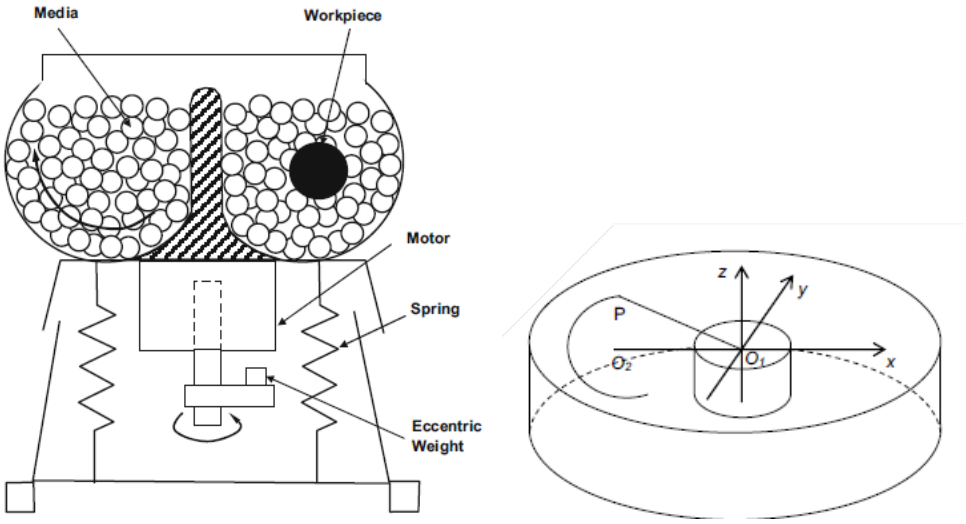

Figure 2.22 Schematic diagram of (left) dome vibrofinishing machine and its (right) XYZ-coordinate representation by Tian et al. [23]

Lastly, Tian et al. [23] utilised a similar flyweight setup to by Zhang et al. [22] machine, that it has no top eccentric weight at the dome as seen in Figure 2.22. A parametric representation in the *x-y-z* coordinates was produced as well as used to generate a kinematic model to establish a material removal model.

2.4 Summary of Literature Review

The literature review reveals that there is limited industrial practice and published research on the domeless process, indicating a relatively new and underexplored area. In order to address this gap, this thesis aims to conduct trials to assess whether the domeless process can meet the rigorous standards of the aerospace industry in terms of machine parameters, surface roughness, and material removal requirements. The investigation also seeks to explore the impact of factors such as orientation and component-to-machine size ratio on the domeless process, providing valuable insights into its capabilities and limitations.

Furthermore, as the domeless process involves significant changes in machine geometry compared to the conventional machines, which can affect the flow characteristics of the media, it is important to examine and understand the resulting changes in machine efficacy. To achieve this, a comparative study will be conducted

between the domeless process and conventional techniques such as dome and trough machines, utilising theoretical modelling approaches. By analysing and comparing the results, the research aims to enhance the fundamental understanding of the domeless process and its potential advantages and challenges. This summary of the literature review highlights the rationale and justification for undertaking the present study and contributes to the existing body of knowledge in the field of domeless processing.

Chapter 3 Validation of Domeless Vibrofinishing Process to Industrial Standards

This chapter presents a study on the domeless vibrofinishing process to validate its suitability for meeting aerospace industry requirements. The study includes a process KPV study to evaluate the effectiveness of the domeless vibrofinishing process on airfoils at different positions. Experimental trials were conducted on standard vibrofinishers, including dome and trough types, using similar settings, and a cost analysis was performed. The aim was to compare the performance of the domeless process with the standard types, providing valuable insights and validating its effectiveness for aerospace applications.

3.1 Methodology

The aim of the key process variable (KPV) study conducted on the domeless circular vibrofinisher was to investigate the impact of different positions within the vibrofinishing bowl on the surface roughness improvement and material removal of airfoils. Specifically, two KPVs were examined: the angular orientation of the airfoils relative to the media flow, and the radial position of the airfoils within two annular rings. These KPVs were chosen to address the unique characteristic of the domeless design, which enables more convenient processing of annular components. By studying these variables, the study sought to gain a deeper understanding of the domeless vibrofinishing process and validate its applicability in the aerospace industry. Table 3.1 explains the factors of the two KPVs, which comprised of five angular orientations, and two radial positions of the airfoil to be studied. An in-depth explanation on the methodology is explained in the following sections.

Table 3.1 Experimental factors of the KPVs to study

Angular orientation of airfoil (Facing the media flow) Refer to Figure 3.5 for more detail	**Convex 180°**	**Convex 45°**	**90°**	**Concave 45°**	**Concave 180°**
Component-to-Machine Ratio Refer to Figure 3.6 for more detail	***~0.4*** *(2 : 4.75)*		***~0.6*** *(3 : 4.75)*		

3.1.1 Experiment

The domeless vibrofinishing machine used was the ERBA EVP-250 CL, with a working bowl volume of 250 L and driving power of 3 kW. Figure 3.1 shows the schematic drawing and the actual domeless machine.

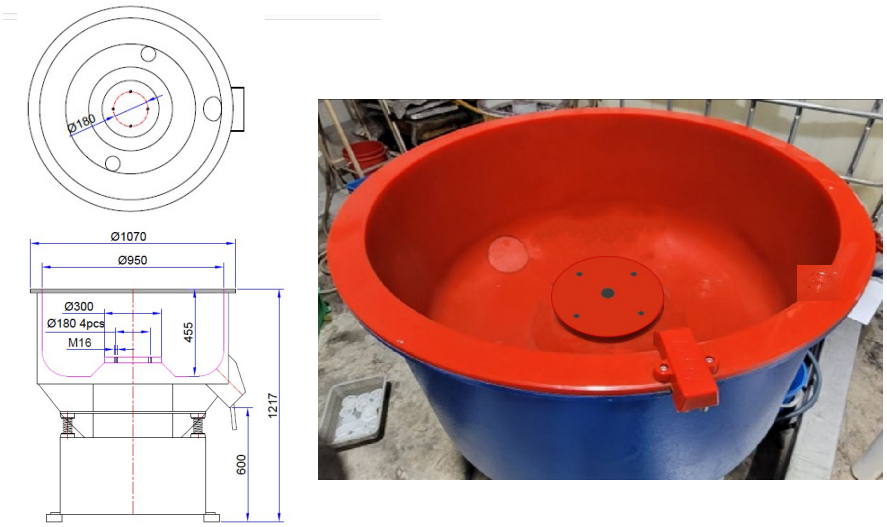

Figure 3.1 ERBA EVP-250 CL

As seen in Figure 3.2, the airfoil made of stainless steel 304 (SUS304), was designed with a concave and convex surface on each side, with a constant thickness of 12 mm, to have an easier measurement methodology.

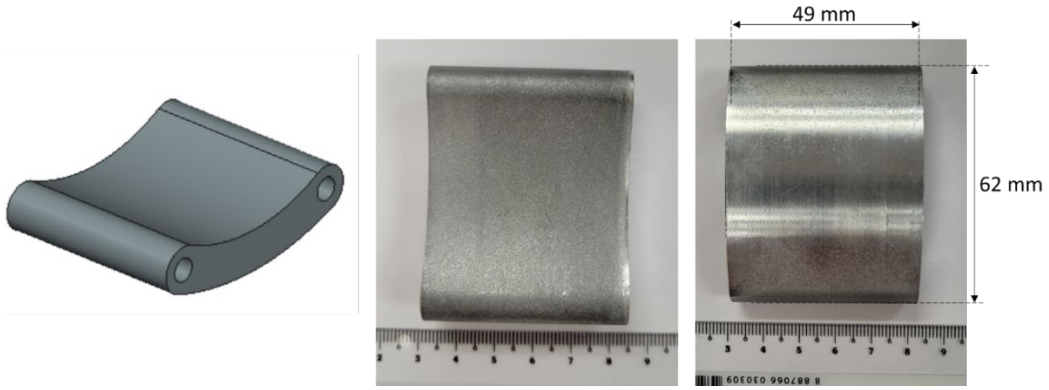

Figure 3.2 Isometric view and actual airfoil taken at each surface with dimension.

The airfoils were designed with two holes at the sides with the design intention to be encapsulated between two annular rings to simulate aerospace components such as a blisk. As seen in Figure 3.3, the assembly of the airfoil with the annular rings comprised of six airfoils (in green) attached between two annular rings – an inner (grey) and an outer (purple) ring. The annular rings had six flat surfaces. This allowed the sides of the airfoils to be flushed to the rings so that media does not interfere with the assembly during vibrofinishing.

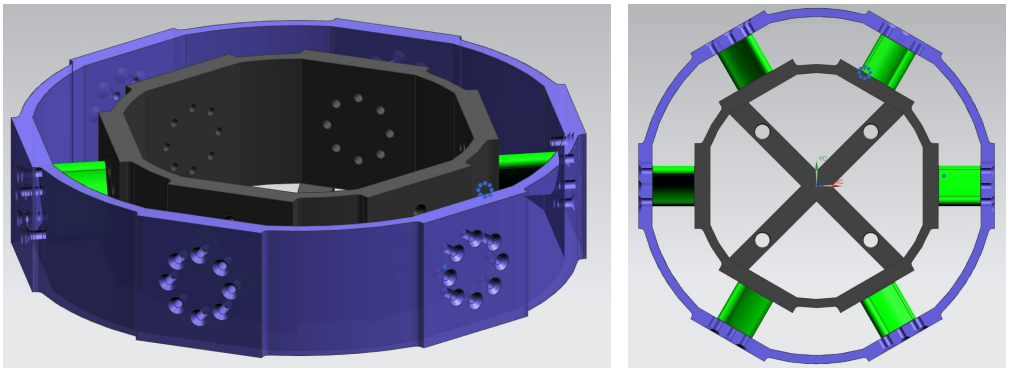

Figure 3.3 Annular Assembly of six airfoils encapsulated between two annular rings

Eight holes at 45° apart were fabricated on the flat surfaces of the annular rings. The holes were used in the assembly by first, fitting two M10 flat head screws through the outer annular ring, through the airfoil and lastly screwing onto the inner ring's threads. The screw length was thoughtfully selected to enable no protrusion during the vibrofinishing. This was to prevent damages to the screw which would cause difficulty during disassembly. Figure 3.4 shows the actual assembly.

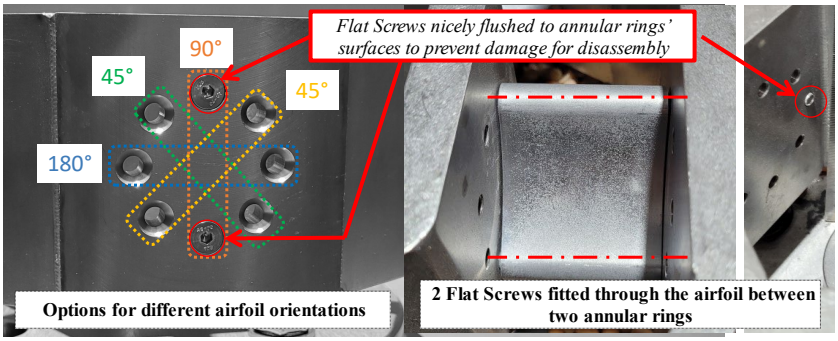

Figure 3.4 Actual assembly of airfoil between two annular rings using two M10 Flat head screws

Figure 3.5 shows these five orientations selected for the KPV study, with Figure 3.5 (a) illustrating the circular cross-section of the annular assembly together with the media flow direction onto the airfoil, and the top view of the actual setup in Figure 3.5 (b).

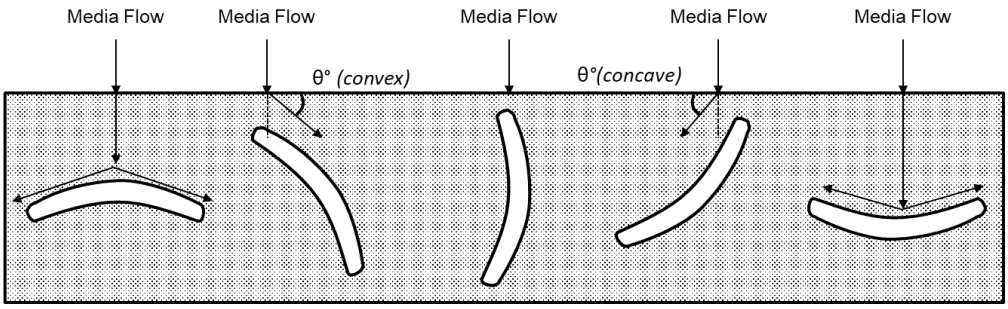

(a)

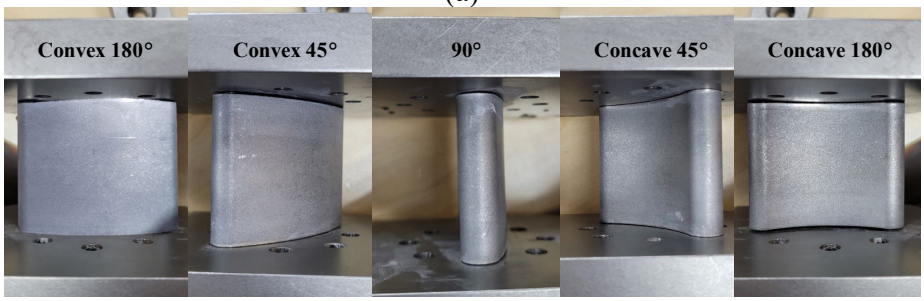

(b)

Figure 3.5 (a) Circular Cross-Section of assembly and (b) Top view of actual setup

To understand the effect of varying diameters between annular components to domeless bowls, a component-to-machine ratio was analysed at two radii of annular assembly. The radial positions of the airfoil were enabled by employing various assemblies of different sized annular rings. Specifically, the two radial positions of

300 mm and 200 mm utilised a 350 mm and 250 mm ring, and a 250 mm and 150 mm ring respectively. Figure 3.6 describes the two assemblies.

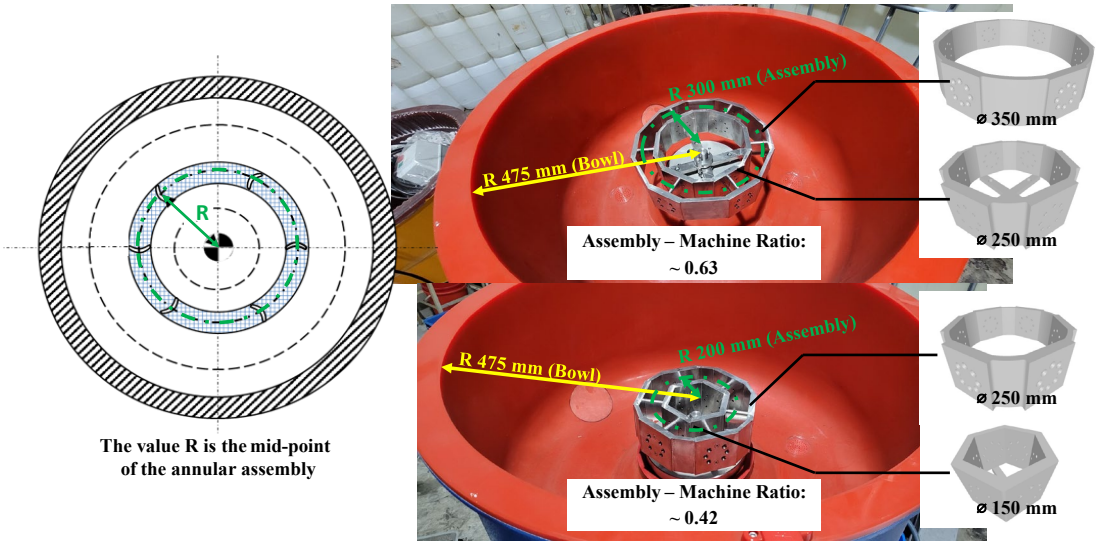

Figure 3.6 Two annular assemblies fixtured in domeless bowl

The annular assembly would be fixtured at the middle of the domeless machine by two fixture rings onto an adaptor plate that is welded onto the annular ring. Figure 3.7 shows a breakdown of the fixture setup.

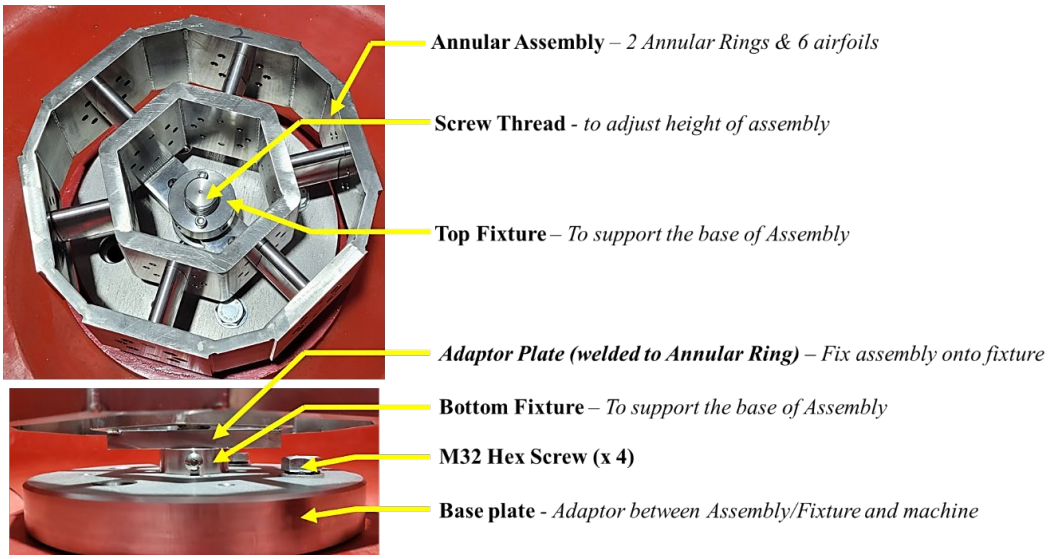

Figure 3.7 Fixture setup of the annular assembly onto the domeless bowl

To ensure the effectiveness of the KPV study, certain parameters, including media,

compound, and process time, were kept constant. Maintaining consistent media selection was particularly important for running the study successfully. This approach allowed for sufficient material removal and surface finishing, enabling a reliable analysis unaffected by airfoil fabrication effects such as machining marks as shown in Figure 3.8.

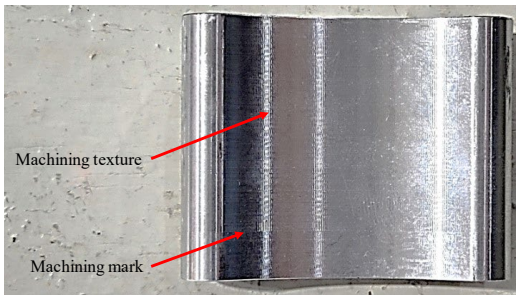

Figure 3.8 Machining mark left on the airfoil during fabrication (CNC milling)

A two-stage vibrofinishing process was employed for this purpose. In the first stage, an ellipse-shaped ceramic PB-grade media measuring 15 x 15 x 5 mm (depicted in Figure 3.9 (a)) was utilised. This media choice, with a 20% abrasive-to-base ratio, facilitated relatively high cutting rates, effectively removing machine marks from the airfoil's surface. In the industry, the removal of machine marks is coined as a ‘deburring’ process. However, for cogent reasoning, stage one will be termed as a surface ‘conditioning’ process instead. In stage two, a cone-shaped plastic XR-grade media measuring 10 x 10 mm (as seen in Figure 3.9b) was employed. This media had a lower cutting rate and aggressiveness, with a 15% abrasive-to-base ratio to generate a matte polishing effect, hence, to be termed as a surface ‘polishing’ process. With a 60 minutes processing time for each stage, there would be sufficient processing on the airfoils to get sufficient material removal and surface finishing to understand the relationship between the KPVs and the outputs concerning material removal and surface finishing. Table 3.2 summaries this two-stage process.

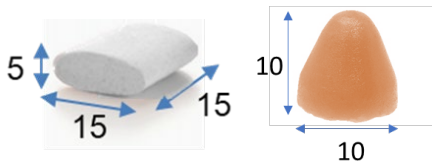

Figure 3.9 (a) Ceramic PB-grade ellipse media (20% abrasive content) (b) Polyester XR-grade cone media (15% abrasive content)

Table 3.2 Parameters kept constant for KPV study

Parameter	**Stage #1 Conditioning**	**Stage #2 Polishing**
Media	PB (15 x 15 x 5 mm)	XR-10 (10 x 10 mm)
Process Time	60 mins	60 mins

Additionally, to ensure the validity and relevance of the KPV study in the aerospace industry, it was crucial to adhere to established standard operating parameters. By incorporating these standard parameters, the scope of the study was effectively streamlined, allowing for a focused investigation of key variables and their impact on the vibratory finishing process. This approach not only ensures consistency and comparability with industry practices but also enhances the reliability and applicability of the study's findings. By following these established standards, the study can provide valuable insights and actionable recommendations that align with real-world operational requirements, making it a valuable resource for professionals and researchers in the aerospace field.

Media entry height: In order to ensure a consistent and controlled experimental environment, it is essential to maintain constant values for the flowability of media and sludge during the vibratory finishing process. The media entry height (labelled as H_{entry}) is the height between the media height and the entry point between the annular surface as depicted in Figure 3.10 (a). H_{entry} can be calculated by subtracting the H_{bowl} with the length between the bowl and media height as shown in Figure 3.10 (b).

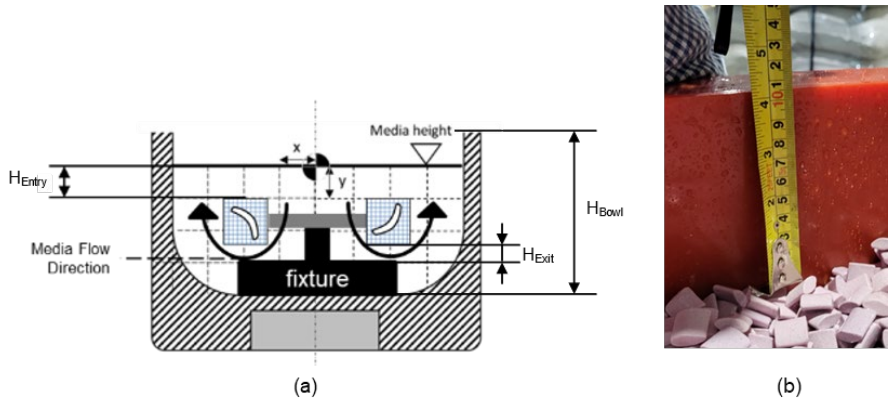

Figure 3.10 (a) Media Flow Height (H_{Entry}) is the depth between media height and the annular component surface and (b) Depth of bowl surface to media height

When the media enters between the annular rings, it establishes contact with the component surface, initiating the material removal and finishing actions through the transmission of energy from the machine vibration to the media and subsequently the component surface. Figure 3.11 illustrates this in various scenarios, with the selection of Figure 3.11 (c) fixed for the experiment.

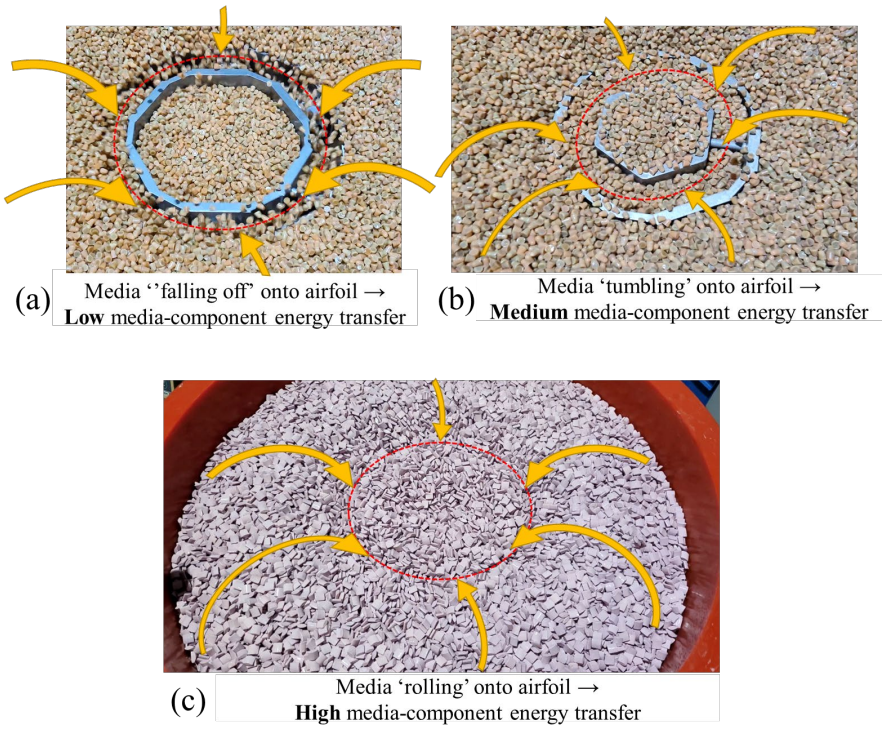

Figure 3.11 Inefficient media-component energy transfer for scenario (a) and (b) when there is insufficient media (or low H_{entry}) and scenario (c) when there is sufficient media

In order to ensure smooth flow of the media and the resulting sludge, which consists of media particles and debris from the components, it was necessary to verify the flowability of the system. To achieve this, the fixture was adjusted to create a 60 mm gap, as depicted in Figure 3.12. The determination of this value involved considering a safety ratio of 1:5. This ratio was obtained by multiplying the longest length of a media, in this case, the 15 mm length of a PB media, by five. The chosen ratio was based on the consideration that it is highly unlikely for five PB media to stack lengthwise and cause media clogging.

Figure 3.12 (a) Media Entry Height (labelled as H_{Entry}) can be measured by subtracting (b) measured from component top surface to media surface on pre-process

Nevertheless, prior to the actual study, a visual inspection was conducted, allowing for the observation of the flow pattern, and ensuring that there were no obstructions or bottlenecks when media enters between the annular assembly. By carefully monitoring and maintaining the flowability of media and sludge, the experiment can be conducted under consistent conditions, enabling accurate data collection and reliable analysis of the vibratory finishing process.

Dosage of compound and water: The dosage of compound and water is a critical parameter that must be carefully controlled in the mass finishing process. It is imperative to maintain a consistent and optimal dosage throughout the experiment. The continuous, open-loop process of compound and water ensures the constant removal of sludge, which is vital for achieving reliable and efficient results. By

establishing the appropriate dosage, the overall processing efficiency can be maximised. Too much compound and insufficient water will lead to excessive soap-like bubbles, hampering the effectiveness of the process. On the other hand, too little compound and excessive water will result in an inadequate "soaping" effect, diminishing the compound's ability to perform its intended tasks and potentially causing damage to the components and machine lining. Through a method of trial and error, the optimal dosage ratio is determined and then maintained consistently throughout the entire process. For example, an industrial practice often involves a ratio of 1:5, meaning 1 litre of compound is used for every 5 litres of water in a 100-litre volume. Additionally, adhering to standard practice, an open system approach is employed, where compound and water are continuously added while simultaneously discharging sludge. This ensures a constant flow of compound and water, facilitating effective material removal and maintaining the desired processing conditions. By emphasising the importance of maintaining a constant and appropriate dosage of compound and water, the mass finishing process can achieve consistent and high-quality results. For this experiment, the compound solution used was SC-588, which was a Spire in-house formulated compound specifically designed for non-ferrous metals to provide soaping effects for process uniformity and anti-rust properties.

Motor RPM and Frequency: In the aerospace industry, maintaining consistent and standardised operational parameters is crucial to ensure optimal results in mass finishing processes. A key aspect of this is establishing constant values for frequency and the motor RPM (Revolutions Per Minute) used to rotate the two eccentric weights. These values play a significant role in achieving the desired finishing outcomes, particularly in terms of a full roll and a good feed speed. By adhering to the industry's recommended practices, it is recommended to set the operational frequency at 50 Hz and the motor RPM of the domeless machine motor at 1400 RPM. This standardisation allows for reliable and predictable results, ensuring that the workpieces undergo a complete roll motion with an appropriate feed speed. Consistency in these operational parameters guarantees that the finishing process is

efficient, effective, and capable of meeting the stringent quality requirements of the aerospace industry.

After the completion of the KPV study, a comparison study was undertaken to investigate and compare the performance of the domeless, dome and trough types. The objective was to determine which machine type is more effective in achieving the desired results. The machine parameters were kept constant, such as frequency at 50 Hz, motor RPM as 1400 RPM, amplitude at 4.5 mm, lead angle at 60° for domeless and dome (Trough at 90° as per industrial requirement). Experimental parameters such as maintaining the same media, compound, process time, and the same two-stage approach were employed. The varying parameters between the machine types were the employment of different fixture method. This is shown in Figure 3.13.

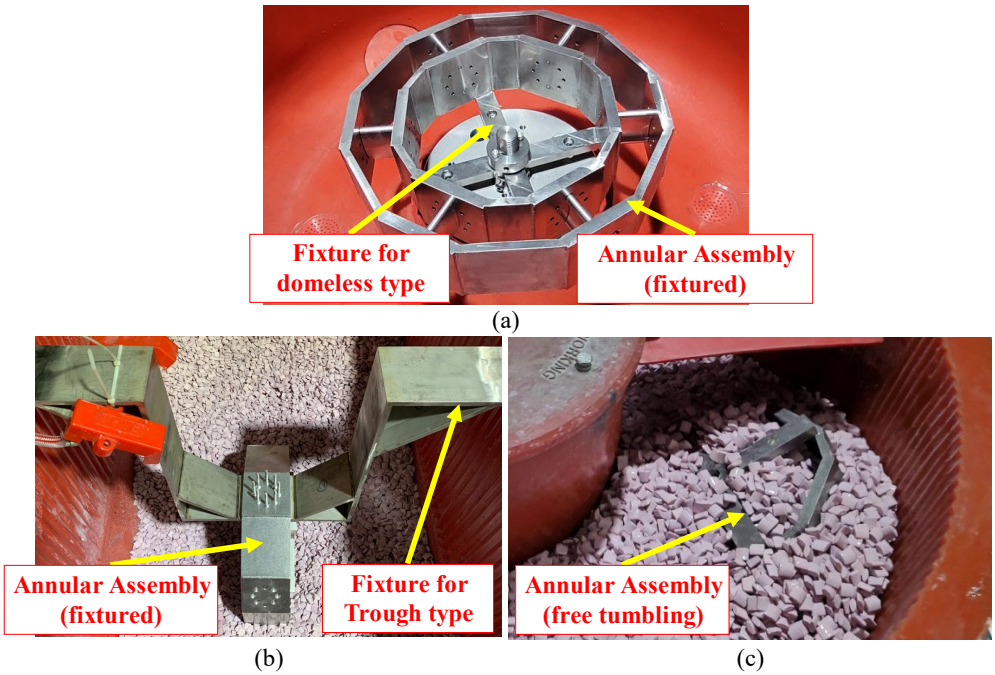

Figure 3.13 Fixturing methods for three vibrofinishing techniques

Resource limitations necessitated the use of a 350 L free tumbling dome round vibrofinishing machine, and an 800 L fixtured domeless round vibrofinishing machine as shown in Figure 3.14.

Figure 3.14 (left) Dome, Circular model EVP-RA 350 (right) Trough model EVT-800

Finally, as seen in Figure 3.15, the setup of the airfoils along various heights along the trough will likely affect the required results due to the varying processing power of the trough-type that increases the deeper the component is located. Hence, two trials were conducted with each of the setup can be found in Table B.0.2 Airfoil positioning for trials on trough machine under the full experimental detail in

Appendix A: Design of Experiment.

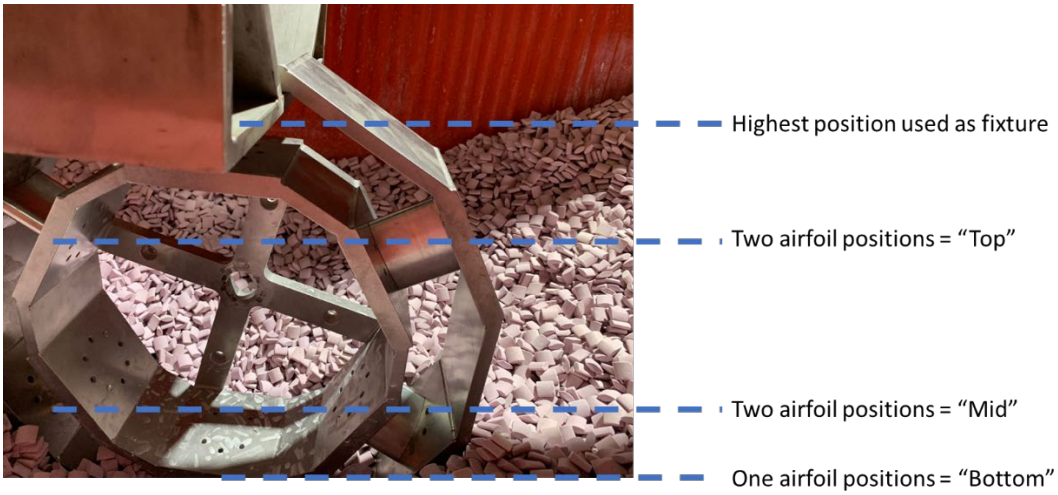

Figure 3.15 Classification of airfoil positions at a trough machine

3.1.2 Validation

To validate the domeless vibrofinishing if viable for the aerospace industry, the surface roughness and material removal after vibrofinishing had to be measured.

Quantifiably, the general surface roughness requirement of an airfoil was that both the concave and convex surfaces of the airfoil had to be below 0.625 µm R_a, with the material removal through the measurement of the airfoil thickness reduction to be below 12.7 µm. The requirements provided were given by Spire Pte Ltd based on their aerospace customers such as Rolls-Royce, GE Aviation e.g.

The surface roughness measurements utilised a Taylor Hobson PGI 2D profilometer at the four profiles as indicated in Figure 3.16 and are categorised as A, B, C and D respectively. The four profiles were selected to study the surface finishing variance along A, B and C. Additionally, profile D signifies the profile of the airflow during operations. Three measurements were taken for all four profiles on both sides of the airfoil, at three intervals - Before vibrofinishing, after surface conditioning, and after surface polishing, a total of 72 measurements for each orientation.

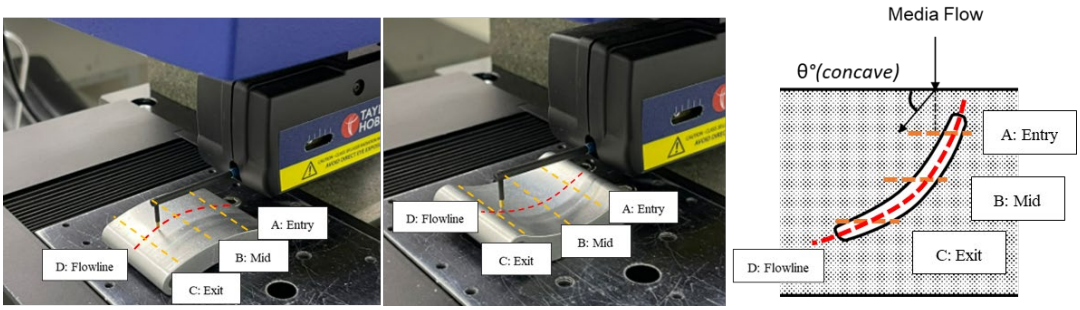

(a) (b)

Figure 3.16 (a) Four profiles per side to be taken on profilometer and (b) Illustration of profiles during processing

The measurement parameters used followed the ISO4288 standard. The data length for all four profiles at 40 mm, which is sufficient as an evaluation length a maximum cutoff length of 8 mm. Figure 3.17 shows a screenshot of the input parameters.

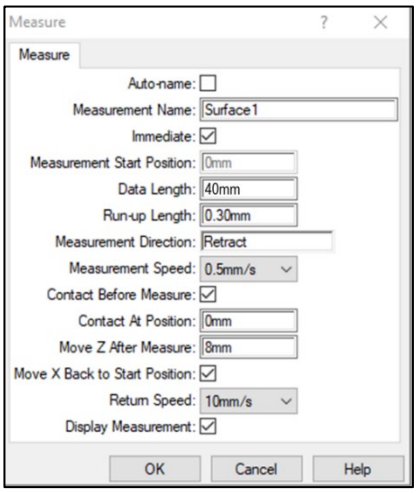

Figure 3.17 Surface roughness measurement parameters from PGI Talysurf software

For the airfoil thickness measurement, a Mitutoyo digital micrometre (Absolute Digimatic 2) was used, as shown in Figure 3.18.

Figure 3.18 Mitutoyo Digital Ball Micrometre to measure thickness of airfoil

An additional measurement on the overall material removal in grams was measured using a Satorius Cubis digital analytical balance of readability of 0.1 mg as seen in Figure 3.19.

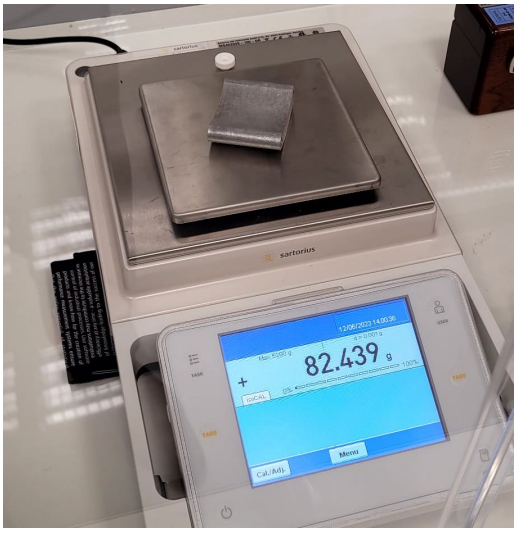

Figure 3.19 Satorius Cubis Digital analytical balance with draft shield

Finally, Figure 3.20 shows the sequence between the experimental trials and the measurements.

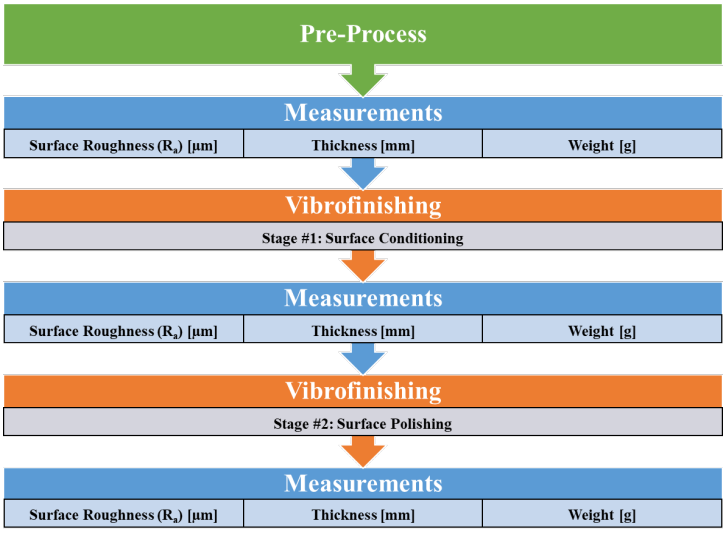

Figure 3.20 Sequence of runs

3.2 Results & Discussion

This chapter presents the findings of the KPV study (Section 3.2.1) and the comparative analysis between the domeless vibrofinishing process and other conventional vibrofinishing techniques (Section 3.2.2). These sections provide valuable insights into the effectiveness of the domeless vibrofinishing process for the aerospace industry and its potential advantages over conventional methods. In Section 3.2.1, the KPV study explores the impact of various parameters on the surface finishing and material removal of the airfoil, with key findings such as the effects of orientation to surface finishing and material removal in a domeless machine, the influence of airfoil orientation to the surface finishing of the airfoil, a study on the indirect media-component interaction from airfoil surfaces not facing the media flow, and the component-to-machine ratio. Furthermore, Section 3.2.2 offers a comprehensive comparison between the domeless vibrofinishing process and established conventional techniques, providing a deeper understanding of its potential benefits and limitations. Together, these findings contribute to the evaluation and validation of the domeless vibrofinishing process for meeting the rigorous requirements of the aerospace industry. The full measurement results can be found in Appendix B: Measurement Results.

3.2.1 KPV Study of Domeless Vibrofinishing Process

The result from the study presents the key findings, namely the effect of airfoil orientation to surface finishing and material removal, the surface finishing gradient along the profile of the airfoil due to orientation, a study of the indirect media-component interaction based on the surface finishing results, and lastly the relation of component-to-machine ratio to the surface finishing results. These findings serve to validate the domeless vibrofinishing process's ability to meet the requirements of the aerospace industry. The following sections will explore each of these key findings in detail, highlighting on their implications on the vibrofinishing process to achieve the desired results.

3.2.1.1 Effect of orientation to surface finishing and material removal

The results demonstrated that the airfoil orientation of 45° provided the highest material removal and surface finishing as compared to the other orientations, with the lowest by the concave surface at 90° orientation. Figure 3.21 shows the average surface roughness improvement from surface conditioning (stage 1) to polishing (stage 2), with measurements taken three times for each stage at each orientation, with a marginal error between each measurement of less than 0.001μm with a standard deviation of below 0.00003. Similarly, Figure 3.22 shows the material removal by measuring both the thickness change and weight loss from pre-process to polishing (stage 2), which also has very low margin of error between each measurement by ± 0.2 μm and ± 0.0001 g respectively and standard deviation of less than 0.00003. Figure 3.23 shows the effect of tool mark removal as part of surface conditioning (stage 1) and after polishing (stage 2).

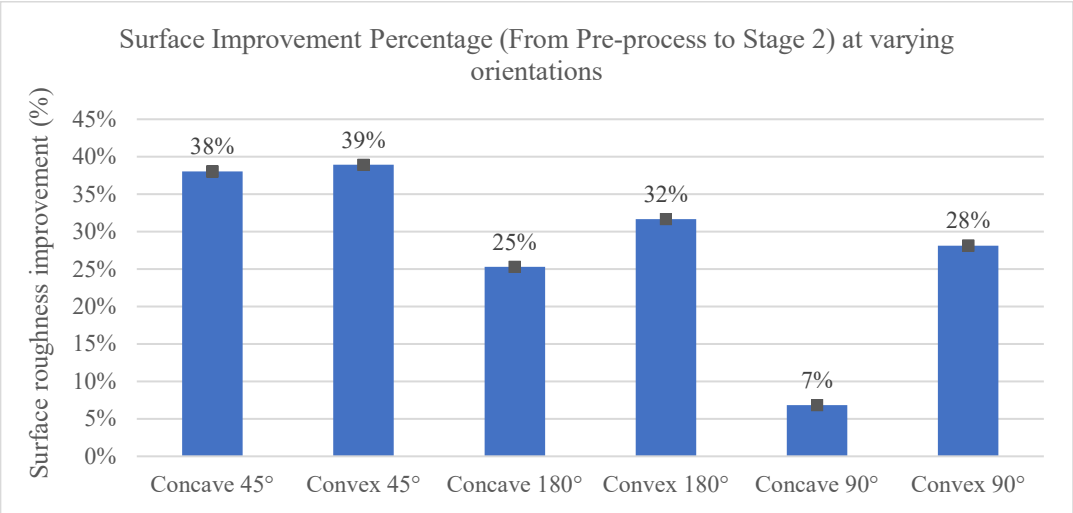

Figure 3.21 Surface Roughness improvement in percentage of varying orientation by domeless vibrofinishing

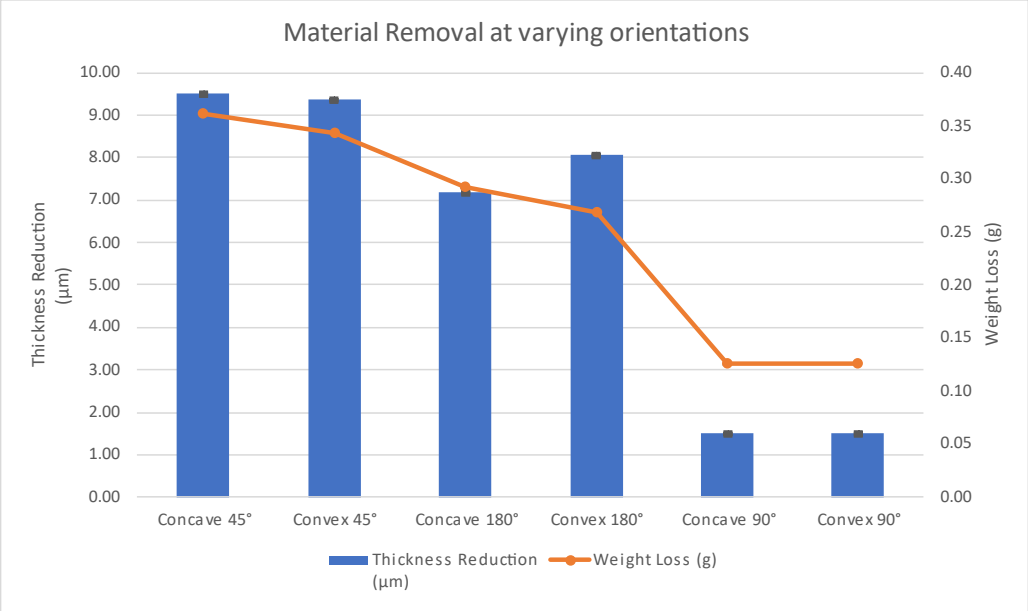

Figure 3.22 Material Removal at varying orientations by domeless vibrofinishing

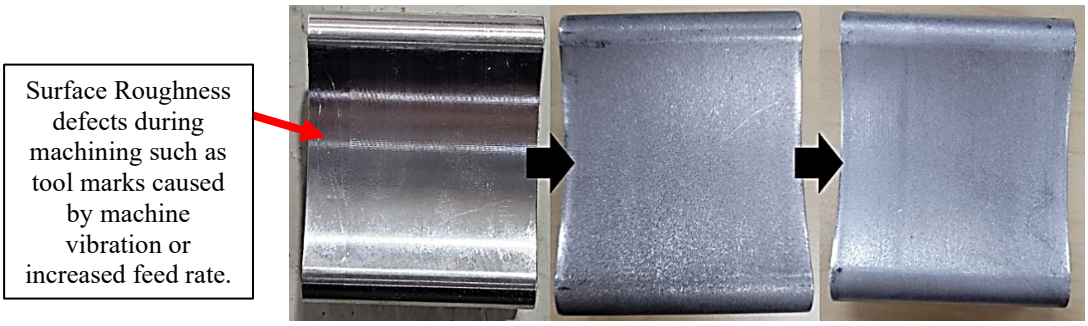

Figure 3.23 Airfoil orientated at 45° from (left to right) pre-process, surface conditioning (stage 1) and polishing (stage 2)

An explanation for the result was likely due to the favourable flowability of the media onto the curved surface of the airfoil to have continuous abrasive motion, in turn allow greater media contact exposure onto the airfoil surface. Many literatures support the statement on how media flowability would provide better surface finishing. For example, in a stream finishing process, Itoh et. al. [24] used a video recording during the process to show that a flat surface increased in media velocity against its surface, with the lowest at 0°, or perpendicular to media flow, and highest at 90° angle to the media flow, which is a parallel flow of the media. This was compared with additional results between 30° and 60°. Similarly, Srivastava, S. et. al. [25] showed that between a parallel (90°), perpendicular (0°) and diagonal (45°) result showed the highest surface finishing at the 90° position, followed by the 45° position. It is noted that these studies, the component surfaces were flat as compared to the curvatures of the airfoil in this study. This shows that media flowability is highly dependent on the exposure of the surface adjacent to the media flow. This was apparent for the results at 90° orientation. Figure 3.24 shows the varying surface finishing improvement in percentage along the concave and convex surfaces at 90° orientation to media flow. The results showed that there is a varying difference between the surfaces exposed to the media flow as compared to the surfaces not exposed, indicated by the red zones. Concave surface had little to no exposure to the media flow hence had the lowest surface finishing, while convex surface had a varying surface finishing result, with profile A and B having a higher exposure than profile C.

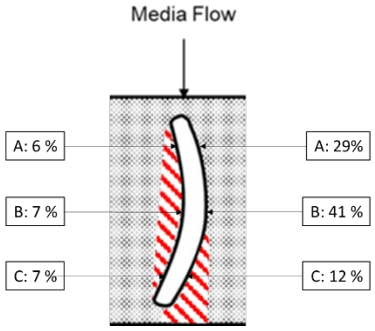

Figure 3.24 Varying surface finishing improvement at 90° orientation to media flow, with red zones indicating no direct exposure to media flow

3.2.1.2 Effect of orientation to surface finishing profile

This section focuses on the relationship between how the media flow interacts along the surface of the airfoil along varying profiles. The results will be shown as a surface roughness improvement in percentage by taking an average of three R_a measurements for each stage, and subtracting the R_a value after surface conditioning (stage 1) to the R_a value of polishing and dividing by the R_a value of surface conditioning (stage 1), bringing to a total of nine measurement per surface profiles A, B, C and D as seen in Figure 3.25.

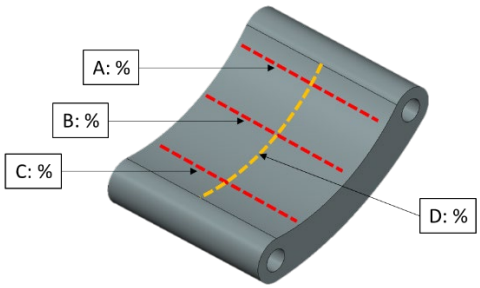

Figure 3.25 Isometric drawing of the airfoil with four measurement profiles

As discussed in the earlier section, media flowability was a critical factor in the surface finishing. The results between surface profiles along the airfoil at each orientation further illustrates this criticality. First, for the orientation of 45°, Figure 3.26 shows that there is a surface finishing gradient profile, with the highest improvement at the initial media-component surface contact at profile A, with

gradually lesser surface finishing along profile B and C. In the context of meeting the requirements, all surface finishing profiles met the requirements of below R_a 0.625 µm.

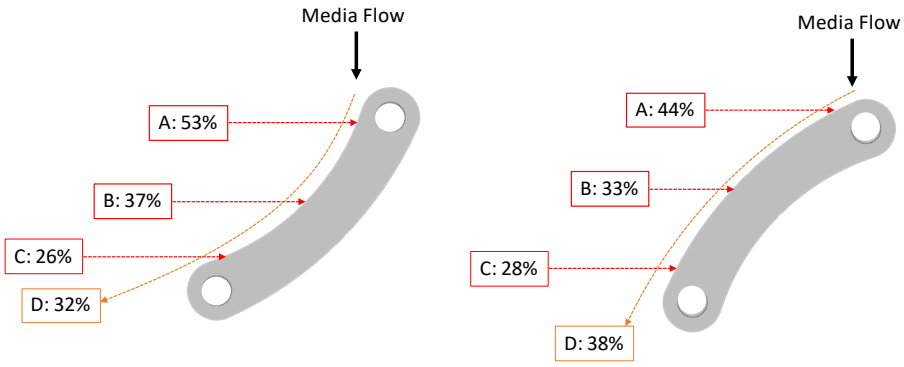

Figure 3.26 Surface finishing improvement profile gradient at 45° orientation

Figure 3.27 shows the surface finishing profile at 180° orientation. As compared to the 45° orientation, there is a relatively even polishing along the profiles for the convex surface, likely due to the accessibility of the media to flow outwards upon media-component contact.

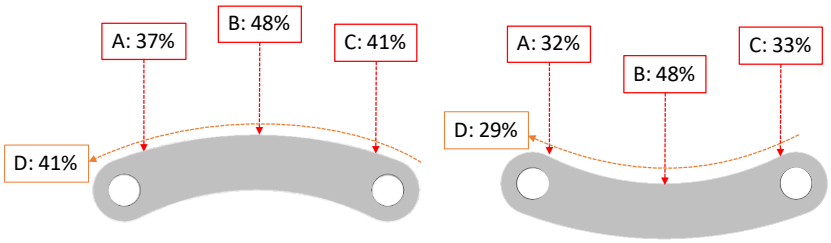

Figure 3.27 Surface finishing improvement profile gradient at 180° orientation

For the concave surface, one key observation was that at surface profile B, there was a significant increase in surface conditioning at stage 1, which led to a high final surface finishing of R_a 0.606 µm. As seen in Figure 3.28, the surface conditioning of the 180° orientation created a higher surface roughness of almost two times than the 45° orientation.

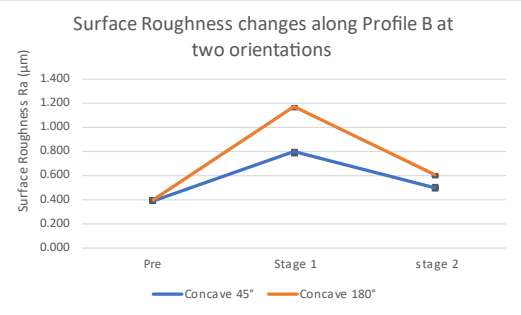

Figure 3.28 Surface finishing along Profile B concave surface at 45° and 180° orientation

The hypothesis for this would be a stagnation of the media flow at the mid-point of the concave surface of the airfoil, specifically at surface profile B as explained in Figure 3.29.

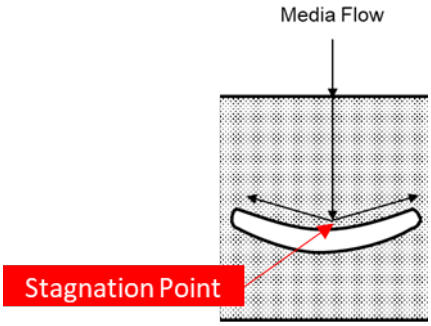

Figure 3.29 Stagnation point due to sudden deceleration by media

A causality of stagnation would be a sudden deceleration of the media upon contact to the component surface. The experimental observation of media surrounding the component surface were generally smaller than the original size and had some broken-up media that coagulated onto the surface together with slurry made up of compound, water, and metallic waste. This seemed to suggest that the coagulation caused undesirable surface finishing.

As seen in Figure 3.30, the overall surface was not completely processed. There were two visible surface types – the base surface which was the original machined surface and pitted-looking points that were the processed surface area generated by the media-component surface interactions. To substantiate the hypothesis, an observation of the image showed that across the profiles of A, B and C, the profile B visibly had

lesser media-component surface interactions inferred from the lesser pitted-looking, matte points as compared to the adjacent profiles of A and C. A lack of processing supports the hypothesis of the stagnation point at the middle of the concave profile.

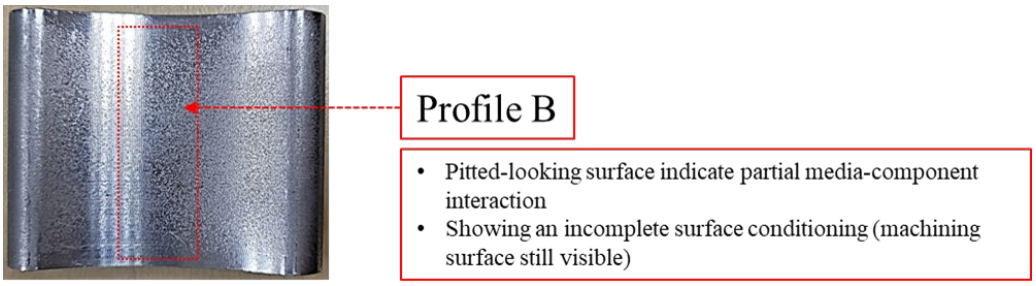

Figure 3.30 An incomplete Surface Condition at 180° Orientation

3.2.1.3 Indirect Media Interaction

Vibrofinishing process works on the principle of abrasive media-component interaction through vibration. As the nature of the vibration causes media to flow based on the direction of roll and feed, a hypothesis would be that surfaces of components not facing the direction of the media flow would not have surface finishing. Figure 3.31 indicates the surfaces at varying orientations that do not have direct contact to the media flow.

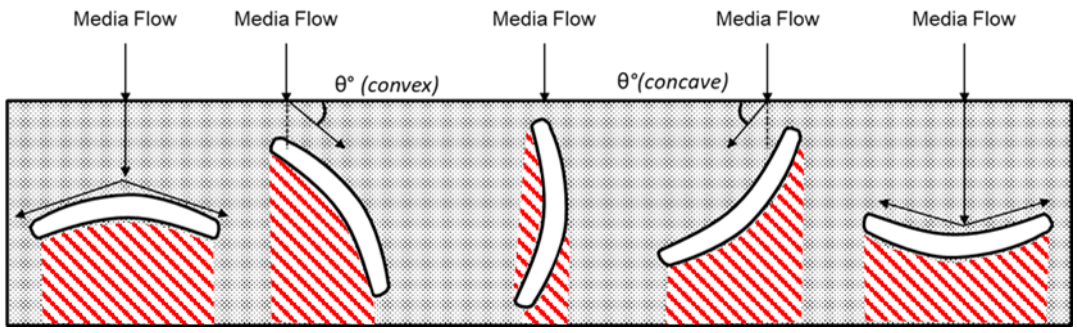

Figure 3.31 Red zones indicate no media flow contact

The alternate hypothesis would be that there would be some surface finishing effects due to localised media-component interaction caused by the vibration. The experimental observation was that the airfoil surfaces supported the alternate

hypothesis as surfaces not in direct contact to the media flow had a significant surface finishing improvement, with the results shown in Figure 3.32. This strongly suggests of the alternate hypothesis to be true.

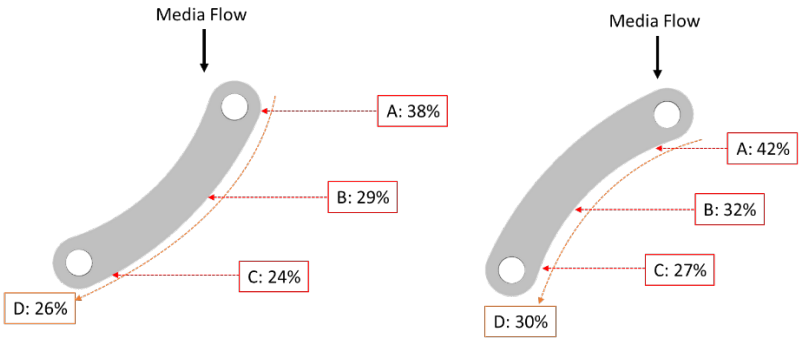

Figure 3.32 Surface finishing improvement profile gradient at 45° orientation underside

In a qualitative example, at the 180° orientation, while the convex surface did not face directly to the media flow as it was obstructed by the opposite concave surface at, the media could be observed to be vibrating downwards and some media flowing inwards to the edges of the convex surface as pointed out in Figure 3.33.

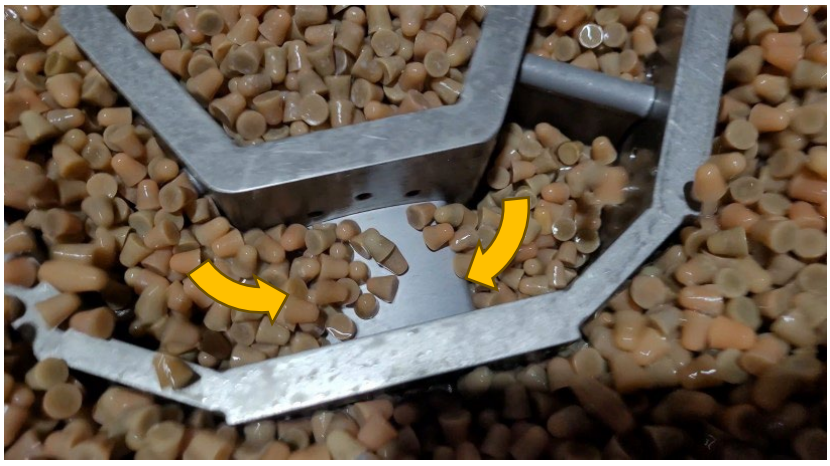

Figure 3.33 Observed media flow direction at 180° orientation

While the experimental results supported the alternate hypothesis, a micro, media-to-media level analysis was further explored to further substantiate the hypothesis. First, the phenomenon is likely due to the indirect or secondary media interactions. When the media is flowing through the vibrofinishing bowl, it undergoes complex motion

patterns, including bouncing, sliding, and cascading. As the media interacts with the workpieces and the walls of the bowl, it generates a dynamic environment within the bowl. This dynamic environment creates a mix of forces and interactions that can indirectly affect surfaces that are not directly exposed to the media flow.

Some mechanisms through which indirect media interactions can occur include:

1. Media Cascade: As the media flows over and around the workpieces, it cascades and creates a turbulent media bed within the bowl. This cascading action causes the media to collide with each other and with the workpieces. These collisions can transfer energy and force to adjacent surfaces, even those not directly exposed to the primary media flow.
2. Media Rebound: When the media impacts the surfaces of the workpieces or the walls of the bowl, it can rebound or bounce off those surfaces. This rebounding action propels the media particles into the surrounding space, allowing them to interact with surfaces in different orientations, including those opposite to the primary media flow.
3. Media Flow Redistribution: The media flow within the bowl is not limited to a single, uniform direction. The movement and interaction of the media particles can cause them to redistribute and reorient within the bowl. This redistribution can bring media particles into contact with surfaces that are not directly exposed to the primary media flow.

These indirect media interactions enable material removal and surface finishing on surfaces that are not in direct contact with the primary media flow. While the intensity of these interactions may be lower compared to surfaces in direct contact with the media flow, they can still contribute to the overall finishing process. The cumulative effects of indirect media interactions, along with other factors such as bowl geometry, media properties, and process parameters, collectively influence the final surface finish on all surfaces within the vibrofinishing bowl.

3.2.1.4 Component-to-Machine ratio

For operators to understand the domeless bowl selection criteria based on component sizing, a study on the component-to-machine ratio was conducted. Two sizes were studied, ratios of 0.4 and 0.6 each. The key observations from this KPV study, shown in Figure 3.34, demonstrated that a smaller component-to-machine ratio resulted in more surface roughness reduction at 45° orientation, but less surface roughness reduction at 180° orientation. This could be attributed to the media rolling mechanisms.

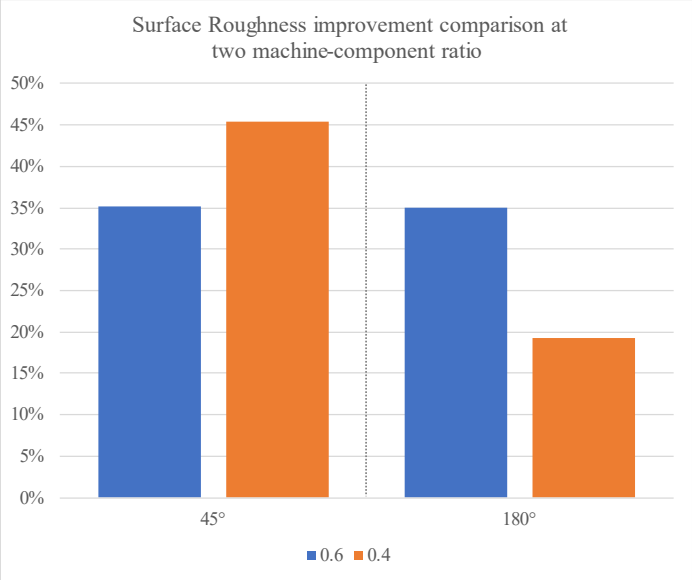

Figure 3.34 Surface Roughness improvement comparison in percentage for two machine-component ratio

The overall rolling motion can be accounted by two sub-mechanisms. The first mechanism is the media roll attributed to the centripetal acceleration of the vibrating, defined as:

$$a_c = \frac{v^2}{r} \tag{3.1}$$

Where a_c is centripetal acceleration or the roll in the *x*-*y* plane, v is velocity of media and r is the radius of the airfoil within bowl. As the radial distance decreases, the centripetal acceleration increases. Hence, a smaller component-to-machine would

give rise to a higher acceleration resulting in a higher aggressive vibrofinishing process.

The second mechanism requires further deconstruction of the media motion in the domeless vibrofinishing. As reviewed in Chapter 2 from the observations by Hashimoto and Johnson [20] [20], when the roll and feed motions were observed in totality as a helical motion while observed in the *x*-*y* plane and *x*-*z* (or *y*-*z*) plane respectively, there were two layer of motions each depending on the depth of the media flow. In the *x*-*z* (or *y*-*z*) plane, the first motion, or for cogency, to be labelled as 'outer roll', was the macro movement of the media flowing from the walls to the centre of the bowl, to which in this experiment, the media falls in between the annular rings onto the airfoils as observed in Figure 3.35, with the green arrow illustrating the inward roll to the middle of the bowl into the component, and the red arrow illustrating the outward roll under the medium.

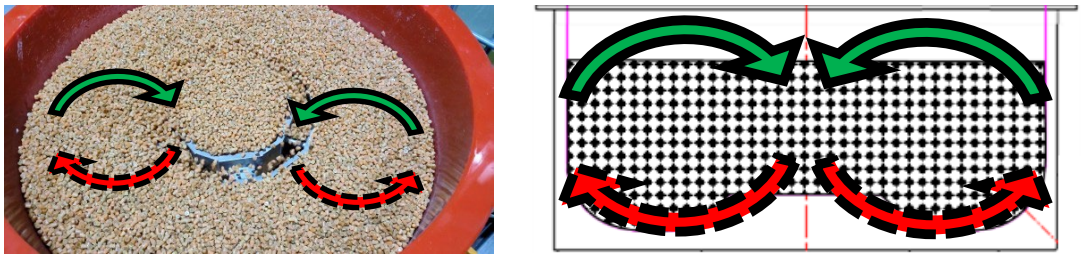

(a) (b)

Figure 3.35 (a) Media flow Macro motion of media in the *x*-*z* plane

The second motion was a multitude of micro circular trajectories under the macro flow, in a counterclockwise rotation downwards and outward towards the walls of the domeless bowl, to be labelled as 'inner roll'. A noteworthy observation by Hashimoto and Johnson [20] [20] was that the amplitude in vertical direction (*z*-axis) increases with increased distance from the centre of the bowl, the amplitude is a constant in the *x* direction. This was due to the nature of the helical flow as well as the curved shaped of the base of the bowl. Similarly, an illustration of these two motions in the domeless bowl was illustrated in Figure 3.36, with the outer roll in green to show the flow into the middle of the bowl, and the red portion of the arrows indicate outward flow, and

the inner rolls with decreasing radii (amplitude) nearing to the centre as shown in orange.

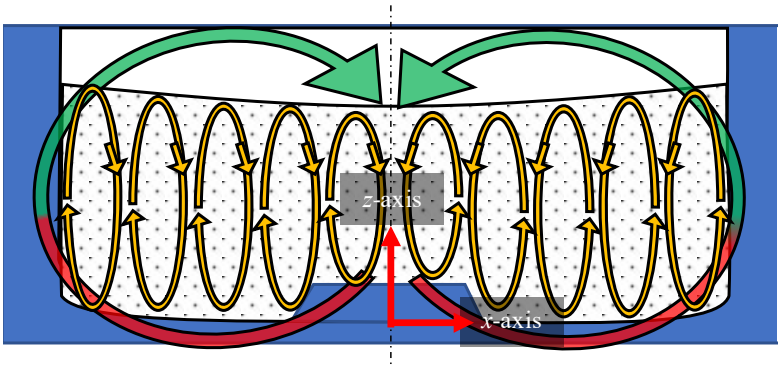

Figure 3.36 Two types of motion in *x-z* plane of a domeless vibrofinisher

With the breakdown and explanations of these two rolling actions, it describes that when the component is placed at certain radial position at the bowl, one form of roll will supersede another, thereby affecting the significant of the orientation of the airfoil to the surface finishing results. An illustration of this analysis can be described in Figure 3.37 at the two component-to-machine ratios.

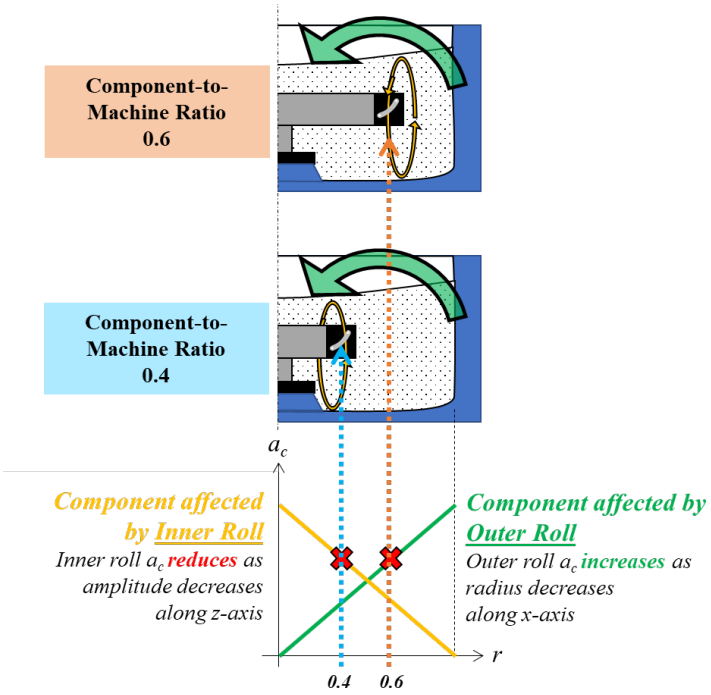

Figure 3.37 Plotted a_c to *r* graph to identify component-to-machine ratio threshold to determine if the airfoil orientation would be significant to the surface finishing result

At the component-to-machine ratio of 0.4, as the airfoil was more affected by the inner roll than the outer roll, there would be a higher influence on the orientation to the surface finishing results. This explains that at orientation of 45°, the surface finishing improvement was much higher. For the case of the surface finishing at 180° orientation at 0.4 ratio, the hypothesis was due to the stagnation as described in the section earlier. At the component-to-machine ratio of 0.6, the orientation was not as significant, therefore the surface finishing was quite even, at around 35% improvement each.

It is noteworthy that specific characteristics of the vibrofinishing setup and the workpiece geometry can influence the extent and effectiveness of indirect media interactions. In this context, the geometry of the annular configuration showed that the roughness as improvements varies based on the airfoil orientations, with surfaces subjected to direct media flow generally tend to have higher surface roughness improvements than surfaces subjected to indirect media interaction. Figure 3.38 illustrates the overall results of the 45° orientation at both surfaces, with variation of within a 10% difference, but still within acceptable values as results met the requirements.

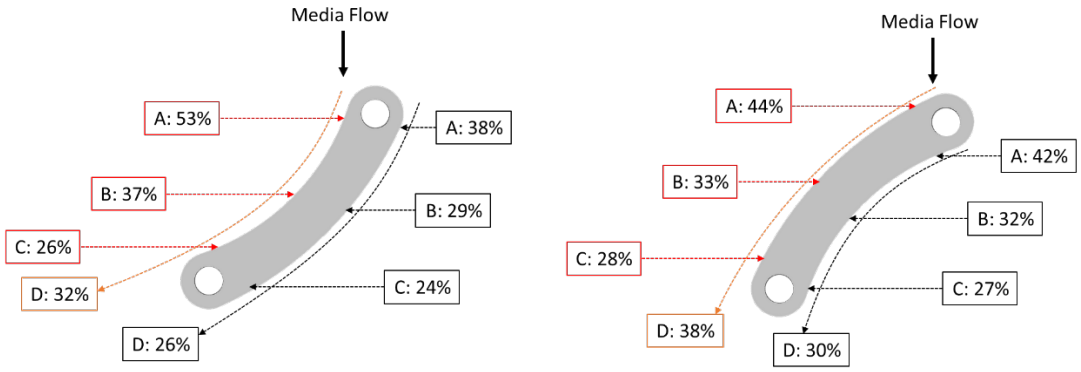

Figure 3.38 Surface finishing improvement results in percentage along both surfaces of the airfoil at 45° orientation

3.2.2 Comparative Analysis and Observations on Differing

Vibrofinishing Processes

Section 3.2.2 delved into a comparative observations and analysis on different types of vibrofinishing techniques. Building upon the KPV study of a domeless vibrofinishing conducted earlier, this chapter extended the investigation to include dome, and trough types to compare their results, with the aim to verify if domeless was able to perform equally or better to conventional techniques. This would validate domeless vibrofinishing to industrial standards.

Furthermore, this section focused beyond the technical aspects and conducted a cost analysis of the three vibrofinishing types. Evaluating the cost-effectiveness and efficiency of each technique adds a practical dimension to the comparison, enabling informed decision-making for surface finishing applications to the aerospace industry.

3.2.2.1 Dome vs Domeless

A comparison was done between the R 200 mm annular setup on the dome and domeless by analysing the data obtained on surface finish and material removal.

As shown in Figure 3.39, the domeless showed a higher surface finishing improvement at the 45° orientation as compared to the dome. The 180° orientation had marginal differences. Finally, at 90° orientation, the convex surface had a much better surface finishing for the domeless, while the concave surface had marginal differences.

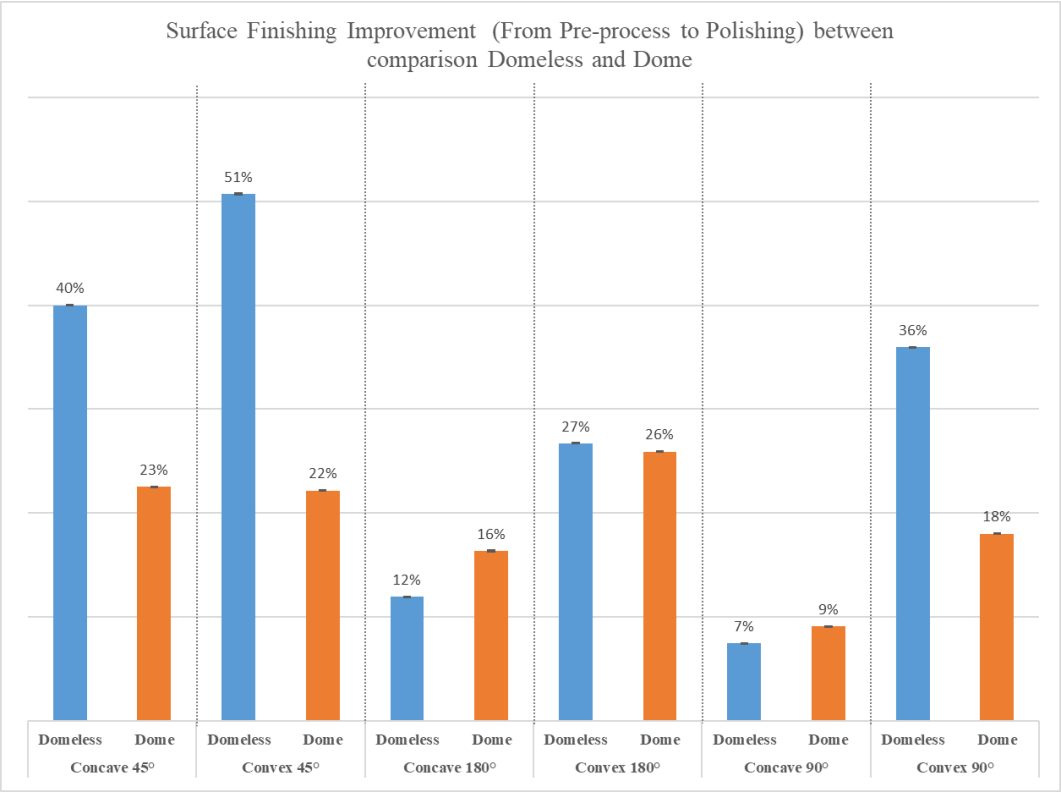

Figure 3.39 Surface Finishing Improvement comparison between Domeless and Dome process at various orientations

For the material removal comparison as shown in Figure 3.40, the domeless process resulted in a higher material removal in terms of the change of thickness at all orientations as compared to the dome process. The weight loss, however, was higher for the dome process at 45° orientation of around ± 0.1 g. The other orientations were marginally different. Notably, the results met the surface finishing requirements of less than 0.625 µm R_a while maintaining the thickness requirement of below 12.7 µm.

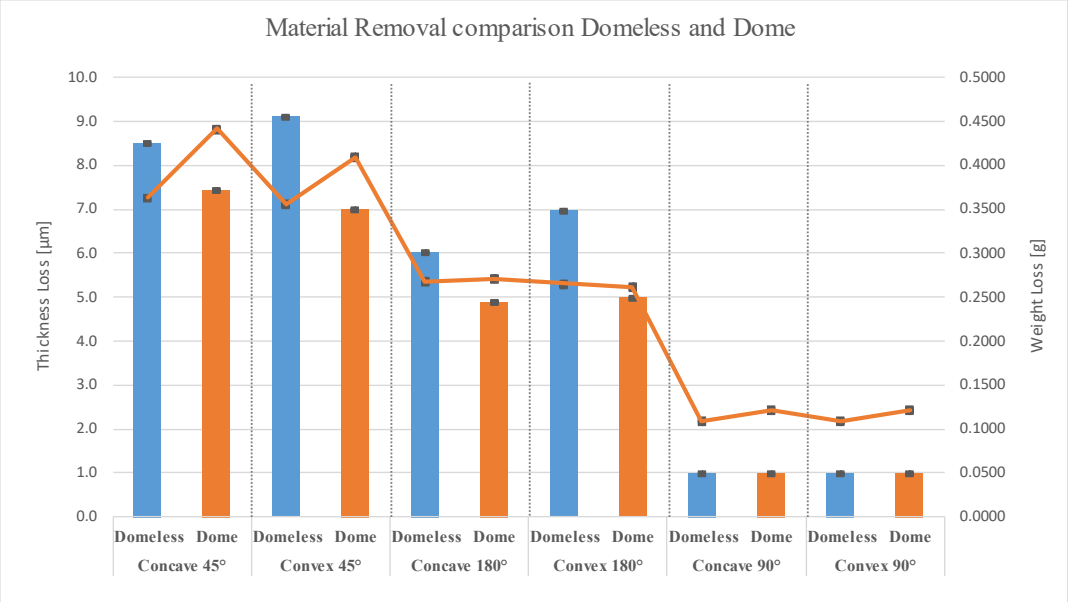

Figure 3.40 Material Removal comparison between Domeless and Dome process

A key reasoning for the results was due to the method of fixture between dome and domeless. The experimental image is shown in Figure 3.41.

Figure 3.41 Free vs fixed fixturing between dome and domeless vibrofinishing process

Fixtured components in a vibrofinishing process generally achieve better surface finishing and material removal compared to free tumbling components due to several factors:

1. Stability and Control: When components are fixtured in a vibrofinishing process, they are held securely in place, minimising their movement within the vibratory chamber. This fixturing provides stability to the components, ensuring consistent

contact with the abrasive media. With reduced movement and better control over the component's position, there is a higher relative velocity of the media onto the component. Additionally, there is more predictable and uniform interaction between the media and the component, leading to improved surface finishing.

2. Targeted Surface Treatment: Fixturing allows for specific areas of the component to be exposed to the abrasive media, enabling targeted surface treatment. By selectively exposing certain surfaces such as varying the orientation in this experiment, the contact area between the media and the component is focused on that targeted surface. By fixturing the component in a way that exposes specific areas, the media's force is concentrated on those regions, resulting in more intense abrasion and better surface finishing in those targeted areas.
3. Enhanced Abrasive Action: The fixturing of components can promote better interaction between the abrasive media and the component's surface. Fixtures can act as a channel that guide the media's movement, directing it to specific areas of the component and its surface, leading to targeted removal of imperfections, burrs, or irregularities, and resulting in improved surface finishing.

It is important to note that the suitability of fixturing versus free tumbling depends on the specific component, its geometry, and the desired surface finishing requirements. While fixtured components generally offer better control and targeted treatment, free tumbling may be preferred for certain parts that require a more random or generalised surface finish. Therefore, understanding the characteristics and goals of the component and the intended application is crucial in determining the most appropriate approach within the vibrofinishing process.

One key limitation of the dome configuration during this comparison was the component-to-machine ratio. Due to the presence of the dome, the ratio was significantly larger as compared to the domeless setup. This caused the component within the dome process to get periodically trapped. This also meant that during this entrapment, there was unintended processing on the fixture. Figure 3.42 illustrates

these occurrences.

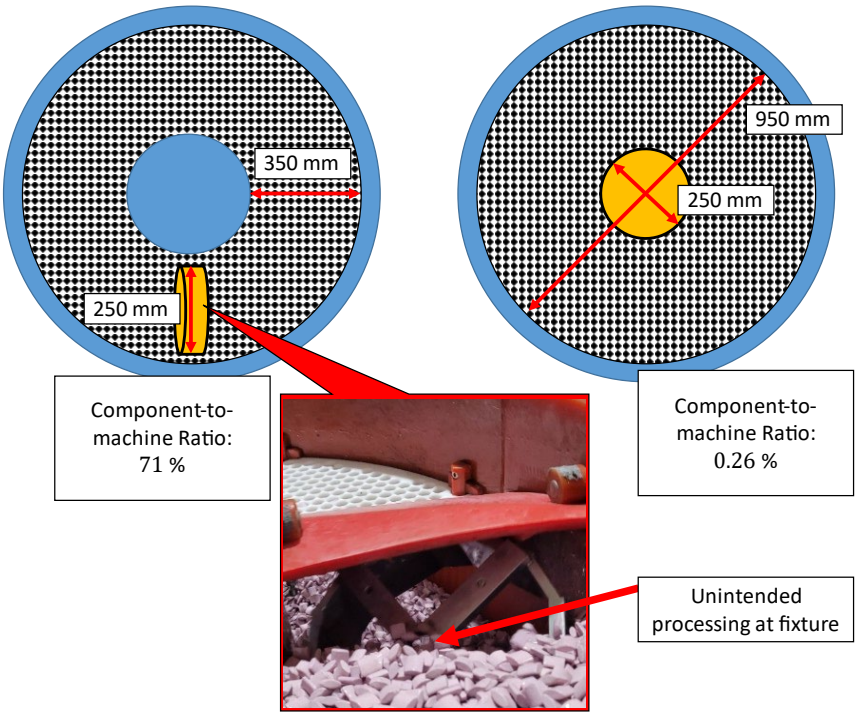

Figure 3.42 High component-to-machine ratio cause entrapment at dome vibrofinishing

In conclusion, domeless performed better than the dome vibrofinishing. Though a reason may be due to the high component-to-machine ratio for the dome that caused operational inefficiencies, by considering a larger bowl, potential additional cost considerations would have to be considered.

3.2.2.2 Trough vs Domeless

This comparison was done between the R 300 mm annular setup on the trough and domeless. Overall, the domeless outperformed the trough vibrofinishing in terms of surface finishing and material removal at all orientations. The results are shown in Figure 3.43 and Figure 3.44 respectively.

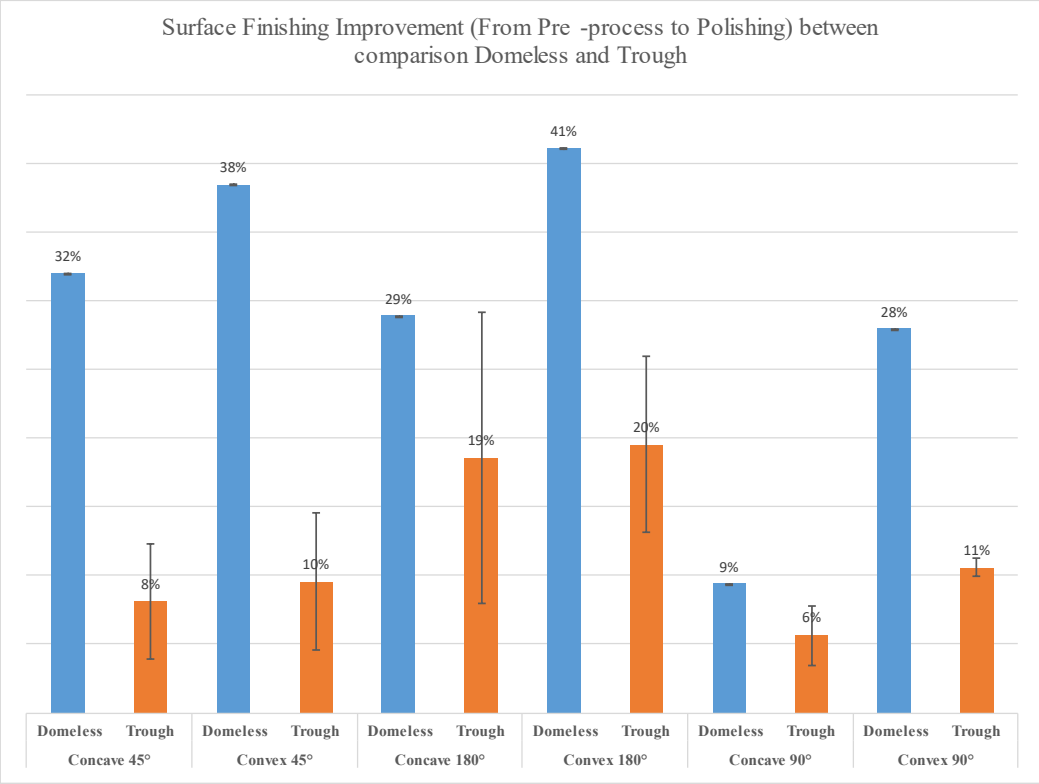

Figure 3.43 Surface Finishing Improvement comparison between Domeless and Trough process

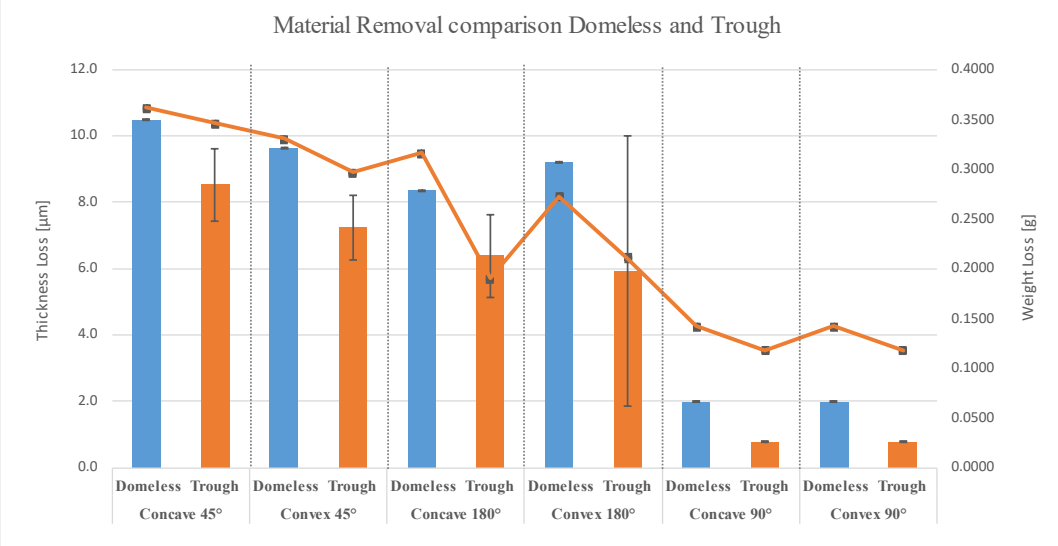

Figure 3.44 Material Removal comparison between Domeless and Trough process

One key pointer to highlight was the limitation of the fixture at the trough process which caused a large error bar at each of the orientation. The reason was due to the

placement of the airfoil at various depth which heavily affected the surface finishing and material removal results. As explained in the methodology, processing power increases with the dept of the airfoil in the trough. Therefore, the approach adopted was to conduct each orientation at varying heights to obtain a range of results based on the individual airfoil positioning in each trial. To enhance the accuracy of the comparative results and minimise the error bar, the consideration could be made to design a fixture that would rotate the component for equal processing. However, it was noted that implementing a rotating fixture would incur higher costs.

3.2.2.3 Cost Analysis

A cost analysis was conducted to compare and understand the economic differences to utilise the domeless vibrofinishing process, as compared to dome and trough processes. The results here would prove practical feasibility of the domeless vibrofinishing technique that would be key to drive industry adoption.

This section focuses on the processing of annular components, which are the main target components in this thesis. It is important to note that there are two main forms of annular components, one with an annular outer ring and one without, such as a nozzle guide vane and turbine disk, respectively, as seen in Figure 3.45. In this cost analysis, a component with an annular outer ring was considered.

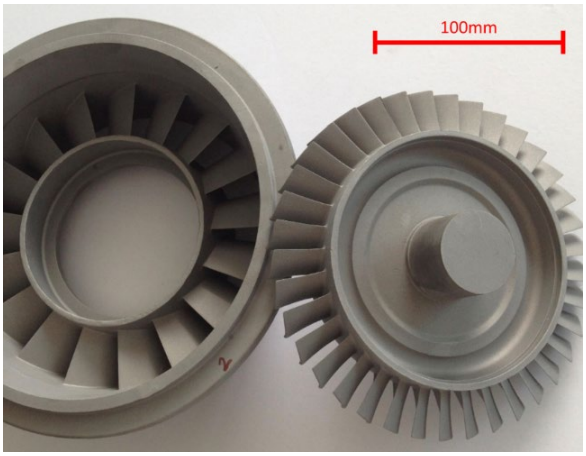

Figure 3.45 (left) nozzle guide vane and (right) turbine disk [26]

As indicated in Chapter 2.2.1, dome and trough bowls are commonly used in the industry to polish annular components but only applicable for larger sized components and are fully annular (not sectioned). At Table 3.3, a schematic drawing of such industrial practice was presented, together with the proposed domeless process for a similar component for comparison.

A noteworthy point was that the dome and trough had to be scaled larger. This was to accommodate a low enough component-to-machine ratio for process operability. Common operational issues stemmed from a high component-to-machine ratio were component damage to Polyurethane (PU) or component being lodged between PU wall and separation flap.

Table 3.3 Schematic drawings of the current industrial practice of annular aerospace component polishing and proposed new method

Machine type / Component	Current industry practice		Proposed new method
	800 L Dome bowl *	**350 L Trough ***	**350 L Domeless bowl**
With outer ring (e.g., nozzle guide vane)	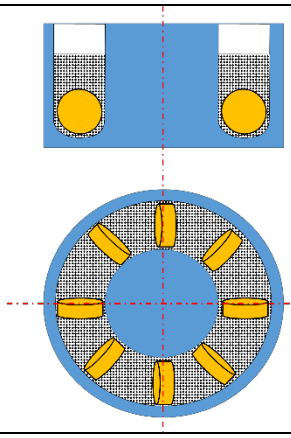	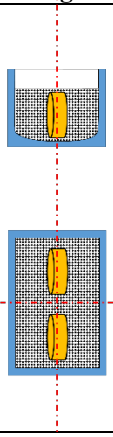	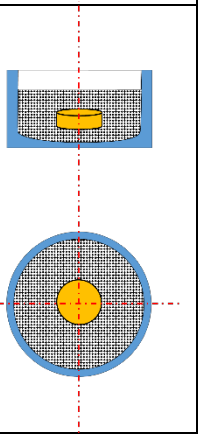

Note: Free tumbling is also an option

Together with Spire Pte Ltd's consultancy, equipment setup assumptions were made to ensure fair comparison. These assumptions were based on industrial requirements to ensure the lowest operational risks, highest throughput while maintaining within a reasonable cost:

1. Machine size: Dome bowl requires a larger size to fit the annular component. To put into operational perspective, an 800 L dome bowl is required to fit a 300 mm diameter component when a 350 L domeless bowl is sufficient. This is crucial for a shopfloor setup when space constraint and optimisation is critical.

   Additionally, due to the absence of a dome in a domeless type vibrofinishing machine, there will be more volume of media required to be added in. A simple estimation for a 350 L bowl requires about 10% more media, in turn requiring a higher consumable usage. This estimation is calculated based on the dome volume over the total volume and will be considered in the analysis.

2. Number of (annular) components: An 800 L dome bowl can fit up to eight components together with PU dividers. Similarly for trough type, it would be able to fit up to two components with an outer annular ring.

   For the domeless bowl, although only one component was considered in this comparison, it is also noteworthy that multiple components could be stacked for the domeless bowl. This is similar to a multi-stage blisk drum. Due to the lack of process testing and understanding, the worst-case scenario of only one component was used for this study.

3. Setup cost: For the dome bowl and trough PU dividers, there is a need to customise it based on the number of parts per cycle. Based on the pricing provided by a vibrofinisher OEM introduced by Spire Pte Ltd, the add-on cost for a PU divider costed an approximately 19% (dome bowl) and 11% (trough) extra. For context, the actual costing amount was dependant on the machine size therefore a percentage was provided instead. Between the dome and trough, the cost range could amount between SGD 10,000 to SGD 47,500 and SGD 5,500 to SGD

27,500 respectively. In addition, fixture would be required for the dome and trough depending on the use case. In comparison, domeless only require a fixture, which by comparison would be much cheaper. Domeless also does not require dividers.

To ensure a fair comparison, the following operation and result assumptions were made on all three processes:

1. Negligible difference in operating expenses. (i.e., electricity, air, water)
2. Capital expenditure (CapEx) based on Spire Pte Ltd base cost.
3. Fixed processing time with the same amplitude and frequency. This meant that motor configuration such as motor size, quantity of flyweights and adjustment (phase) angles are adjusted accordingly to meet these specifications.
4. Domeless bowl to be used as baseline in this study, set at value of one.

Finally, the cost ratio analysis through a Pugh Matrix method was to be calculated based on the summation of each specification's ratio multiply by its weightage:

$$Cost\ Ratio\ of\ machine\ type\ (\%) = \sum Specification\ \times Weightage\ (\%) \qquad (3.2)$$

Table 3.4 CapEx and OpEx comparison (%) between current practice vs proposed new vibrofinishing method

Machine type / **Specification (weightage %)**		***Current industry practice***		***Proposed new method***	***Remarks***
		Dome bowl (800 L)	**Trough (350 L)**	**Domeless bowl (350 L)**	
Machine cost	**40%**	1.60 (64 %)	1.20 (48 %)	1.00 (40 %)	• *800 L Dome costs 60% more* • *350 L Trough cost 20% more*
Divider/Fixture cost	**10%**	1.38 (13.8 %)	1.11 (11 %)	1.00 (10 %)	• *Dome divider cost increased significantly due to larger machine size*
Consumable cost	**5%**	2.30 (11.5 %)	1.00 (5 %)	1.00 (5 %)	• *Dome media and compound cost increased significantly (2.3x) due to larger machine size*
Process time / Productivity	**20%**	0.125 (2.5 %)	0.50 (10 %)	1.00 (20 %)	• *Dome – 8 pcs / run* • *Trough – 2 pcs / run* • *Domeless – 1 pc / run*
Manual handling of components	**5%**	2.00 (10 %)	1.50 (7.5 %)	1.00 (5 %)	• *Amount calculated based on manhours required to handle loading/unloading of divider, fixture, and component*

Operational space required	**20%**	2.93 (58.5 %)	1.79 (35.8 %)	1.00 (20 %)	• *Amount calculated based on each machine square meter multiply by per square meter rental cost.* • *Dome - ⌀ 1.8 m → 2.63 m^2* • *Trough – 1.5 m* x *1.05 m → 1.61 m^2* • *Domeless - ⌀ 1.07 m → 0.90 m^2*
Cost Ratio (%)		**160.3 %**	**117.3 %**	**100 %**	

Based on the results, the 800 L dome bowl requires a 60.3 % higher CapEx and OpEx while a 350 L trough requires 17.3 % higher CapEx and OpEx cost to domeless bowl. The results indicated that the domeless bowl had a lower cost ratio compared to the dome bowl and trough. However, it is important to note that these results are indicative and further process development and optimisation are required for a comprehensive understanding of the domeless vibrofinishing technique.

In conclusion, the analysis presented in this section provides insights into the economic viability of adopting the domeless vibrofinishing technique for annular components. The domeless bowl offers advantages in terms of machine size, uniformity of surface finish, and setup costs compared to the dome bowl and trough. However, further research and development are necessary to refine the process and fully evaluate its potential benefits.

Chapter 4 Fundamental Study of Domeless Vibrofinishing Machine

This chapter presents a fundamental study of the domeless vibrofinishing machine by creating a model of the machine. The model is employed to theoretically derive a key machine parametric configuration, the flyweight setting, for the domeless vibrofinishing. A validation of the derived configuration is also conducted. Finally, a model comparison between domeless and dome vibrofinishing through a theoretical analysis of machine outputs' such as vibratory force and displacement was studied.

4.1 Methodology

This section focuses on establishment of a mechanical vibration system to model a domeless machine, and a set of vibrational and excitation force equations based on the created model.

4.1.1 Model

To understand the fundamentals of domeless, circular vibrofinishing machine, a scaled model can be designed based on existing models of a dome, circular vibratory process readily available (as reviewed in Chapter 2).

The domeless, circular vibrofinishing machine can be modelled using a spring-dampening-load dynamic system in *x*-*y*-*z* axes as seen in Figure 4.1.

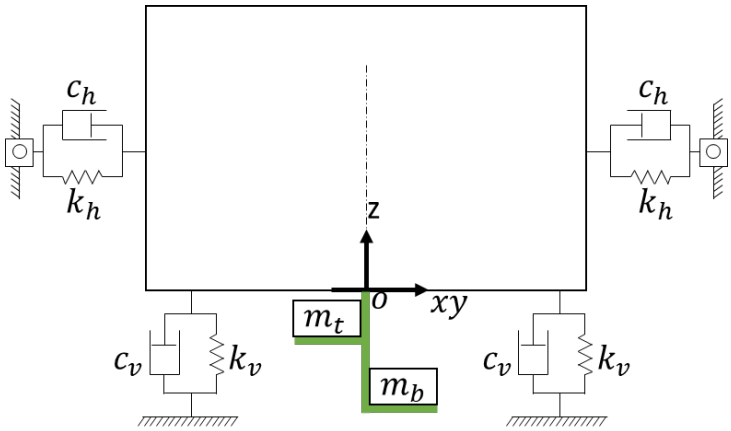

(a) Front View

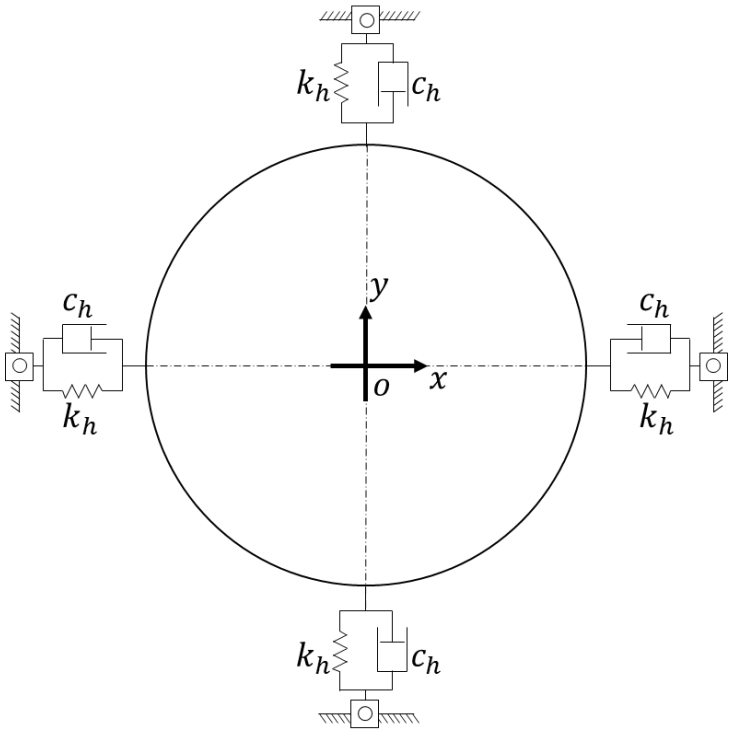

(b) Top View

Figure 4.1 Dynamic Model of domeless vibrofinishing bowl with indicative position of eccentric weights attached under the bowl

With reference to the model of the dome vibrofinishing machine by Hashimoto and Johnson [20] [20], we can simplify the bowl as a charged cuboid-body with mass, *M*, representing the total mass which includes the mass of the bowl, media, component,

fixture, liquid compound, and water. This mass M is induced with forced vibration by two eccentric plates with attached flyweights along two ends of a motor shaft. The motor rotates and generates a centrifugal force to trigger the forced vibration. At the same time, a moment of inertia J is generated from the centrifugal force. The two eccentric plates are labelled top and bottom plates and are respectively labelled as m_t, m_b, with their rotational movement along the motor shaft as angular velocity, Ω. The alignment angle between the two masses will be labelled as the phase angle, φ. The distance from the centroid which is the motor axial shaft to the centroid of the flyweights is labelled as r.

Similar to Figure 4.1, the springs supporting the mass, M, are consolidated into 4 spring/dampener at the corners on the body vertically (z-axis) while horizontally (x-y-axes) supported by 4 spring/dampener as well. To which the springs are labelled as k_h and k_v in the horizontal and vertical direction respectively, and dampeners labelled as c_h and c_v in the horizontal and vertical direction respectively as well.

The distance of the vertical springs from the centroid of M is labelled as L. Finally, mass M is understood to rotate along the x and y axes but not along the z axis. Therefore, there is a rotational angle along x and y axes, θ_x and θ_y respectively. The full representation is drawn in Figure 4.2.

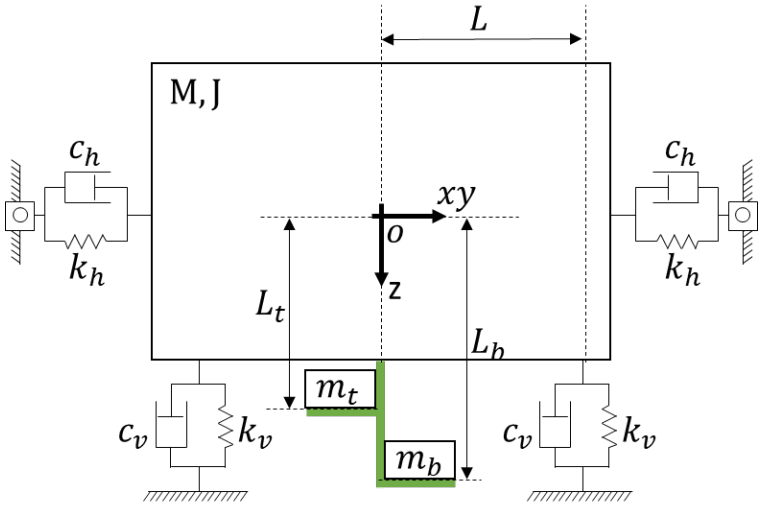

(a) Front View

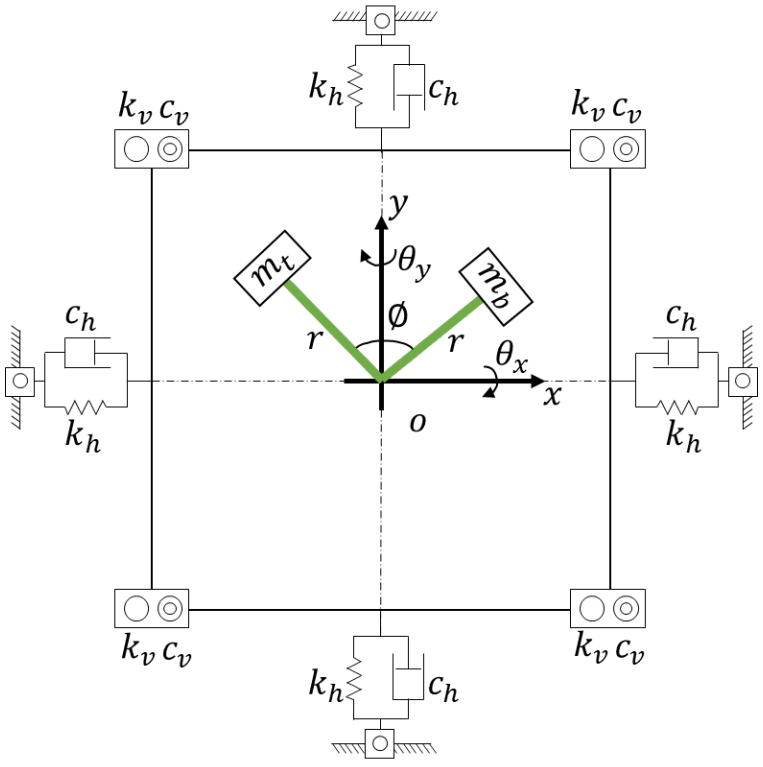

(b) Top View

Figure 4.2 Domeless vibrofinishing machine modelled as a mechanical vibration system

4.1.2 Equations

A set of parametric equations can be used to explain the model, as represented in Figure 3.3. By using Newton's Second Law, the forces in a mechanical vibration system in the *x-y-z* coordinate can be established as follows:

$$F_x = M\ddot{x} + C_h\dot{x} + K_h x \tag{4.1}$$

$$F_y = M\ddot{y} + C_h\dot{y} + K_h y \tag{4.2}$$

$$F_z = M\ddot{z} + C_h z + K_h z \tag{4.3}$$

With the nature of the bowl vibration, we can assume small values for θ_x and θ_y which approximated as $\sin\theta_x \approx \theta_x$, $\cos\theta_x \approx 1$, $\sin\theta_y \approx \theta_y$ and $\cos\theta_y \approx 1$. Therefore, F_z can be equated as:

$$F_z = F_x\theta_x + F_y\theta_y \tag{4.4}$$

The angular motion equations are established as follows:

$$P_X = J\ddot{\theta}_x + (C_v L^2)\dot{\theta}_x + (K_v L^2)\theta_x \tag{4.5}$$

$$P_y = J\ddot{\theta}_y + (C_v L^2)\dot{\theta}_y + (K_v L^2)\theta_y \tag{4.6}$$

$$P_z = J\ddot{\theta}_z = 0 \tag{4.7}$$

where $C_v = 4c_v$, $K_v = 4k_v$, $C_h = 2c_h$, $K_h = 2k_h$.

Using Figure 4.2 to establish the dynamic positioning of top and bottom eccentric masses m_t and m_b during processing, we can establish the linear and rotational forces along *x-y* axes as:

$$F_x = r\Omega^2[m_t \cos\Omega t + m_b \cos(\Omega t + \varphi)] \tag{4.8}$$

$$F_y = r\Omega^2[m_t \sin\Omega t + m_b \sin(\Omega t + \varphi)] \tag{4.9}$$

$$P_X = r\Omega^2[m_t L_t \sin\Omega t + m_b L_b \sin(\Omega t + \varphi)] \tag{4.10}$$

$$P_y = r\Omega^2[m_t L_t \cos\Omega t + m_b L_b \cos(\Omega t + \varphi)] \tag{4.11}$$

Finally, the motion equations of (4.1) - (4.3), (4.5) and (4.6) can be solved to yield free and forced vibrations. A general solution of the second order differential equation of each of the equations (4.1) - (4.3), (4.5) and (4.6) can be summated by the auxiliary solution with subscript *c* to label the free vibrations equations and particular solution subscript *p* to label the forced vibration equations. This is to follow the model of Hashimoto and Johnson [20] to enable comparison in the subsequent section. Therefore, $x = x_c + x_p$, $y = y_c + y_p$, $z = z_c + z_p$, $\theta_x = \theta_{xc} + \theta_{xp}$ and $\theta_y = \theta_{yc} + \theta_{yp}$.

It is also noted that there is a slight variation to equations (4.10) and (4.11) for a domeless bowl due to the change in direction of L_t as compared to a dome bowl. Hence, the free vibrations in the *x*-*y*-*z* coordinates and their rotational axes, except for rotation along *z* axis, are represented by the following equations:

$$x_c = A_1 e^{-\zeta_h \omega_{nh} t} \sin(\omega_{dh} t - \psi_1) \tag{4.12}$$

$$y_c = A_2 e^{-\zeta_h \omega_{nh} t} \sin(\omega_{dh} t - \psi_2) \tag{4.13}$$

$$z_c = A_3 e^{-\zeta_v \omega_{nh} t} \sin(\omega_{dv} t - \psi_3) \tag{4.14}$$

$$\theta_{xc} = A_4 e^{-\zeta_h \omega_{nh} t} \sin(\omega_{dh} t - \psi_4) \tag{4.15}$$

$$\theta_{yc} = A_5 e^{-\zeta_h \omega_{nh} t} \sin(\omega_{dh} t - \psi_5) \tag{4.16}$$

where A_1 – A_5 are arbitrary constants, ψ_1 to ψ_5 are alignment (phase) angles determined by arbitrary constants. ζ represents the damping factors, ω_n represents natural frequency and ω_d represent damped natural frequency, with all three having subscripts to represent their directions – *v* for vertical, *h* for horizontal and θ for rotational. Each of them can be calculated with the following equations:

$$\zeta_h = \frac{C_h}{2\sqrt{MK_h}} \tag{4.17}$$

$$\omega_{nh} = \sqrt{\frac{K_h}{M}} \tag{4.18}$$

$$\omega_{dh} = \left(\sqrt{1-\zeta_h^2}\right)\omega_{nh} \tag{4.19}$$

$$\zeta_v = \frac{C_v}{2\sqrt{MK_v}} \tag{4.20}$$

$$\omega_{nh} = \sqrt{\frac{K_v}{M}} \tag{4.21}$$

$$\omega_{dv} = \left(\sqrt{1-\zeta_v^2}\right)\omega_{nv} \tag{4.22}$$

$$\zeta_\theta = \frac{C_v L}{2\sqrt{MK_v}} \tag{4.23}$$

$$\omega_{n\theta} = \sqrt{\frac{K_v L^2}{J}} \tag{4.24}$$

$$\omega_{d\theta} = \left(\sqrt{1-\zeta_\theta^2}\right)\omega_{n\theta} \tag{4.25}$$

The forced vibrations generated by the rotational angular velocity Ω of eccentric masses m_t and m_b are represented by the auxiliary equations of equations (3.1) – (3.5) in the *x*-*y*-*z* coordinates and their rotational axes, except for rotation along *z* axis, by the following equations:

$$x_p = G_x cos(\Omega t - \Phi_1) \tag{4.26}$$

$$y_p = G_y sin(\Omega t - \Phi_1) \tag{4.27}$$

$$z_p = constant \tag{4.28}$$

$$\theta_{xp} = E_x sin(\Omega t - \Phi_2) \tag{4.29}$$

$$\theta_{yp} = E_y cos(\Omega t - \Phi_2) \tag{4.30}$$

where Φ is the alignment or phase angle and variables *G*, *E* are variables, with their subscripts to represent their directional axis, are determined by the following equations:

$$G_x = \frac{F_x}{\sqrt{(C_h\Omega)^2 + (K_h - M\Omega^2)^2}} \tag{4.31}$$

$$G_y = \frac{F_y}{\sqrt{(C_h\Omega)^2 + (K_h - M\Omega^2)^2}} \tag{4.32}$$

$$E_x = \frac{P_x}{\sqrt{(C_v L^2\Omega)^2 + (K_v L^2 - J\Omega^2)^2}} \tag{4.33}$$

$$E_y = \frac{P_y}{\sqrt{(C_v L^2\Omega)^2 + (K_v L^2 - J\Omega^2)^2}} \tag{4.34}$$

$$\Phi_1 = \tan^{-1}\frac{C_h\Omega}{(K_h - M\Omega^2)} \tag{4.35}$$

$$\Phi_2 = \tan^{-1}\frac{C_h L^2\Omega}{(K_h L^2 - J\Omega^2)} \tag{4.36}$$

The equations (3.1) to (3.36) will be used on the model done in section 4.1.1 for the comparison of a key machine parametric configuration which is the flyweight setting between conventional and new settings specific to domeless type at both theoretical and experimental.

4.2 Results & Discussion

Utilising the created model served as a foundation for achieving several objectives. The first objective was to conduct a comprehensive comparison of a key machine parameter configuration, specifically the flyweight setting, between conventional settings and new settings specific to the domeless type. This comparison was carried out through theoretical analysis and experimental investigations. Additionally, the

model was employed to analyse and compare machine outputs, such as vibratory force and displacement, between domeless and dome vibrofinishing techniques.

4.2.1 Flyweight configuration

Conventionally, in a fully laden dome vibrofinishing, achieving a 4.5 mm amplitude would utilise a top and bottom flyweight configuration of 1:1. For domeless vibrofinishing, due to the lack of the dome which causes variations such as the laden weight and position of flyweights, the flyweight configuration would be completely different in order to achieve a similar amplitude. This section aims to utilise the created model and established equations to identify the right flyweight configuration. Parameters to be used in the equation would utilise the domeless vibrofinishing machine (ERBA EVP-250 CL) provided by Spire Pte Ltd.

Based on the model created, *x-y-z* axes was assigned as shown in Figure 4.3. The amplitude can be converted into *x-z* axis based on the amplitude and lead angle values during operations. The conversion is shown in Figure 4.4.

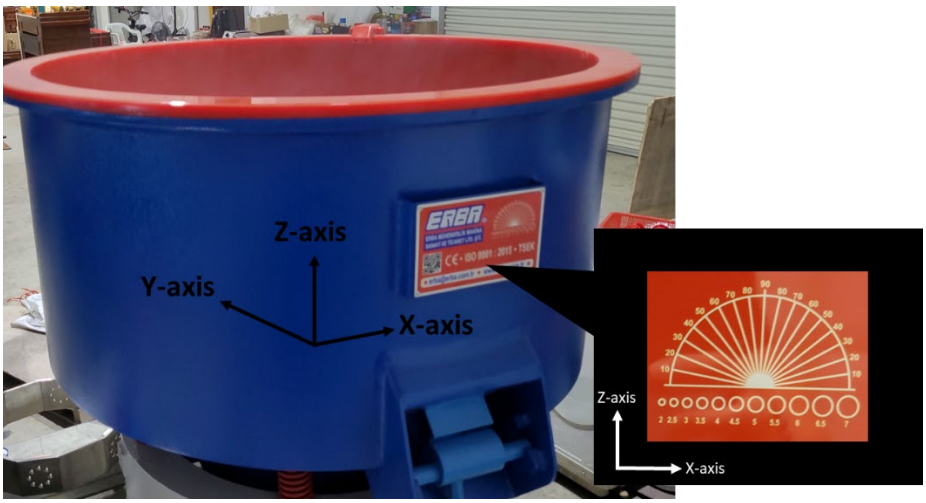

Figure 4.3 Assigning 3-axis to domeless machine

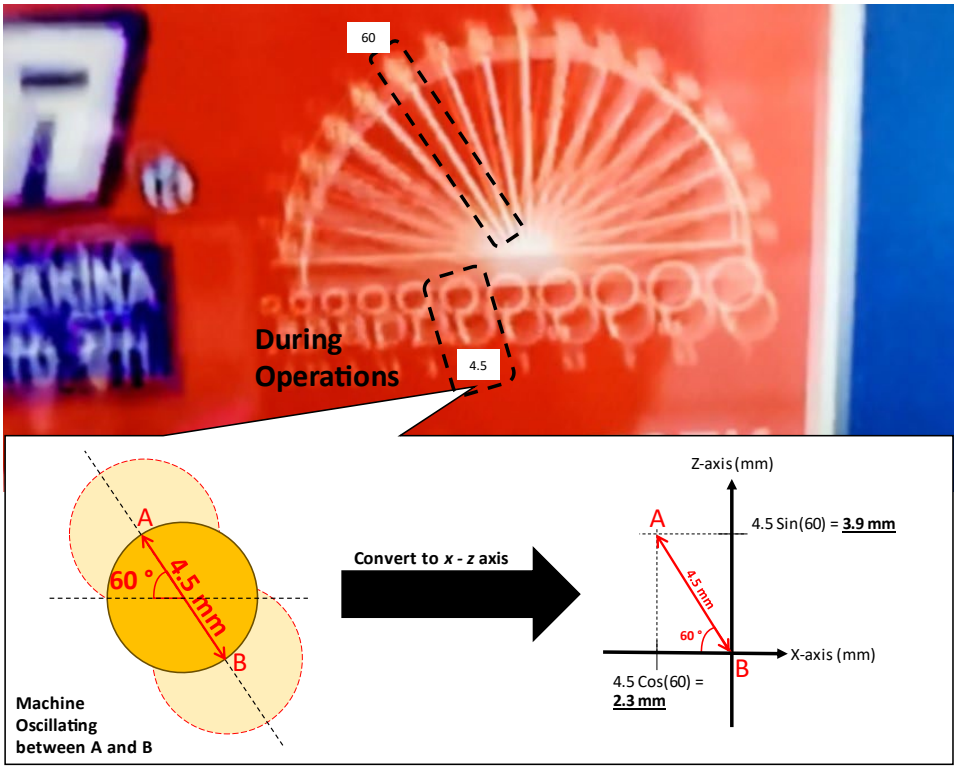

Figure 4.4 Amplitude converted to *x*-*z* axis

The next step was to validate the displacement along the x-axis was 2.3 mm using the displacement equation of $x = x_c + x_p$ based on the two forms of vibration derived at equations (4.12) and (4.26), where:

$$x_c = A_1 e^{-\zeta_h \omega_{nh} t} \sin(\omega_{dh} t - \psi_1)$$

$$x_p = G_x cos(\Omega t - \Phi_1)$$

The displacement along *x*-axis is therefore extended as follow:

$$x = A_1 e^{-\zeta_h \omega_{nh} t} \, sin(\omega_{dh} t - \psi_1) + \left[\left(\frac{r\Omega^2 [m_t \cos \Omega t + m_b \cos(\Omega t + \varphi)]}{\sqrt{(C_h \Omega)^2 + (K_h - M\Omega)^2)^2}} \right) \cos\left(\Omega t - tan^{-1} \frac{C_h \Omega}{(K_h - M\Omega^2)} \right) \right] \quad (4.37)$$

Parameters for the vibration model were: K_h = 31.8 N/mm, C_h = 0.0444 N s/mm, C_v = 0.011 N s/mm, ζ_h = 0.0014, ζ_v = 0.0031, ζ_u = 0.0031, ω_{nh} = 20.1 rad/s, ω_{nv} = 44.6

rad/s, ω_{nu} = 45.1 rad/s, ω_{dh} = 20.1 rad/s, ω_{dv} = 44.6 rad/s and ω_{du}=45.1 rad/s.

Machine parameters were on the usage of the ERBA EVP-250 CL domeless vibrofinisher and were selected with industrial practiced values as follows: φ = 60°, Ω = 1400 RPM, M = 3380 N, L_t =340 mm, L_b = 700 mm, r = 50 mm, and L = 350 mm.

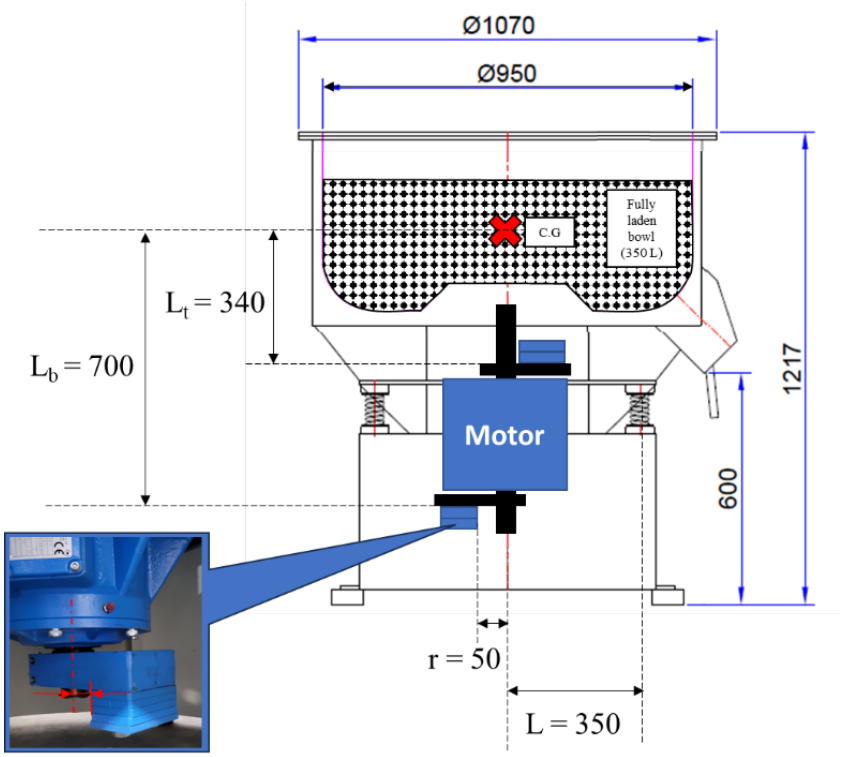

Figure 4.5 Additional machine dimensions of ERBA EVP-250 CL domeless vibrofinisher

Total mass (M) calculated based on volume of a fully media ladened domeless bowl, multiplied by the media density of 1.43 g/cm^3. Finally, the mass of a single flyweight was measured at 2.255 kg, and therefore weight of 22.12 N. In this theoretical analysis, the selection was based on a fixed top flyweight setting of two pieces (22.12 N) to ensure a good feed rate which was tested briefly and described in Section 2.3.2. To increase the amplitude, an addition of one flyweight would be added per trial until the *x*-axis amplitude value of 2.3 mm was obtained. The arbitrary constants A_1 and ψ_1 were to be adjusted to best fit the experimental data to keep the graph in a constant frequency and amplitude. Table 4.1 shows the results of this theoretical analysis with

the validated flyweight setting resulting in the targeted amplitude value plotted in Figure 4.6.

Table 4.1 Theoretical experiment for flyweight setting

Trial	Top Flyweight		Bottom Flyweight		Amplitude (x-axis) (mm)
	Qty	(N)	Qty	(N)	
1	2	44.24	2	44.24	1.26
2	2	44.24	3	66.36	1.58
3	2	44.24	4	88.49	1.91
4	2	44.24	5	110.61	2.23

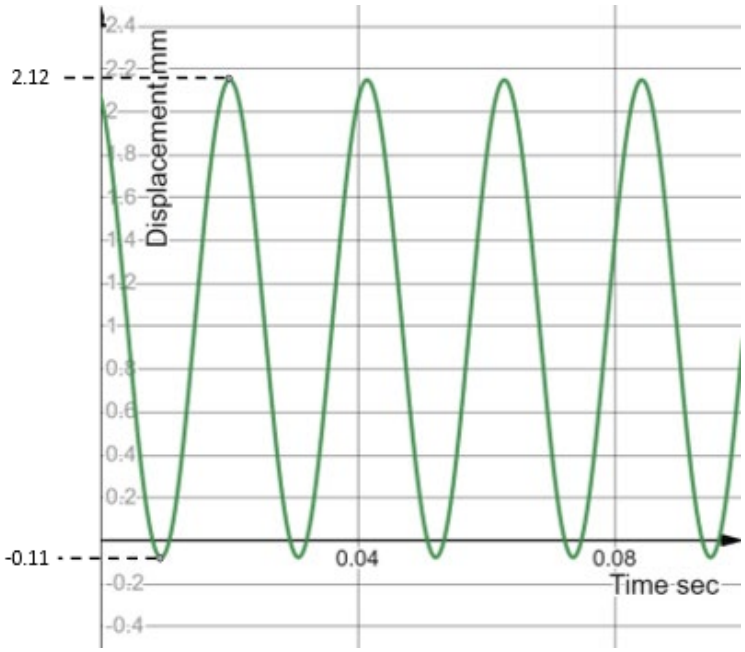

Figure 4.6 Machine oscillation during vibration in the x-axis, representing amplitude in x-axis

As shown by the results, the conventional method of top to bottom flyweight ratio at 1:1 would o produce an amplitude of 1.26 mm in the x-axis, which would only amount to an amplitude of 2.5 mm. In this theoretical experiment, it was validated that to achieve an amplitude of 4.5 mm at a lead angle of 60°, the top to bottom flyweight ratio was found to be 2:5. This flyweight setting would be validated with experimental results in the next section.

4.2.1.1 Experimental results and validation of proposed flyweight setting

In accordance with industrial practice, the flyweight setting in the domeless vibrofinishing machine was adjusted in a trial-and-error to achieve the amplitude and lead angle of 4.5 mm and 60° respectively. As explained in Section 2.3.2, a visual inspection on the Vibroscope was done to check these parameters physically. Based on the results obtained in the previous section, two flyweight variations were focused – one was the conventional method of a 1:1 flyweight setting, and the proposed flyweight setting of 2:5 as summarised in Table 4.2. An additional 1:1 flyweight setting of 1 piece each was conducted as a baseline.

Table 4.2 Experiment trials for flyweight setting

Trial	Test (Flyweight setting)	Quantity	
		Top Flyweight	Bottom Flyweight
1	1:1	1	1
2	1:1	2	2
3	2:5	2	5

During the initial trial, the placement of a single flyweight at both the top and bottom positions of the domeless vibrofinishing machine led to a relatively low degree of off-balanced movement. This outcome can be attributed to the absence of eccentric vibration, resulting in vertical bouncing of the domeless bowl. This behaviour, as illustrated in Figure 4.7, was predominantly observed along the z-axis in accordance with the model. Consequently, the absence of media roll and feed was observed under these conditions.

Figure 4.7 Domeless Bowl movement in the 90° lead angle due to the lack of eccentric mass to tilt the vibration

In the second trial, an additional flyweight was introduced at both the top and bottom positions. This modification resulted in the occurrence of roll and feed motions, albeit at a low level. As depicted in Figure 4.8 (a) a snapshot of the trial demonstrated a subtle rolling effect, with the media at the top exhibiting limited downward movement. Consequently, the media at the outer diameter of the bowl tended to accumulate and stack on top of each other, as opposed to rolling back down and inward, as depicted in Figure 4.8 and highlighted. Furthermore, Figure 4.9 revealed that the amplitude and frequency of the motion corresponded to only 2 mm and an angle of 60°, respectively, as highlighted in yellow. The insufficient rolling action resulted in decreased flowability and subsequently hindered the processing of the component.

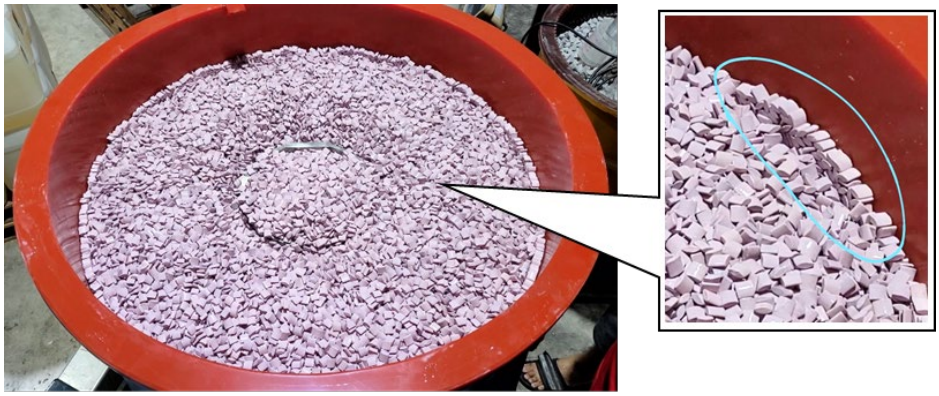

Figure 4.8 Low amplitude caused by undesirable flyweight setting would cause a media stacking effect

Figure 4.9 Visual analysis of the amplitude and lead angle based on the Vibroscope

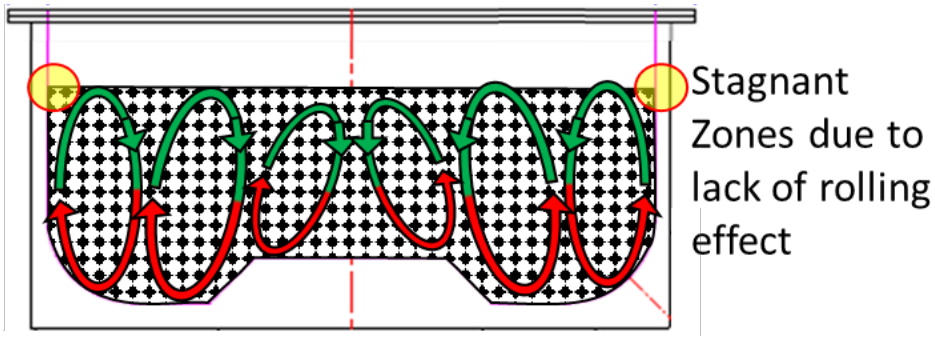

Figure 4.10 Stagnant zones in domeless bowl would happen at a bad flyweight setting

In the final trial, three additional flyweights were added to the setup in order to increase the amplitude of the motion. This adjustment was consistent with the theoretical findings discussed in the previous section with the modified flyweight configuration of 2:5 successfully achieved the desired amplitude of 4.5 mm and a lead angle of 60°. Figure 4.11 visually represents the final arrangement of the bottom flyweight in the domeless vibrofinishing machine.

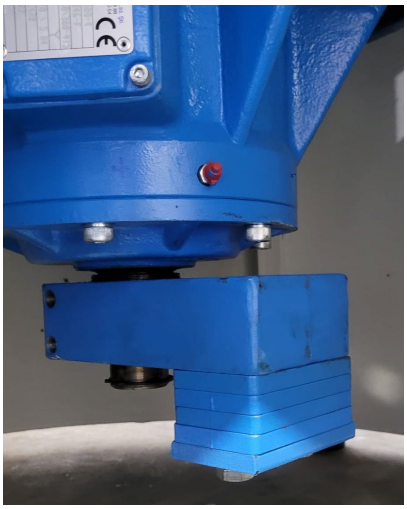

Figure 4.11 Five flyweight setup at bottom of motor

Finally, a quick plot of the excitation moment in the x-axis showed that in theory, the flyweight setting of 2:5 had a larger excitation moment than the 1:1 setting by 129%.

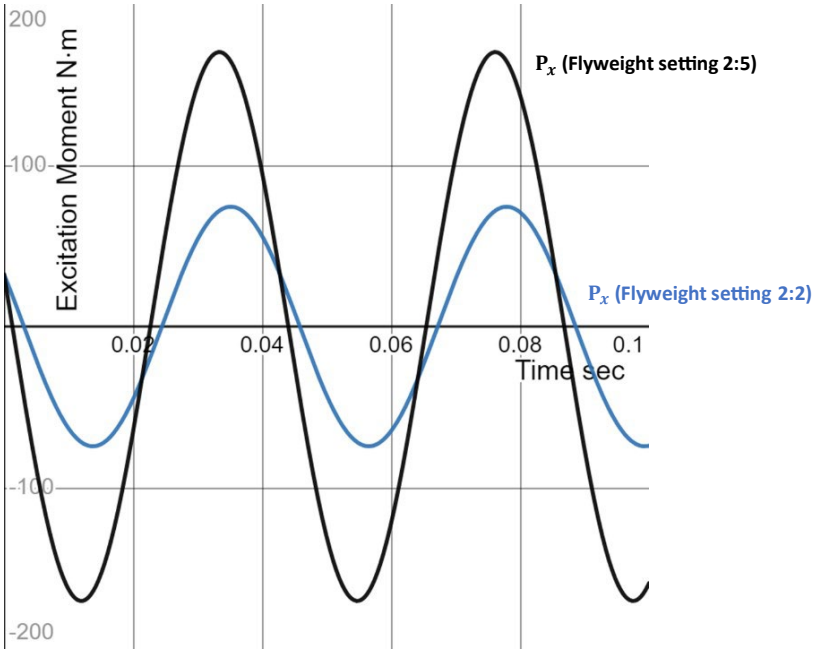

Figure 4.12 Excitation Moment (M_x) in the horizontal direction between two flyweight settings

4.2.2 Theoretical Comparison Domeless and Dome Vibrofinishing

This section focused on using the proposed model of the domeless vibrofinishing to scale and compare against Hashimoto and Johnson's mechanical vibration model of a dome vibrofinisher [20] to make a direct comparison on the two vibrofinishing machines. The model comparison investigated the machines' outputs during the bowl vibration such as the forces generated, and the amount of displacement created. These outputs focus on the linear (x-y) axes and the rotational (θ_x-θ_y) axes.

For a fair comparison, the domeless machine model from section 4.1.1 was scaled to Hashimoto and Johnson's dome vibrofinishing model [20] as shown in Figure 4.13. The main difference between the two machines was primarily the positions of the eccentric plates, m_t and m_b, labelled from the c as L_t and L_b respectively.

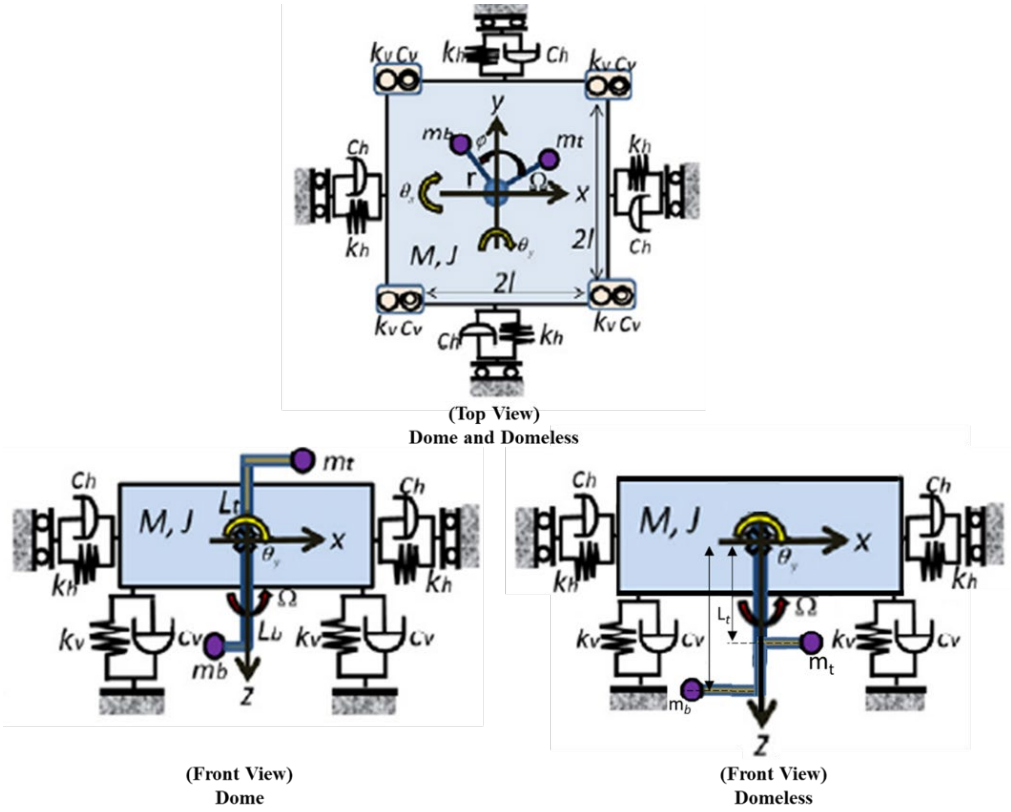

Figure 4.13 Schematic drawing of domeless-type designed from dome-type [20]

By taking the values provided in their study with some calculations to scale the dome type to domeless type, a parameter table can be established in Table 4.3. It is noted that in the cited study, it was not mentioned if the theoretical calculations were based off experimental setup, specifically the bowl dimensions to draft the cuboid-body, but as experimental and theoretical values were in agreement, this thesis would consider both as references in this comparison study.

Table 4.3 Parameters to be used for comparison

Parameter	Symbol	Dome	Domeless
Phase angle (Alignment Angle between eccentric plates)	φ	90° ≈ 1.5708 rad/s	
Angular velocity	Ω	1400 RPM ≈ 146.9 rad/s	
Frequency	Hz	50 Hz	
Spring constant - vertical	k_v	39.2 N/mm	
Spring constant - horizontal	k_h	15.9 N/mm	
Damping constant - vertical	c_v	0.0055 N s/mm	
Damping constant - horizontal	c_h	0.0222 N s/mm	
Damping factors - vertical	ζ_v	0.0031	
Damping factors - horizontal	ζ_h	0.0014	
Damping factors - angular	ζ_θ	0.0031	
Natural frequency - vertical	ω_{nv}	44.6 rad/s	
Natural frequency - horizontal	ω_{nh}	20.1 rad/s	
Natural frequency – angular	$\omega_{n\theta}$	45.1 rad/s	
Damping frequency - horizontal	ω_{dv}	44.6 rad/s	
Damping frequency - vertical	ω_{dh}	20.1 rad/s	
Damping frequency - Angular	$\omega_{d\theta}$	45.1 rad/s	
Horizontal length of vertical springs to mass M centroid	L	180 mm	
Horizontal length of eccentric plate to mass M centroid	r	50 mm	
Vertical length of top eccentric plate to mass M centroid	L_t	145 mm	200 mm
Vertical length of bottom eccentric plate to mass M centroid	L_b	255 mm	300 mm
Top eccentric plate and flyweight (pre-assigned) weight	$m_t \cdot g$	8.4 N*	8.4 N (2 plates)
Bottom eccentric plate and flyweight (pre-assigned) weight	$m_b \cdot g$	9.3 N*	21.0 N (5 plates)
Ratio of top eccentric plate and flyweight and bottom eccentric plate and flyweight	m_t/m_b	1 (round up)	0.4
Body weight	M · g	772.3 N	816.1 N

*Based on weight referred from Hashimoto and Johnson [20]

To ensure a proper baseline comparison, machine setups that are similar in nature for both types such as springs, and dampeners were kept constant. The process setup such as alignment (phase) angle and angular velocity were also set similar. Additionally,

natural constants and factors were set similar. Therefore, the similar values are as follows: φ, Ω, Hz, k_v, k_h, c_v, c_h, ζ_h, ζ_v, ζ_θ, ω_{nh}, ω_{nv}, $\omega_{n\theta}$, ω_{dh}, ω_{dv}, $\omega_{d\theta}$, L, and r.

Additionally, positions L_t and L_b for the domeless bowl were scaled to the dome bowl as referenced to Hashimoto and Johnson [20], and were estimated at 200 mm and 300 mm respectively. A schematic drawing shown in Figure 4.14.

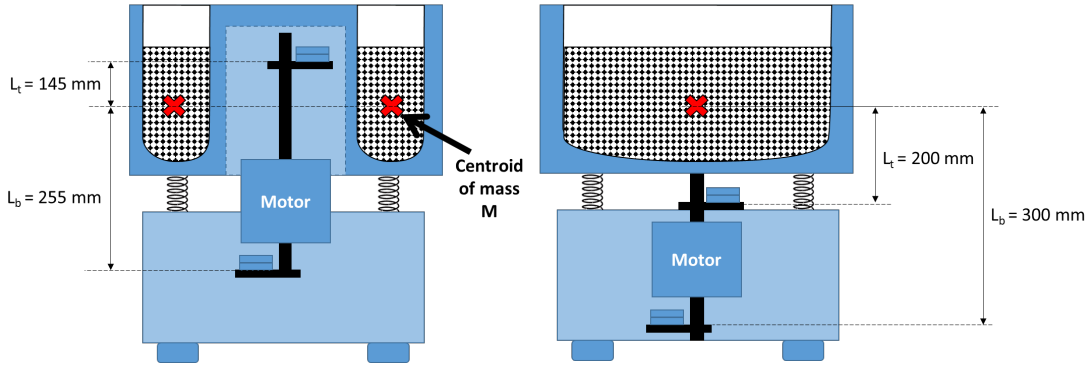

Figure 4.14 Schematic drawings of estimated positions and dimensions of L_t and L_b of (left) dome and (right) domeless

The values of eccentric masses, m_t and m_b of the domeless bowl utilised the proposed flyweight setting of 2:5 as discussed in the previous section.

Finally, the body mass M of dome machine was calculated based on similar media (Al_2O_3 spherical dia. 5 mm) of density 1.43 g/cm^3 and component mass (hardened steel cylindrical roller of dia. 15 mm x L22 mm, HRC62) from Hashimoto and Johnson [20]. As the mass M of dome type will account for the additional volume due to the lack of a dome, came to a calculated approximation of 3.123 L, giving a total weight amount to 816.1 N. The detailed calculations are appended in Appendix .

4.2.2.1 Linear and Rotational Excitation Force Comparison

Figure 4.15 compared the dome and domeless types in terms of the external forces generated along the x and y axes during machine operation at a motor rotational speed of 1400 RPM. These forces, which drive the vibration motion, are calculated using Equation (4.8) and (4.9). The results clearly show that the domeless bowl produces a higher excitation force compared to the dome type, with an 80.5% increase.

Specifically, the dome type has an excitation force of 2.44 kN, while the domeless type has a higher force of 1.35 kN.

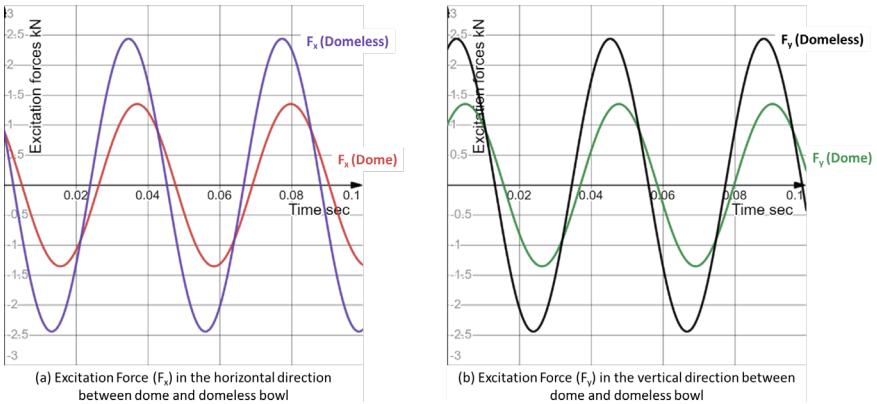

Figure 4.15 Comparison of excitation forces caused by the forced vibration along (a) *x*-axis and (b) *y*-axis

Figure 4.16 compares the dome and domeless types in terms of the external moments generated along the *x* and *y* axes. These moments, which contribute to the vibration motion, are calculated using Equation (4.8) and (4.9) for the domeless type and sourced from the study for the dome type [20]. The results indicate that the domeless type has a higher peak amplitude of 144.5% in excitation moment compared to the dome type, measuring 703.5 kN for the domeless type and 287.7 kN for the dome type. Additionally, it is noteworthy that there is a phase shift of approximately 50%.

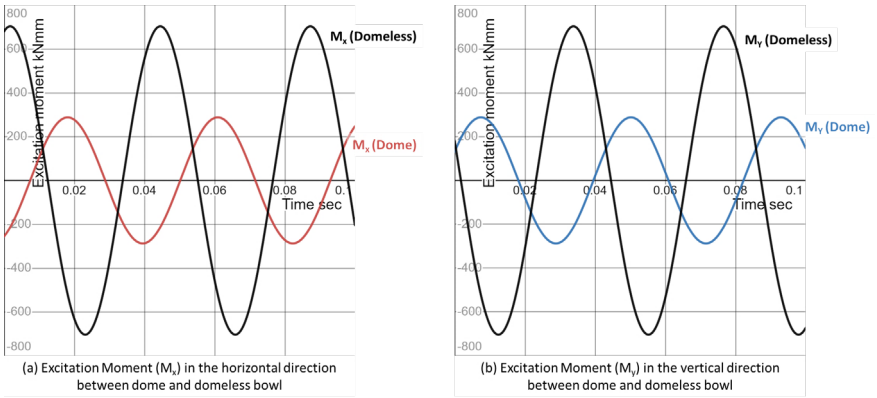

Figure 4.16 Comparison of excitation moment caused by the forced vibration along (a) *x*-axis and (b) *y*-axis

The enhanced processing power of the domeless bowl can be attributed to two notable qualitative factors. Firstly, the augmented bottom eccentric weight (m_b) within the

domeless bowl contributes to its superior performance. This increased weight distribution amplifies the energetic effects, resulting in enhanced material removal capabilities. Secondly, by positioning the motor and eccentric plates farther away from the centroid mass M (L_b), the domeless bowl harnesses a greater force and moment. This deliberate arrangement unlocks a heightened potential for dynamic agitation and material interaction.

4.2.2.2 Linear and Rotational Displacement Comparison

This section presents a comparison of the linear and rotational displacements between the dome and domeless bowls. Figure 4.17 illustrated the linear displacement results and showed that the domeless bowl exhibited an approximately 44.7% higher than that of the dome bowl, at 1.47 mm and 0.81 mm respectively.

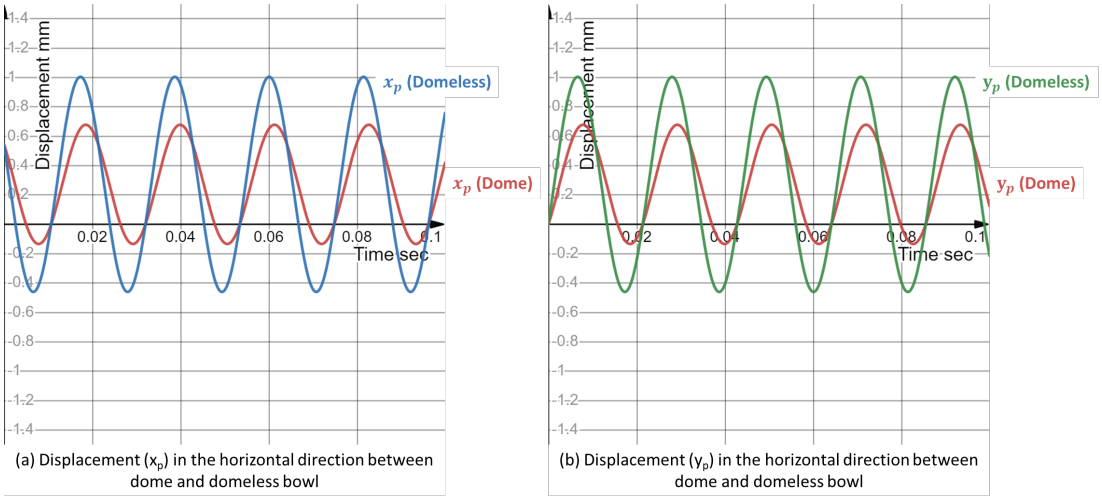

Figure 4.17 Theoretical comparison between dome and domeless bowl by the displacement of the bowl (body mass M) caused by the forced vibration along (a) *x*-axis and (b) *y*-axis

Similarly, Figure 4.18 illustrates a rotational displacement increase of approximately 51.5% for the domeless bowl compared to the dome bowl, which amounted to 1.47 mm and 0.81 mm, respectively. It was noted that there was a minor time shift between the domeless and dome process. This shift qualitatively implied a slower initiation of vibration to steady state by the domeless bowl likely due to the increased in inertia due to the further positioning of the centroid of mass M to the eccentric weights.

However, despite this shift, the unchanged peak-to-peak distance suggests comparable feed rates and minimal impact on productivity.

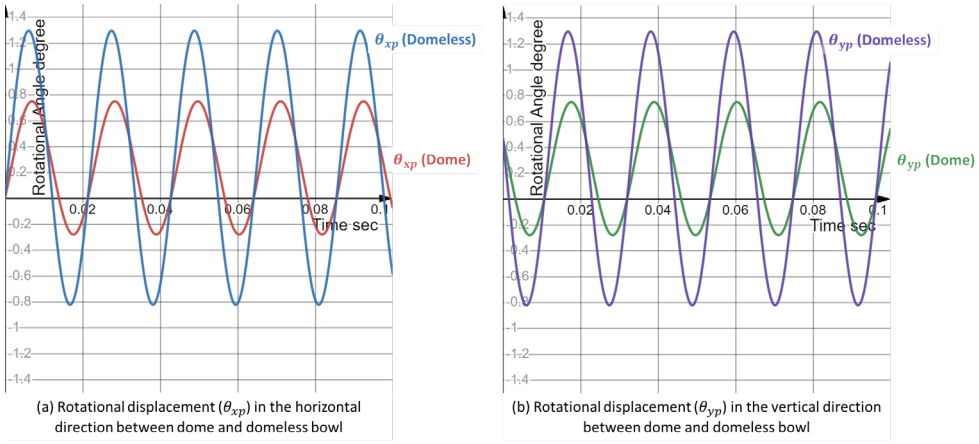

Figure 4.18 Theoretical comparison between dome and domeless bowl by the rotational displacement of the bowl (body mass M) caused by the forced vibration along (a) *x*-axis and (b) *y*-axis

Finally, an additional observation was that the peaks and valleys of both linear and rotational displacements occur at different times. Replotting from Figure 4.18 to place the *x*-*y* axes for each type of displacement as shown in Figure 4.19, both graphs illustrated that both linear and rotational displacements of *x* and *y* axes were in a phase inversion.

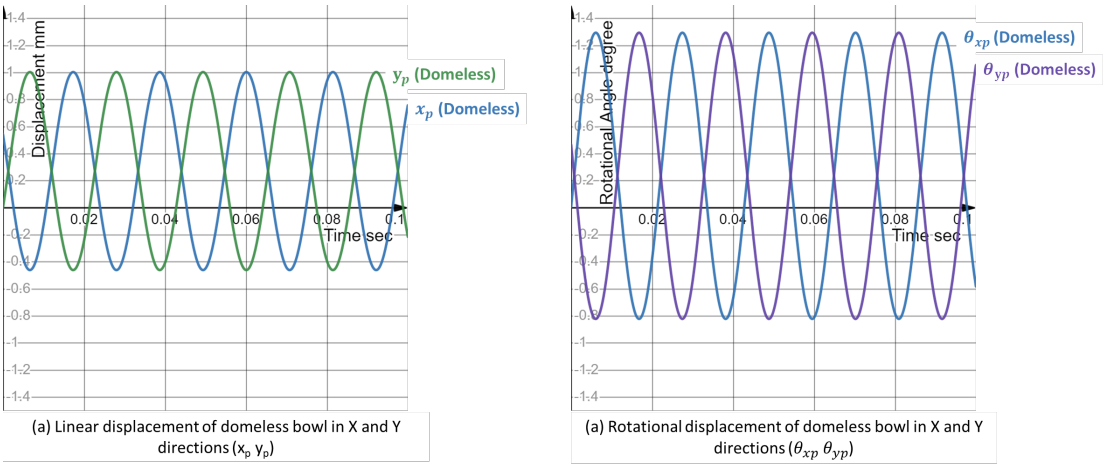

Figure 4.19 (a) Linear and (b) Rotational displacements of domeless bowl

As shown in Figure 4.20, this phase inversion was essentially a theoretical description of the domeless bowl direction during vibration, which allowed a derivation of the amplitude and lead angle of theoretically at 2.06 mm and 45 ° respectively.

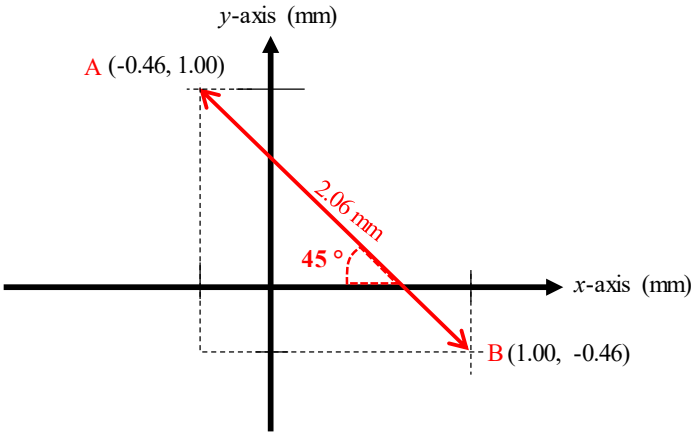

Figure 4.20 Theoretical description on the domeless bowl vibration to calculate amplitude and lead angle

In summary, the findings of the study demonstrate that the domeless bowl exhibits substantially greater linear and rotational displacements when compared to the dome type.

4.2.2.3 Comparison on flyweight configuration

An additional theoretical analysis to compare the domeless and dome in a similar flyweight setting of 1:1 was conducted. Figure 4.21 shows that with an equivalent flyweight configuration, the domeless bowl has exhibited a higher excitation moment of 351.4 kN mm, signifying a notable 22% increase as compared to the dome bowl's excitation moment of 287.7 kN mm. This substantiated the potential for higher energy output by the domeless bowl design which may help in increasing mass finishing productivity.

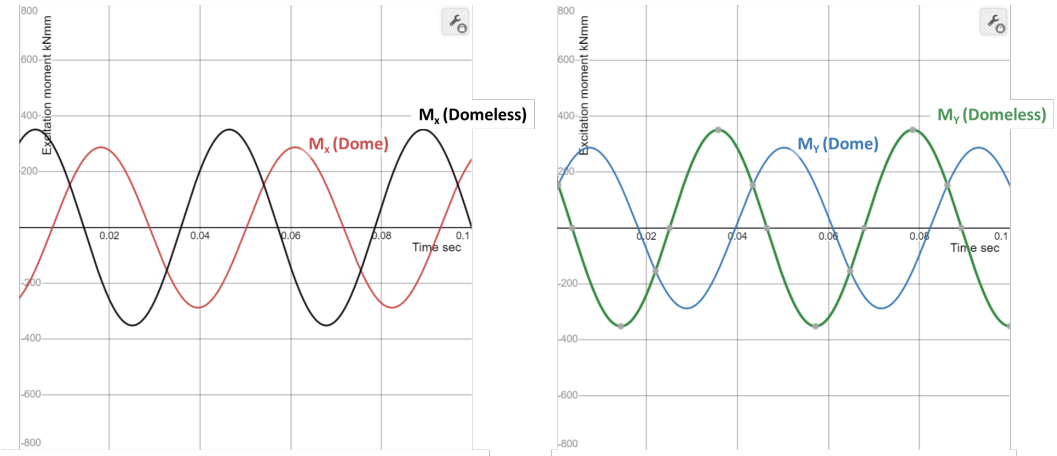

(a) Excitation Moment (M_x) in the horizontal direction between dome and domeless bowl with same flyweight setting

(b) Excitation Moment (M_y) in the vertical direction between dome and domeless bowl with same flyweight setting

Figure 4.21 A 22% higher excitation moment for domeless bowl compared to dome bowl with same flyweight setting of 1:1

Chapter 5 **Conclusion and Future Work**

This chapter presents the thesis summary of findings and proposed future works.

5.1 Summary of findings

This thesis proposed a new vibratory finishing machine with a unique design – domeless, non-elevating and circular vibratory finishing bowl - to be deployed for the aerospace industry, both in MRO (remanufacturing) and new-make (manufacturing). The key limitations based on the literature review were the lack of process know-how of the domeless vibrofinisher in terms of understanding the potential capability of processing aerospace components, especially annular-shaped components. Additionally, the domeless vibrofinisher had limited literature on the machine know-how that would allow practitioners to utilise as an initial guideline when deciding on setting up their own equipment.

The first step in this work was to validate the domeless vibrofinisher process through an experimental KPV study to ensure it met the surface finishing and material removal requirements of aerospace industry. The KPV study analysed the processing capabilities of a domeless process on an airfoil assembled between two annular rings, at various positions on the domeless machine at various orientations to the media flow to study the effects of airfoil orientation and the component-to-machine ratio.

The findings demonstrated that the optimal position for surface finishing was at a 45-degree angle at both concave and convex surfaces, as it allows for the highest surface roughness improvement and material removal, with the lowest processing result by the concave surface at the 90-degree angle. Notably, the results met the surface finishing requirements of less than 0.625 μm R_a while maintaining the thickness requirement of below 12.7 μm. The results were attributed based on the favourable flowability of the media onto the airfoil surface, ensuring continuous abrasive motion. On the other hand, certain positions of the airfoil, such as when the concave surface

is positioned at 180°, can lead to reduced media flow or to cause stagnation, resulting in less effective material removal and surface finishing in that particular area.

Furthermore, the study revealed that surfaces that are not in direct contact with the media flow would still undergo surface finishing through indirect media interactions. These interactions occur due to mechanisms such as media cascade, media rebound, and media flow redistribution. Although the intensity of these interactions may be lower compared to surfaces in direct contact with the media flow, they contribute to the overall finishing process. The results showed that with a good orientation such as at 45°, the overall surface finishing between both surfaces were within a 10% difference.

The findings also demonstrated that the component-to-machine ratio was only critical when the component was large enough within the domeless bowl. The results suggested that at a larger ratio, the surface finishing would be uniformed at 45 and 180-degrees. At a smaller component-to-machine ratio, the orientation of the airfoil was more significant towards the surface finishing results.

The KPV study was subsequently verified with an experimental comparative analysis to convention processes used in the aerospace industry. First, between the domeless and dome vibrofinishing, the domeless configuration demonstrating a higher surface finishing improvement at the 45° orientation as compared to the dome configuration by more than two times. The 180° orientation had marginal differences, and at 90° orientation, the convex surface had a twice the surface finishing for the domeless compared to dome, while the concave surface had marginal differences. For the material removal, the domeless process resulted in a higher material removal in terms of the change of thickness at all orientations as compared to the dome process. The weight loss, however, was higher for the dome process at 45° orientation of around ± 0.1 g. The other orientations were marginally different. Next, compared to the domeless and trough vibrofinishing, the domeless showed significantly better surface finishing and material removal results, but due to the fixed method of the trough as compared to industrial methods to include a rotational fixture to enable potential

uniformity, the results for the trough had high error margins that would need further validation.

Finally, the KPV study was further augmented with an economic comparative analysis between conventional methods and the proposed domeless bowl, based on the costs required in terms of machine and setup costs with considerations on the productivity and operational costs. The result illustrated that among the three, the dome bowl cost at least 60% more than the domeless bowl due to the increased operational size it required to ensure a right component-to-machine ratio to ensure good processing while preventing component damages. The trough process accounted an extra cost of 17%. Though the added quantity of component per run increased the productivity and reduced the cost weightage, the additional costs such as the dividers, and manual handling of the component would make the domeless process a potential viable solution for the industry.

Next, a comprehensive domeless machine fundamental study was conducted by examining prevailing literature and industrial practices on the dome vibrofinisher to propose and establish a spring-dampening-load dynamic model and a set of vibrational and excitation force equations. A theoretical analysis of a key machine parameter, the flyweight configuration, was conducted on Spire Pte Ltd's domeless machine, to propose a new flyweight configuration. The result provided an ideal top-to-bottom flyweight ratio for the domeless vibrofinishing to be 2:5 to achieve the required amplitude of 4.5 mm. The proposed 2:5 configuration was experimentally verified by conducting trials together with the conventional configuration of 1:1. Finally, a theoretical comparison between the domeless and dome vibrofinishing machines was conducted to analyse machine outputs such as excitation forces, vibrational displacements, and flyweight configuration between conventional and the proposed configuration. The results theoretically demonstrated that the domeless configuration give rise the following effects with respect to the dome configuration:

- 80.5% higher excitation force

- 144.5% higher excitation
- 44.7% higher linear displacement
- 51.5% higher rotational displacement

In summary, the findings of the theoretical study demonstrated that the domeless bowl exhibited substantially greater machine outputs at similar machine inputs such as the motor rotational speed of 1400 RPM and frequency of 50 Hz, as compared to the dome vibrofinishing.

In conclusion, an in-depth study into the process and machine of the domeless vibrofinishing process provided valuable insights into the interplay of key process parameters such as airfoil orientations and component-to-machine ratio configurations, together with a fundamental understanding on key machine settings such as the flyweight configuration, for achieving optimal surface roughness and material removal. The findings contribute to the development of effective strategies for surface finishing in aerospace applications, with the domeless vibrofinishing technique showing promise for cost-effective and efficient processing of annular components. This knowledge will assist practitioners in selecting the most suitable vibrofinishing approach for their specific requirements, optimising surface finishing processes, and enhancing overall productivity.

5.2 Future Work

Further research can explore improvement to domeless vibrofinishing such as looking at improving the machine, consumables, or the process parameters. Other aspects such as the applicability of the thesis findings to other industries and competition, expanding on the cost analysis of different vibrofinishing techniques and even including sustainability aspects to the analysis. A more in-depth proposal is discussed in this section below.

- Optimisation of Process Parameters

In this study, the proposed vibratory finishing machine demonstrated promising

results in the aerospace industry for both MRO and new-make applications. To further enhance its performance and efficiency, future research should focus on optimising the key process parameters of the machine. Specifically, investigations should be conducted to determine the optimal vibration frequency, amplitude, and media-to-part ratio for different types of aerospace components. By systematically varying these parameters and evaluating their effects on surface finish quality, processing time, and material removal rate, it will be possible to establish an optimised parameter range that maximises the machine's effectiveness. This optimisation process can be guided by design of experiments (DOE) methodology, statistical analysis, and empirical validation. The findings from this research will contribute to the knowledge base and provide practical guidelines for operating the vibratory finishing machine in various aerospace manufacturing scenarios.

- Comparative Analysis with Other Finishing Techniques

While the proposed vibratory finishing machine has shown promise, it is important to compare its performance with other commonly used finishing techniques in the aerospace industry. Future research should involve a comprehensive comparative analysis that includes abrasive flow machining, shot peening, and barrel tumbling. This analysis will enable a better understanding of the specific advantages and limitations of each technique and their suitability for different aerospace applications. By evaluating factors such as surface finish quality, material removal efficiency, process flexibility, and cost-effectiveness, a comprehensive comparison can be made. Additionally, opportunities for integrating or hybridising these techniques with the proposed vibratory finishing machine should be explored to further enhance the finishing process and meet the evolving needs of the aerospace industry.

- Advanced Media Development

The media used in the vibratory finishing process plays a critical role in achieving the desired surface finish quality. Therefore, future research should focus on the development of specialised media tailored to the requirements of the proposed

vibratory finishing machine. This may involve exploring novel media compositions, shapes, and sizes that can improve the efficiency and consistency of the finishing process for different aerospace materials, including aluminium alloys, titanium alloys, and composites. Research efforts should also be directed towards understanding the wear characteristics of the media and developing strategies for optimising media life and performance. Furthermore, investigations into the recycling and reclamation of used media can contribute to reducing waste and promoting sustainability in the aerospace manufacturing process.

- Real-time Monitoring and Control

To ensure consistent and high-quality surface finishing, future research should aim to develop a real-time monitoring and control system for the vibratory finishing machine. This system would incorporate sensors and data acquisition techniques to measure and analyse various process parameters, including vibration levels, media wear, and part dimensions. By implementing closed-loop control algorithms, the system can optimise the finishing process in real-time, adjusting the machine parameters to achieve the desired surface finish quality based on feedback from the monitoring system. This integration of advanced sensing and control technologies will not only enhance process efficiency but also provide valuable insights into process optimisation and quality assurance.

- Environmental Sustainability

With increasing emphasis on environmental sustainability, it is crucial to explore methods for reducing the environmental impact of the vibratory finishing process. Future research should investigate alternative media materials that are more environmentally friendly, such as biodegradable or recyclable media options. Additionally, efforts should be made to develop recycling and reclamation techniques for used media to minimise waste generation. Furthermore, optimisation of energy consumption and the development of energy-efficient operating strategies can significantly reduce the carbon footprint associated with the vibratory finishing

process. A comprehensive assessment of the environmental impact, along with the development of sustainable practices, will contribute to the long-term viability and acceptance of the proposed vibratory finishing machine in the aerospace industry.

- Application to Other Industries

While this study focuses on the application of the proposed vibratory finishing machine in the aerospace industry, future research should explore its potential applicability in other industries. By adapting the machine design and process parameters to meet the specific requirements and challenges of different industries, such as automotive, medical devices, or precision engineering, the utility of the machine can be extended. This research should involve conducting feasibility studies and pilot tests to assess the effectiveness and adaptability of the machine in different industrial contexts. The findings will contribute to expanding the practical applications of the vibratory finishing machine, providing opportunities for diversification and market penetration beyond the aerospace sector.

These future works chapters provide insightful directions for further research and development of the proposed vibratory finishing machine. They address key aspects such as process optimisation, comparative analysis, media development, monitoring and control, environmental sustainability, and broader industrial applications. Undertaking these future works will contribute to the continuous improvement and wider adoption of the proposed machine, thus enhancing the competitiveness and efficiency of the aerospace industry and potentially other industries as well.

References

[1] D. Parker, K. Riley, S. Robinson, H. Symington, J. T. (. Hollins), K. J. (VTT), S. R. (. Economy) and D. P. (. Delft), "Remanufacturing Market Study," November 2015.

[2] C.-M. Lee, W.-S. Woo and Y.-H. Roh, "Remanufacturing: Trends and issues," *International Journal of Precision Engineering and Manufacturing-Green Technology,* vol. 4, no. 1, January 2017.

[3] L. K. Gillespie, Mass Finishing Handbook, 2006.

[4] D. Davidson, "Mass Finishing Processes Explained," *Subtractive Manufacturing Technology Blog,* 21 October 2017.

[5] R. Steinhilper and F. Weiland, "Exploring New Horizons for Remanufacturing an Up-to-date Overview of Industries, Products and Technologies," *Procedia CIRP,* vol. 29, 2015.

[6] A. Gopinath, A. Lim, B. Nagarajan, C. C. Wong, R. Maiti and S. Castagne, "Introduction of Enhanced Compressive Residual Stress Profiles in Aerospace Components Using Combined Mechanical Surface Treatments," IOP Conference Series: Materials Science and Engineering, vol. 157, November 2016.

[7] B. Kennedy, "Advanced Workpiece Materials Present Challenges to Providers of Deburring, Finishing Tools," SME Media, 1 November 2017. [Online]. Available: https://www.sme.org/technologies/articles/2017/november/advanced-workpiece-materials-present-challenges-to-providers-of-deburring-finishing-tools/ . [Accessed 25 June 2021].

[8] INOVATEC MACHINERY, “Polishing of various turbine blades,” [Online]. Available: https://www.inovatecmachinery.com/turbine-blade-polishing. [Accessed 3 June 2021].

[9] Rosler, “Aero Engine / Airframe Preparation and Finishing,” [Online].

[10] P. Geng, G. Qin, L. Chen, J. Zhou and Z. Zou, “Simulation of plastic flow driven by periodically alternating pressure and related deformation mechanism in linear friction welding,” *Materials & Design,* vol. 178, September 2019.

[11] C. M. Cotell, S. J. F. A. and S. J. A., “Surface Engineering,” vol. 5, 1994.

[12] A. Yabuki, M. R. Baghbanan and J. K. Spelt, “Contact forces and mechanisms in a vibratory finisher,” *Wear,* vol. 252, p. 7–8, April 2002.

[13] D. Regen, “High-Energy Mass Finishing,” PF Products Finishing, 7 Jan 1999. [Online]. Available: https://www.pfonline.com/articles/high-energy-mass-finishing. [Accessed 2 June 2021].

[14] K. Ahluwalia, R. Mediratta and S. H. Yeo, “Experimental Investigation of Fixtured Vibratory Finishing,” *The World Congress on Engineering,* p. 714–718, July 2016.

[15] G. Feldmann, C. C. Wong, W. Wei and T. Haubold, “Application of Vibropeening on Aero – Engine Component,” *Procedia CIRP,* vol. 13, p. 423 – 428, 2014.

[16] W. P. Nebiolo, “Products Finishing,” 10 October 2013. [Online]. Available: https://www.pfonline.com/articles/considerations-regarding-the-proper-loading-of-vibratory-finishing-bowls-for-optimal-quality-performance-and-throughput-efficiency. [Accessed 10 June 2023].

[17] M. D. Sangid, J. A. Stori and P. M. Ferriera, “Process characterization of vibrostrengthening and application to fatigue enhancement of aluminum

aerospace components—part I. Experimental study of process parameters," *The International Journal of Advanced Manufacturing Technology,* pp. 5-8, March 2011.

[18] Fintek, "Stream Finishing Turbine Blades For Maximum Surface Performance.".

[19] J. Domblesky, V. Cariapa and R. Evans, "Investigation of vibratory bowl finishing," *International Journal of Production Research,* vol. 41, no. 16, January 2003.

[20] F. Hashimoto and S. P. Johnson, "Modeling of vibratory finishing machines," *CIRP Annals - Manufacturing Technology,* vol. 64, pp. 345-348, 2015.

[21] Rösler, "Röslerblog," 25 October 2022. [Online]. Available: https://roslerblog.com/2022/10/25/how-to-use-a-vibrascope-to-measure-vibratory-bowl-amplitude-and-frequency/. [Accessed 25 May 2023].

[22] C. Zhang, W. Liu, S. Wang, Z. Liu, M. Morgan and X. Liu, "Dynamic modeling and trajectory measurement on vibratory finishing," *The International Journal of Advanced Manufacturing Technology,* vol. 106, pp. 1-2, January 2020.

[23] Y. B. Tian, Z. W. Zhong and S. J. Tan, "Kinematic analysis and experimental investigation on vibratory finishing," *International Journal Advanced Manufacturing Technology,* vol. 86, pp. 3113-3121, 2016.

[24] S. Itoh, J. W. K. Ho, C. Turangan and S. Wan, "In Situ Measurement of Granular Pressure and Velocity on Component Surfaces in Stream Finishing," *International Conference on Advanced Surface Enhancement,* vol. 1, no. 1, pp. 226 - 233, 2019.

[25] S. Srivastava, C. Z. Qin and S. Castagne, "Effect of Workpiece Orientation, Lubrication and Media Geometry on the Effectiveness of Vibratory Finishing

of Al6061," *4th International Conference on Material Science and Engineering Technology,* vol. 30, 2015.

[26] Alibaba, "China supplier 165mm nozzle guide vane and turbine disc parts for rc jet engine," [Online]. Available: https://www.alibaba.com/product-detail/China-supplier-165mm-nozzle-guide-vane_62344696812.html. [Accessed 1 July 2022].

[27] University of Wisconsin-Stout Physics Department, "Density of Steel - The Physics Factbook," 20 January 1998. [Online]. Available: . (URL: http://physics.uwstout.edu/StatStr/statics/Stress/strsp35b.htm). [Accessed 15 July 2022].

[28] REM Chemicals Inc., Training Manual for Vibratory Finishing, Southington, 1995.

[29] Inovatec Machinery, "An Introduction to Vibratory Deburring.".

[30] J. R. Davis and Ed., "Metals Handbook Desk Edition.," *ASM International,* 1998.

[31] Nebiolo and W. P., Vibratory Bowl Optimization by Proper Mechanical Set-up and the Use of Chemical Accelerators to Virtually Eliminate Hand Polishing of Steel Parts, REM Chemicals, Inc..

[32] Clark, Remanufacturing in Malaysia - An Assessment of the Current and Future Remanufacturing Industry, 2015.

[33] Y. Xu and W. Feng, "Develop a cost model to evaluate the economic benefit of remanufacturing based on specific technique," *Journal of Remanufacturing,* vol. 4, no. 1, December 2014.

[34] D. A. Davidson, "Surface condition impacts part performance," *Metal Finishing,* vol. 105, no. 2, Feburary 2007.

[35] “Intergranular Corrosion Testing: An Overview of ASTM A262,” January 2019. [Online]. Available:

https://www.element.com/nucleus/2017/intergranular-corrosion-testing-astm-a262. [Accessed 3 June 2021].

[36] C. Cotell, J. Sprague and F. Smidth, ASM handbook. Vol. 5 : Surface engineering, vol. 5, ASM International, 1994.

[37] K. M. K. A. &. S. H. Y. B. J. Wong, “Effects of high frequency vibratory finishing of aerospace components,” *Journal of Mechanical Science and Technology,* vol. 33, no. 4, pp. 1809 - 1815, 2019.

[38] Y. L. K. S. W. G. L. T. Stephen Wan, “A material removal and surface roughness evolution model for loose abrasive polishing of free form surfaces,” *International Journal Abrasive Technology,* vol. 6, no. 4, pp. 269 - 285, 2014.

[39] K. M. K. A. a. S.-H. Y. Ben Jin Wong, “Minimum surface roughness using rule-based modeling of the vibratory finishing process in a high-frequency bowl system,” *Proc IMechE Part B: Journal Engineering Manufacture,* vol. 234, no. 11, pp. 1415 - 1421, 2020.

Appendix A: **Design of Experiment**

Table B.0.1 Design of Experiment

Trial	Annular setup	Media	Machine	Concave 45°	Convex 45°	Concave 180°	Convex 180°	90°	Filler
1	big	PI -> XR	Domeless	#1	#2	#3	#4	#5	#62
2	small	PI -> XR	Domeless	#6	#7	#8	#9	#10	#62
5	small	PI -> XR	Dome	#12	#13	#14	#15	#16	#62
6	big	PI -> XR	Trough	#17	#18	#19	#20	#21	Fixture
7	big	PI -> XR	Trough	#22	#23	#24	#25	#26	Fixture

Table B.0.2 Airfoil positioning for trials on trough machine

Trial	Orientation	Airfoil #	Position
6	Concave 45°	#17	Top
	Convex 45°	#18	Mid
	Concave 180°	#19	Bottom
	Convex 180°	#20	Mid
	90°	#21	Top
7	Concave 45°	#22	Mid
	Convex 45°	#23	Top
	Concave 180°	#24	Mid
	Convex 180°	#25	Bottom
	90°	#26	Top

Appendix B: **Measurement Results**

Airfoil	Radial Position [mm]	Orientation (main surface)	Machine	Fixture method	Pre-Process (main surface)																				
					A: Entry					B: Mid					C: Exit					D: Flowline				
					1	2	3	Mean	SD	1	2	3	Mean	SD	1	2	3	Mean	SD	1	2	3	Mean	SD
1	300	Concave 45°	Domeless	Big	0.438	0.437	0.438	0.438	0.001	0.390	0.390	0.390	0.390	0.000	0.498	0.498	0.498	0.498	0.000	0.383	0.383	0.383	0.383	0.000
2	300	Convex 45°	Domeless	Big	0.390	0.390	0.390	0.390	0.000	0.359	0.359	0.359	0.359	0.000	0.401	0.401	0.401	0.401	0.000	0.375	0.375	0.375	0.375	0.000
3	300	Concave 180°	Domeless	Big	0.412	0.412	0.412	0.412	0.000	0.400	0.400	0.400	0.400	0.000	0.441	0.441	0.441	0.441	0.000	0.375	0.375	0.375	0.375	0.000
4	300	Convex 180°	Domeless	Big	0.453	0.453	0.453	0.453	0.000	0.365	0.365	0.365	0.365	0.000	0.368	0.368	0.368	0.368	0.000	0.467	0.467	0.467	0.467	0.000
5	300	Concave 90°	Domeless	Big	0.422	0.422	0.422	0.422	0.000	0.397	0.397	0.397	0.397	0.000	0.402	0.402	0.402	0.402	0.000	0.406	0.406	0.406	0.406	0.000
6	200	Concave 45°	Domeless	Small	0.400	0.400	0.400	0.400	0.000	0.399	0.399	0.399	0.399	0.000	0.406	0.406	0.406	0.406	0.000	0.356	0.356	0.356	0.356	0.000
7	200	Convex 45°	Domeless	Small	0.450	0.450	0.450	0.450	0.000	0.372	0.372	0.372	0.372	0.000	0.398	0.398	0.398	0.398	0.000	0.376	0.376	0.376	0.376	0.000
8	200	Concave 180°	Domeless	Small	0.413	0.413	0.413	0.413	0.000	0.347	0.347	0.347	0.347	0.000	0.417	0.417	0.417	0.417	0.000	0.456	0.456	0.456	0.456	0.000
9	200	Convex 180°	Domeless	Small	0.393	0.393	0.393	0.393	0.000	0.392	0.392	0.392	0.392	0.000	0.406	0.406	0.406	0.406	0.000	0.379	0.379	0.379	0.379	0.000
10	200	Concave 90°	Domeless	Small	0.346	0.346	0.346	0.346	0.000	0.374	0.374	0.374	0.374	0.000	0.379	0.379	0.379	0.379	0.000	0.383	0.383	0.383	0.383	0.000
12	200	Concave 45°	Dome	Free	0.358	0.358	0.358	0.358	0.000	0.386	0.386	0.386	0.386	0.000	0.391	0.391	0.391	0.391	0.000	0.355	0.355	0.355	0.355	0.000
13	200	Convex 45°	Dome	Free	0.360	0.360	0.360	0.360	0.000	0.388	0.388	0.388	0.388	0.000	0.393	0.393	0.393	0.393	0.000	0.386	0.386	0.386	0.386	0.000
14	200	Concave 180°	Dome	Free	0.359	0.358	0.359	0.359	0.001	0.387	0.387	0.387	0.387	0.000	0.392	0.392	0.392	0.392	0.000	0.347	0.347	0.347	0.347	0.000
15	200	Convex 180°	Dome	Free	0.378	0.378	0.378	0.378	0.000	0.406	0.406	0.406	0.406	0.000	0.411	0.411	0.411	0.411	0.000	0.396	0.396	0.396	0.396	0.000
16	200	Concave 90°	Dome	Free	0.364	0.364	0.364	0.364	0.000	0.392	0.392	0.392	0.392	0.000	0.397	0.397	0.397	0.397	0.000	0.401	0.401	0.401	0.401	0.000
17	300	Concave 45°	Trough	Top	0.372	0.372	0.372	0.372	0.000	0.400	0.400	0.400	0.400	0.000	0.405	0.405	0.405	0.405	0.000	0.421	0.421	0.421	0.421	0.000
18	300	Convex 45°	Trough	Mid	0.376	0.376	0.376	0.376	0.000	0.404	0.404	0.404	0.404	0.000	0.409	0.409	0.409	0.409	0.000	0.452	0.452	0.452	0.452	0.000
19	300	Concave 180°	Trough	Bottom	0.357	0.357	0.357	0.357	0.000	0.385	0.385	0.385	0.385	0.000	0.390	0.390	0.390	0.390	0.000	0.455	0.455	0.455	0.455	0.000
20	300	Convex 180°	Trough	Mid	0.405	0.405	0.405	0.405	0.000	0.433	0.433	0.433	0.433	0.000	0.438	0.438	0.438	0.438	0.000	0.404	0.404	0.404	0.404	0.000
21	300	Concave 90°	Trough	Top	0.362	0.362	0.362	0.362	0.000	0.390	0.390	0.390	0.390	0.000	0.395	0.395	0.395	0.395	0.000	0.471	0.471	0.471	0.471	0.000
22	300	Concave 45°	Trough	Mid	0.361	0.362	0.361	0.361	0.001	0.389	0.389	0.389	0.389	0.000	0.394	0.394	0.394	0.394	0.000	0.380	0.380	0.380	0.380	0.000
23	300	Convex 45°	Trough	Top	0.382	0.382	0.382	0.382	0.000	0.410	0.410	0.410	0.410	0.000	0.415	0.415	0.414	0.415	0.001	0.438	0.438	0.438	0.438	0.000
24	300	Concave 180°	Trough	Mid	0.392	0.392	0.392	0.392	0.000	0.420	0.420	0.420	0.420	0.000	0.425	0.425	0.425	0.425	0.000	0.482	0.482	0.482	0.482	0.000
25	300	Convex 180°	Trough	Bottom	0.383	0.383	0.383	0.383	0.000	0.411	0.411	0.411	0.411	0.000	0.416	0.416	0.416	0.416	0.000	0.456	0.456	0.456	0.456	0.000
26	300	Concave 90°	Trough	Top	0.347	0.347	0.347	0.347	0.000	0.375	0.375	0.375	0.375	0.000	0.380	0.380	0.380	0.380	0.000	0.420	0.420	0.420	0.420	0.000

Airfoil	Radial Position [mm]	Orientation (main surface)	Machine	Fixture method	Deburring (main surface)																				
					A: Entry					B: Mid					C: Exit					D: Flowline				
					1	2	3	Mean	SD	1	2	3	Mean	SD	1	2	3	Mean	SD	1	2	3	Mean	SD
1	300	Concave 45°	Domeless	Big	0.737	0.737	0.737	0.737	0.000	0.795	0.795	0.795	0.795	0.000	0.770	0.770	0.770	0.770	0.000	0.909	0.909	0.909	0.909	0.000
2	300	Convex 45°	Domeless	Big	0.684	0.684	0.684	0.684	0.000	0.710	0.710	0.710	0.710	0.000	0.572	0.572	0.572	0.572	0.000	0.754	0.754	0.754	0.754	0.000
3	300	Concave 180°	Domeless	Big	0.904	0.904	0.904	0.904	0.000	1.170	1.170	1.170	1.170	0.000	0.894	0.894	0.894	0.894	0.000	0.747	0.747	0.747	0.747	0.000
4	300	Convex 180°	Domeless	Big	0.981	0.981	0.981	0.981	0.000	1.160	1.160	1.160	1.160	0.000	1.020	1.020	1.020	1.020	0.000	1.010	1.010	1.010	1.010	0.000
5	300	Concave 90°	Domeless	Big	0.450	0.450	0.450	0.450	0.000	0.444	0.444	0.444	0.444	0.000	0.501	0.502	0.501	0.501	0.001	0.468	0.468	0.468	0.468	0.000
6	200	Concave 45°	Domeless	Small	0.984	0.984	0.984	0.984	0.000	0.642	0.642	0.642	0.642	0.000	0.768	0.768	0.768	0.768	0.000	0.840	0.840	0.840	0.840	0.000
7	200	Convex 45°	Domeless	Small	0.952	0.952	0.952	0.952	0.000	0.592	0.592	0.592	0.592	0.000	0.733	0.733	0.733	0.733	0.000	0.761	0.761	0.761	0.761	0.000
8	200	Concave 180°	Domeless	Small	0.642	0.642	0.642	0.642	0.000	0.715	0.715	0.715	0.715	0.000	0.674	0.674	0.674	0.674	0.000	0.671	0.671	0.671	0.671	0.000
9	200	Convex 180°	Domeless	Small	0.714	0.714	0.714	0.714	0.000	0.794	0.794	0.794	0.794	0.000	0.703	0.703	0.703	0.703	0.000	0.816	0.816	0.816	0.816	0.000
10	200	Concave 90°	Domeless	Small	0.444	0.444	0.444	0.444	0.000	0.430	0.430	0.430	0.430	0.000	0.441	0.441	0.441	0.441	0.000	0.430	0.430	0.430	0.430	0.000
12	200	Concave 45°	Dome	Free	0.728	0.728	0.728	0.728	0.000	0.808	0.808	0.808	0.808	0.000	0.717	0.717	0.717	0.717	0.000	0.582	0.582	0.582	0.582	0.000
13	200	Convex 45°	Dome	Free	0.825	0.825	0.825	0.825	0.000	0.905	0.905	0.905	0.905	0.000	0.814	0.814	0.814	0.814	0.000	0.663	0.663	0.663	0.663	0.000
14	200	Concave 180°	Dome	Free	0.797	0.797	0.797	0.797	0.000	0.877	0.877	0.877	0.877	0.000	0.786	0.786	0.786	0.786	0.000	0.587	0.587	0.587	0.587	0.000
15	200	Convex 180°	Dome	Free	0.720	0.720	0.720	0.720	0.000	0.800	0.800	0.800	0.800	0.000	0.709	0.709	0.709	0.709	0.000	0.598	0.598	0.598	0.598	0.000
16	200	Concave 90°	Dome	Free	0.746	0.746	0.746	0.746	0.000	0.826	0.826	0.826	0.826	0.000	0.735	0.735	0.735	0.735	0.000	0.488	0.489	0.488	0.488	0.001
17	300	Concave 45°	Trough	Top	0.750	0.750	0.750	0.750	0.000	0.830	0.830	0.830	0.830	0.000	0.739	0.740	0.739	0.739	0.001	0.625	0.625	0.625	0.625	0.000
18	300	Convex 45°	Trough	Mid	0.735	0.735	0.735	0.735	0.000	0.815	0.815	0.815	0.815	0.000	0.724	0.724	0.724	0.724	0.000	0.497	0.497	0.497	0.497	0.000
19	300	Concave 180°	Trough	Bottom	0.736	0.735	0.736	0.736	0.001	0.816	0.816	0.815	0.816	0.001	0.725	0.725	0.725	0.725	0.000	0.686	0.686	0.686	0.686	0.000
20	300	Convex 180°	Trough	Mid	0.777	0.777	0.777	0.777	0.000	0.857	0.857	0.857	0.857	0.000	0.766	0.766	0.766	0.766	0.000	0.638	0.638	0.638	0.638	0.000
21	300	Concave 90°	Trough	Top	0.724	0.724	0.724	0.724	0.000	0.804	0.804	0.804	0.804	0.000	0.713	0.713	0.713	0.713	0.000	0.487	0.487	0.487	0.487	0.000
22	300	Concave 45°	Trough	Mid	0.839	0.839	0.839	0.839	0.000	0.919	0.919	0.919	0.919	0.000	0.828	0.828	0.828	0.828	0.000	0.674	0.673	0.674	0.674	0.001
23	300	Convex 45°	Trough	Top	0.737	0.737	0.737	0.737	0.000	0.817	0.817	0.817	0.817	0.000	0.726	0.726	0.726	0.726	0.000	0.549	0.549	0.549	0.549	0.000
24	300	Concave 180°	Trough	Mid	0.741	0.740	0.741	0.741	0.001	0.821	0.821	0.821	0.821	0.000	0.730	0.730	0.730	0.730	0.000	0.557	0.557	0.556	0.557	0.001
25	300	Convex 180°	Trough	Bottom	0.727	0.727	0.727	0.727	0.000	0.807	0.807	0.807	0.807	0.000	0.716	0.716	0.716	0.716	0.000	0.535	0.534	0.535	0.535	0.001
26	300	Concave 90°	Trough	Top	0.729	0.729	0.729	0.729	0.000	0.810	0.809	0.809	0.809	0.001	0.717	0.719	0.718	0.718	0.001	0.511	0.511	0.511	0.511	0.000

Airfoil	Radial Position [mm]	Orientation (main surface)	Machine	Fixture method	Polishing (main surface)																				
					A: Entry					B: Mid					C: Exit					D: Flowline				
					1	2	3	Mean	SD	1	2	3	Mean	SD	1	2	3	Mean	SD	1	2	3	Mean	SD
1	300	Concave 45°	Domeless	Big	0.346	0.346	0.346	0.346	0.000	0.499	0.499	0.499	0.499	0.000	0.566	0.566	0.566	0.566	0.000	0.618	0.618	0.618	0.618	0.000
2	300	Convex 45°	Domeless	Big	0.386	0.386	0.386	0.386	0.000	0.476	0.476	0.476	0.476	0.000	0.411	0.411	0.411	0.411	0.000	0.464	0.464	0.464	0.464	0.000
3	300	Concave 180°	Domeless	Big	0.614	0.614	0.614	0.614	0.000	0.606	0.606	0.606	0.606	0.000	0.599	0.599	0.599	0.599	0.000	0.531	0.531	0.531	0.531	0.000
4	300	Convex 180°	Domeless	Big	0.614	0.614	0.614	0.614	0.000	0.604	0.604	0.604	0.604	0.000	0.601	0.601	0.601	0.601	0.000	0.595	0.595	0.595	0.595	0.000
5	300	Concave 90°	Domeless	Big	0.423	0.423	0.423	0.423	0.000	0.412	0.412	0.412	0.412	0.000	0.467	0.467	0.467	0.467	0.000	0.424	0.424	0.424	0.424	0.000
6	200	Concave 45°	Domeless	Small	0.455	0.455	0.455	0.455	0.000	0.430	0.430	0.430	0.430	0.000	0.548	0.548	0.548	0.548	0.000	0.504	0.504	0.504	0.504	0.000
7	200	Convex 45°	Domeless	Small	0.496	0.496	0.496	0.496	0.000	0.408	0.408	0.408	0.408	0.000	0.451	0.451	0.451	0.451	0.000	0.375	0.375	0.375	0.375	0.000
8	200	Concave 180°	Domeless	Small	0.563	0.563	0.563	0.563	0.000	0.544	0.544	0.544	0.544	0.000	0.593	0.593	0.593	0.593	0.000	0.591	0.591	0.591	0.591	0.000
9	200	Convex 180°	Domeless	Small	0.588	0.588	0.588	0.588	0.000	0.580	0.580	0.580	0.580	0.000	0.601	0.601	0.600	0.601	0.001	0.598	0.598	0.598	0.598	0.000
10	200	Concave 90°	Domeless	Small	0.420	0.420	0.420	0.420	0.000	0.404	0.404	0.404	0.404	0.000	0.413	0.413	0.413	0.413	0.000	0.398	0.398	0.398	0.398	0.000
12	200	Concave 45°	Dome	Free	0.469	0.469	0.469	0.469	0.000	0.444	0.444	0.444	0.444	0.000	0.562	0.562	0.562	0.562	0.000	0.451	0.451	0.451	0.451	0.000
13	200	Convex 45°	Dome	Free	0.500	0.500	0.500	0.500	0.000	0.475	0.475	0.475	0.475	0.000	0.593	0.593	0.593	0.593	0.000	0.516	0.516	0.516	0.516	0.000
14	200	Concave 180°	Dome	Free	0.466	0.466	0.466	0.466	0.000	0.441	0.441	0.441	0.441	0.000	0.559	0.559	0.559	0.559	0.000	0.491	0.491	0.491	0.491	0.000
15	200	Convex 180°	Dome	Free	0.491	0.491	0.491	0.491	0.000	0.466	0.466	0.466	0.466	0.000	0.584	0.584	0.584	0.584	0.000	0.443	0.443	0.443	0.443	0.000
16	200	Concave 90°	Dome	Free	0.475	0.475	0.475	0.475	0.000	0.450	0.450	0.450	0.450	0.000	0.568	0.568	0.568	0.568	0.000	0.444	0.444	0.444	0.444	0.000
17	300	Concave 45°	Trough	Top	0.477	0.477	0.477	0.477	0.000	0.452	0.452	0.452	0.452	0.000	0.570	0.570	0.570	0.570	0.000	0.593	0.593	0.593	0.593	0.000
18	300	Convex 45°	Trough	Mid	0.523	0.523	0.523	0.523	0.000	0.498	0.498	0.498	0.498	0.000	0.616	0.616	0.616	0.616	0.000	0.432	0.432	0.432	0.432	0.000
19	300	Concave 180°	Trough	Bottom	0.483	0.483	0.483	0.483	0.000	0.458	0.458	0.458	0.458	0.000	0.576	0.576	0.576	0.576	0.000	0.507	0.507	0.507	0.507	0.000
20	300	Convex 180°	Trough	Mid	0.470	0.470	0.470	0.470	0.000	0.445	0.445	0.445	0.445	0.000	0.563	0.563	0.563	0.563	0.000	0.542	0.542	0.542	0.542	0.000
21	300	Concave 90°	Trough	Top	0.546	0.546	0.546	0.546	0.000	0.521	0.521	0.521	0.521	0.000	0.639	0.639	0.639	0.639	0.000	0.452	0.452	0.452	0.452	0.000
22	300	Concave 45°	Trough	Mid	0.472	0.472	0.472	0.472	0.000	0.447	0.447	0.447	0.447	0.000	0.565	0.565	0.565	0.565	0.000	0.599	0.599	0.599	0.599	0.000
23	300	Convex 45°	Trough	Top	0.474	0.474	0.474	0.474	0.000	0.449	0.450	0.449	0.449	0.001	0.567	0.567	0.567	0.567	0.000	0.516	0.516	0.516	0.516	0.000
24	300	Concave 180°	Trough	Mid	0.487	0.487	0.487	0.487	0.000	0.462	0.462	0.462	0.462	0.000	0.580	0.580	0.580	0.580	0.000	0.495	0.495	0.495	0.495	0.000
25	300	Convex 180°	Trough	Bottom	0.464	0.464	0.464	0.464	0.000	0.439	0.439	0.439	0.439	0.000	0.557	0.557	0.557	0.557	0.000	0.406	0.406	0.406	0.406	0.000
26	300	Concave 90°	Trough	Top	0.498	0.498	0.498	0.498	0.000	0.473	0.473	0.473	0.473	0.000	0.591	0.591	0.591	0.591	0.000	0.490	0.490	0.490	0.490	0.000

Airfoil	Radial Position [mm]	Orientation (main surface)	Machine	Fixture method	Pre-Process (opposite surface)																				
					A: Entry					B: Mid					C: Exit					D: Flowline				
					1	2	3	Mean	SD	1	2	3	Mean	SD	1	2	3	Mean	SD	1	2	3	Mean	SD
1	300	Concave 45°	Domeless	Big	0.487	0.487	0.487	0.487	0.000	0.456	0.456	0.456	0.456	0.000	0.498	0.498	0.498	0.498	0.000	0.456	0.456	0.456	0.456	0.000
2	300	Convex 45°	Domeless	Big	0.410	0.410	0.410	0.410	0.000	0.379	0.379	0.379	0.379	0.000	0.421	0.421	0.421	0.421	0.000	0.382	0.382	0.382	0.382	0.000
3	300	Concave 180°	Domeless	Big	0.488	0.488	0.488	0.488	0.000	0.457	0.457	0.457	0.457	0.000	0.399	0.399	0.399	0.399	0.000	0.421	0.421	0.421	0.421	0.000
4	300	Convex 180°	Domeless	Big	0.447	0.447	0.447	0.447	0.000	0.416	0.416	0.416	0.416	0.000	0.458	0.458	0.458	0.458	0.000	0.485	0.485	0.485	0.485	0.000
5	300	Concave 90°	Domeless	Big	0.398	0.398	0.398	0.398	0.000	0.363	0.363	0.363	0.363	0.000	0.392	0.392	0.392	0.392	0.000	0.386	0.386	0.386	0.386	0.000
6	200	Concave 45°	Domeless	Small	0.453	0.453	0.453	0.453	0.000	0.422	0.422	0.422	0.422	0.000	0.464	0.464	0.464	0.464	0.000	0.396	0.396	0.396	0.396	0.000
7	200	Convex 45°	Domeless	Small	0.493	0.493	0.493	0.493	0.000	0.462	0.462	0.462	0.462	0.000	0.504	0.504	0.504	0.504	0.000	0.478	0.478	0.478	0.478	0.000
8	200	Concave 180°	Domeless	Small	0.478	0.478	0.478	0.478	0.000	0.447	0.447	0.446	0.447	0.001	0.489	0.489	0.489	0.489	0.000	0.411	0.411	0.411	0.411	0.000
9	200	Convex 180°	Domeless	Small	0.402	0.402	0.402	0.402	0.000	0.428	0.428	0.428	0.428	0.000	0.440	0.440	0.440	0.440	0.000	0.366	0.366	0.367	0.366	0.001
10	200	Concave 90°	Domeless	Small	0.385	0.385	0.385	0.385	0.000	0.372	0.372	0.372	0.372	0.000	0.363	0.363	0.363	0.363	0.000	0.383	0.383	0.383	0.383	0.000
12	200	Concave 45°	Dome	Free	0.406	0.406	0.406	0.406	0.000	0.375	0.375	0.375	0.375	0.000	0.417	0.417	0.417	0.417	0.000	0.486	0.486	0.486	0.486	0.000
13	200	Convex 45°	Dome	Free	0.418	0.418	0.418	0.418	0.000	0.387	0.387	0.387	0.387	0.000	0.429	0.429	0.429	0.429	0.000	0.381	0.381	0.381	0.381	0.000
14	200	Concave 180°	Dome	Free	0.421	0.421	0.421	0.421	0.000	0.390	0.390	0.390	0.390	0.000	0.432	0.432	0.432	0.432	0.000	0.417	0.416	0.417	0.417	0.001
15	200	Convex 180°	Dome	Free	0.422	0.422	0.422	0.422	0.000	0.391	0.391	0.391	0.391	0.000	0.433	0.433	0.433	0.433	0.000	0.462	0.462	0.462	0.462	0.000
16	200	Concave 90°	Dome	Free	0.397	0.397	0.397	0.397	0.000	0.425	0.425	0.425	0.425	0.000	0.384	0.384	0.384	0.384	0.000	0.387	0.387	0.387	0.387	0.000
17	300	Concave 45°	Trough	Top	0.407	0.407	0.407	0.407	0.000	0.376	0.376	0.376	0.376	0.000	0.418	0.418	0.418	0.418	0.000	0.412	0.412	0.412	0.412	0.000
18	300	Convex 45°	Trough	Mid	0.403	0.403	0.403	0.403	0.000	0.372	0.372	0.372	0.372	0.000	0.414	0.414	0.414	0.414	0.000	0.452	0.452	0.452	0.452	0.000
19	300	Concave 180°	Trough	Bottom	0.401	0.401	0.401	0.401	0.000	0.370	0.370	0.370	0.370	0.000	0.412	0.412	0.412	0.412	0.000	0.474	0.474	0.474	0.474	0.000
20	300	Convex 180°	Trough	Mid	0.366	0.366	0.366	0.366	0.000	0.394	0.394	0.393	0.394	0.001	0.353	0.353	0.353	0.353	0.000	0.364	0.364	0.364	0.364	0.000
21	300	Concave 90°	Trough	Top	0.430	0.430	0.430	0.430	0.000	0.399	0.400	0.399	0.399	0.001	0.441	0.441	0.441	0.441	0.000	0.378	0.378	0.378	0.378	0.000
22	300	Concave 45°	Trough	Mid	0.412	0.412	0.412	0.412	0.000	0.381	0.381	0.381	0.381	0.000	0.423	0.423	0.423	0.423	0.000	0.479	0.479	0.479	0.479	0.000
23	300	Convex 45°	Trough	Top	0.405	0.405	0.405	0.405	0.000	0.374	0.374	0.374	0.374	0.000	0.416	0.416	0.416	0.416	0.000	0.416	0.416	0.416	0.416	0.000
24	300	Concave 180°	Trough	Mid	0.438	0.438	0.438	0.438	0.000	0.407	0.407	0.407	0.407	0.000	0.449	0.449	0.449	0.449	0.000	0.423	0.423	0.423	0.423	0.000
25	300	Convex 180°	Trough	Bottom	0.461	0.461	0.461	0.461	0.000	0.430	0.430	0.430	0.430	0.000	0.472	0.472	0.472	0.472	0.000	0.347	0.347	0.347	0.347	0.000
26	300	Concave 90°	Trough	Top	0.420	0.420	0.420	0.420	0.000	0.389	0.389	0.389	0.389	0.000	0.431	0.431	0.431	0.431	0.000	0.404	0.404	0.404	0.404	0.000

Airfoil	Radial Position [mm]	Orientation (main surface)	Machine	Fixture method	Deburring (opposite surface)																				
					A: Entry					B: Mid					C: Exit					D: Flowline				
					1	2	3	Mean	SD	1	2	3	Mean	SD	1	2	3	Mean	SD	1	2	3	Mean	SD
1	300	Concave 45°	Domeless	Big	0.781	0.781	0.781	0.781	0.000	0.807	0.807	0.807	0.807	0.000	0.669	0.669	0.669	0.669	0.000	0.561	0.561	0.561	0.561	0.000
2	300	Convex 45°	Domeless	Big	0.704	0.704	0.704	0.704	0.000	0.730	0.730	0.730	0.730	0.000	0.592	0.592	0.592	0.592	0.000	0.706	0.706	0.706	0.706	0.000
3	300	Concave 180°	Domeless	Big	0.795	0.795	0.795	0.795	0.000	0.821	0.821	0.821	0.821	0.000	0.683	0.683	0.683	0.683	0.000	0.607	0.607	0.607	0.607	0.000
4	300	Convex 180°	Domeless	Big	0.740	0.741	0.741	0.741	0.001	0.767	0.767	0.767	0.767	0.000	0.629	0.629	0.629	0.629	0.000	0.512	0.512	0.512	0.512	0.000
5	300	Concave 90°	Domeless	Big	0.666	0.666	0.666	0.666	0.000	0.789	0.789	0.789	0.789	0.000	0.587	0.587	0.587	0.587	0.000	0.651	0.651	0.651	0.651	0.000
6	200	Concave 45°	Domeless	Small	0.800	0.800	0.800	0.800	0.000	0.826	0.826	0.826	0.826	0.000	0.688	0.689	0.688	0.688	0.001	0.464	0.464	0.464	0.464	0.000
7	200	Convex 45°	Domeless	Small	0.802	0.802	0.802	0.802	0.000	0.828	0.828	0.828	0.828	0.000	0.690	0.690	0.690	0.690	0.000	0.641	0.641	0.641	0.641	0.000
8	200	Concave 180°	Domeless	Small	0.790	0.790	0.790	0.790	0.000	0.816	0.816	0.816	0.816	0.000	0.677	0.678	0.678	0.678	0.001	0.597	0.597	0.597	0.597	0.000
9	200	Convex 180°	Domeless	Small	0.784	0.784	0.784	0.784	0.000	0.810	0.810	0.810	0.810	0.000	0.671	0.672	0.672	0.672	0.001	0.520	0.520	0.520	0.520	0.000
10	200	Concave 90°	Domeless	Small	0.726	0.726	0.726	0.726	0.000	0.646	0.646	0.646	0.646	0.000	0.610	0.610	0.611	0.610	0.001	0.809	0.809	0.809	0.809	0.000
12	200	Concave 45°	Dome	Free	0.701	0.699	0.700	0.700	0.001	0.726	0.726	0.726	0.726	0.000	0.687	0.688	0.689	0.688	0.001	0.718	0.718	0.718	0.718	0.000
13	200	Convex 45°	Dome	Free	0.711	0.712	0.712	0.712	0.001	0.738	0.738	0.738	0.738	0.000	0.600	0.600	0.600	0.600	0.000	0.597	0.598	0.596	0.597	0.001
14	200	Concave 180°	Dome	Free	0.715	0.715	0.715	0.715	0.000	0.741	0.741	0.741	0.741	0.000	0.603	0.603	0.603	0.603	0.000	0.658	0.658	0.658	0.658	0.000
15	200	Convex 180°	Dome	Free	0.716	0.716	0.716	0.716	0.000	0.742	0.742	0.742	0.742	0.000	0.604	0.604	0.604	0.604	0.000	0.729	0.729	0.729	0.729	0.000
16	200	Concave 90°	Dome	Free	0.792	0.792	0.792	0.792	0.000	0.818	0.818	0.818	0.818	0.000	0.780	0.780	0.780	0.780	0.000	0.644	0.644	0.644	0.644	0.000
17	300	Concave 45°	Trough	Top	0.701	0.701	0.701	0.701	0.000	0.727	0.727	0.727	0.727	0.000	0.689	0.689	0.689	0.689	0.000	0.675	0.675	0.675	0.675	0.000
18	300	Convex 45°	Trough	Mid	0.697	0.698	0.697	0.697	0.001	0.723	0.723	0.723	0.723	0.000	0.685	0.685	0.685	0.685	0.000	0.711	0.710	0.710	0.710	0.001
19	300	Concave 180°	Trough	Bottom	0.695	0.695	0.695	0.695	0.000	0.721	0.721	0.721	0.721	0.000	0.683	0.683	0.683	0.683	0.000	0.763	0.763	0.763	0.763	0.000
20	300	Convex 180°	Trough	Mid	0.809	0.809	0.809	0.809	0.000	0.835	0.835	0.835	0.835	0.000	0.697	0.697	0.697	0.697	0.000	0.572	0.572	0.572	0.572	0.000
21	300	Concave 90°	Trough	Top	0.724	0.724	0.724	0.724	0.000	0.750	0.750	0.750	0.750	0.000	0.712	0.712	0.712	0.712	0.000	0.605	0.605	0.605	0.605	0.000
22	300	Concave 45°	Trough	Mid	0.706	0.706	0.706	0.706	0.000	0.732	0.732	0.732	0.732	0.000	0.594	0.594	0.594	0.594	0.000	0.762	0.762	0.762	0.762	0.000
23	300	Convex 45°	Trough	Top	0.699	0.699	0.699	0.699	0.000	0.725	0.725	0.725	0.725	0.000	0.586	0.587	0.587	0.587	0.001	0.678	0.678	0.678	0.678	0.000
24	300	Concave 180°	Trough	Mid	0.732	0.732	0.732	0.732	0.000	0.758	0.758	0.758	0.758	0.000	0.620	0.620	0.620	0.620	0.000	0.716	0.716	0.716	0.716	0.000
25	300	Convex 180°	Trough	Bottom	0.755	0.755	0.755	0.755	0.000	0.781	0.781	0.781	0.781	0.000	0.643	0.643	0.643	0.643	0.000	0.546	0.546	0.546	0.546	0.000
26	300	Concave 90°	Trough	Top	0.714	0.714	0.714	0.714	0.000	0.740	0.740	0.740	0.740	0.000	0.602	0.602	0.602	0.602	0.000	0.646	0.646	0.646	0.646	0.000

Airfoil	Radial Position [mm]	Orientation (main surface)	Machine	Fixture method	Polishing (opposite surface)																				
					A: Entry					B: Mid					C: Exit					D: Flowline				
					1	2	3	Mean	SD	1	2	3	Mean	SD	1	2	3	Mean	SD	1	2	3	Mean	SD
1	300	Concave 45°	Domeless	Big	0.483	0.483	0.483	0.483	0.000	0.573	0.573	0.573	0.573	0.000	0.508	0.508	0.508	0.508	0.000	0.417	0.417	0.417	0.417	0.000
2	300	Convex 45°	Domeless	Big	0.406	0.406	0.406	0.406	0.000	0.496	0.496	0.496	0.496	0.000	0.431	0.431	0.430	0.431	0.001	0.496	0.496	0.496	0.496	0.000
3	300	Concave 180°	Domeless	Big	0.418	0.418	0.418	0.418	0.000	0.508	0.508	0.508	0.508	0.000	0.443	0.443	0.443	0.443	0.000	0.473	0.473	0.473	0.473	0.000
4	300	Convex 180°	Domeless	Big	0.551	0.551	0.551	0.551	0.000	0.534	0.534	0.534	0.534	0.000	0.598	0.598	0.598	0.598	0.000	0.444	0.444	0.443	0.444	0.001
5	300	Concave 90°	Domeless	Big	0.476	0.476	0.476	0.476	0.000	0.466	0.466	0.466	0.466	0.000	0.514	0.514	0.514	0.514	0.000	0.469	0.469	0.469	0.469	0.000
6	200	Concave 45°	Domeless	Small	0.498	0.498	0.498	0.498	0.000	0.508	0.508	0.508	0.508	0.000	0.523	0.523	0.523	0.523	0.000	0.354	0.353	0.354	0.354	0.001
7	200	Convex 45°	Domeless	Small	0.501	0.502	0.501	0.501	0.001	0.511	0.511	0.511	0.511	0.000	0.526	0.525	0.526	0.526	0.001	0.499	0.499	0.499	0.499	0.000
8	200	Concave 180°	Domeless	Small	0.487	0.487	0.487	0.487	0.000	0.497	0.497	0.497	0.497	0.000	0.512	0.513	0.512	0.512	0.001	0.432	0.432	0.432	0.432	0.000
9	200	Convex 180°	Domeless	Small	0.506	0.506	0.506	0.506	0.000	0.516	0.516	0.516	0.516	0.000	0.531	0.531	0.531	0.531	0.000	0.389	0.389	0.389	0.389	0.000
10	200	Concave 90°	Domeless	Small	0.467	0.467	0.467	0.467	0.000	0.430	0.430	0.430	0.430	0.000	0.549	0.549	0.549	0.549	0.000	0.518	0.518	0.518	0.518	0.000
12	200	Concave 45°	Dome	Free	0.502	0.502	0.502	0.502	0.000	0.492	0.492	0.492	0.492	0.000	0.427	0.427	0.427	0.427	0.000	0.531	0.531	0.530	0.531	0.001
13	200	Convex 45°	Dome	Free	0.514	0.514	0.514	0.514	0.000	0.503	0.504	0.504	0.504	0.001	0.469	0.469	0.469	0.469	0.000	0.465	0.465	0.465	0.465	0.000
14	200	Concave 180°	Dome	Free	0.517	0.516	0.517	0.517	0.001	0.507	0.507	0.507	0.507	0.000	0.472	0.471	0.471	0.471	0.001	0.493	0.493	0.493	0.493	0.000
15	200	Convex 180°	Dome	Free	0.502	0.502	0.501	0.502	0.001	0.512	0.512	0.512	0.512	0.000	0.537	0.537	0.537	0.537	0.000	0.590	0.590	0.590	0.590	0.000
16	200	Concave 90°	Dome	Free	0.524	0.524	0.524	0.524	0.000	0.612	0.612	0.612	0.612	0.000	0.549	0.549	0.549	0.549	0.000	0.528	0.528	0.528	0.528	0.000
17	300	Concave 45°	Trough	Top	0.579	0.579	0.579	0.579	0.000	0.529	0.529	0.529	0.529	0.000	0.514	0.514	0.513	0.514	0.001	0.597	0.597	0.597	0.597	0.000
18	300	Convex 45°	Trough	Mid	0.599	0.599	0.599	0.599	0.000	0.539	0.539	0.539	0.539	0.000	0.574	0.574	0.574	0.574	0.000	0.600	0.601	0.600	0.600	0.001
19	300	Concave 180°	Trough	Bottom	0.597	0.597	0.597	0.597	0.000	0.607	0.606	0.607	0.607	0.001	0.622	0.622	0.622	0.622	0.000	0.621	0.621	0.621	0.621	0.000
20	300	Convex 180°	Trough	Mid	0.474	0.474	0.474	0.474	0.000	0.476	0.476	0.476	0.476	0.000	0.499	0.498	0.499	0.499	0.001	0.480	0.479	0.478	0.479	0.001
21	300	Concave 90°	Trough	Top	0.476	0.476	0.476	0.476	0.000	0.573	0.573	0.573	0.573	0.000	0.471	0.471	0.471	0.471	0.000	0.538	0.538	0.538	0.538	0.000
22	300	Concave 45°	Trough	Mid	0.608	0.608	0.608	0.608	0.000	0.568	0.568	0.568	0.568	0.000	0.583	0.583	0.583	0.583	0.000	0.633	0.633	0.633	0.633	0.000
23	300	Convex 45°	Trough	Top	0.501	0.501	0.501	0.501	0.000	0.491	0.491	0.491	0.491	0.000	0.526	0.526	0.526	0.526	0.000	0.595	0.595	0.595	0.595	0.000
24	300	Concave 180°	Trough	Mid	0.584	0.584	0.584	0.584	0.000	0.564	0.564	0.564	0.564	0.000	0.458	0.459	0.459	0.459	0.001	0.601	0.601	0.600	0.601	0.001
25	300	Convex 180°	Trough	Bottom	0.457	0.457	0.457	0.457	0.000	0.447	0.447	0.447	0.447	0.000	0.482	0.482	0.482	0.482	0.000	0.439	0.439	0.439	0.439	0.000
26	300	Concave 90°	Trough	Top	0.535	0.535	0.535	0.535	0.000	0.596	0.596	0.596	0.596	0.000	0.541	0.541	0.541	0.541	0.000	0.581	0.581	0.580	0.581	0.001

Airfoil	Radial Position [mm]	Orientation	Machine	Fixture method	Pre				Stage 1				Stage 2				Thickness Loss [mm]
					B: Mid [mm]	B: Mid [mm]	B: Mid [mm]	SD	B: Mid [mm]	B: Mid [mm]	B: Mid [mm]	SD	B: Mid [mm]	B: Mid [mm]	B: Mid [mm]	SD	
1	300	Concave 45°	Domeless	Big	10.5039	10.5036	10.5037	0.0002	10.4941	10.4941	10.4941	0.0000	10.4932	10.4932	10.4933	0.0001	0.0105
2	300	Convex 45°	Domeless	Big	10.5183	10.5185	10.5184	0.0001	10.5100	10.5101	10.5101	0.0001	10.5087	10.5089	10.5087	0.0001	0.0096
3	300	Concave 180°	Domeless	Big	10.5083	10.5083	10.5083	0.0000	10.5013	10.5013	10.5012	0.0001	10.4999	10.5000	10.4999	0.0001	0.0084
4	300	Convex 180°	Domeless	Big	10.5429	10.5425	10.5428	0.0002	10.5370	10.5370	10.5369	0.0001	10.5335	10.5335	10.5336	0.0001	0.0092
5	300	Concave 90°	Domeless	Big	10.5125	10.5125	10.5124	0.0001	10.5111	10.5110	10.5109	0.0001	10.5104	10.5105	10.5105	0.0001	0.0020
6	200	Concave 45°	Domeless	Small	10.4980	10.4982	10.4982	0.0001	10.4911	10.4913	10.4911	0.0001	10.4896	10.4896	10.4897	0.0001	0.0085
7	200	Convex 45°	Domeless	Small	10.5010	10.5011	10.5010	0.0001	10.4932	10.4932	10.4935	0.0002	10.4920	10.4919	10.4919	0.0001	0.0091
8	200	Concave 180°	Domeless	Small	10.5015	10.5015	10.5014	0.0001	10.4967	10.4964	10.4964	0.0002	10.4954	10.4954	10.4955	0.0001	0.0060
9	200	Convex 180°	Domeless	Small	10.5450	10.5448	10.5449	0.0001	10.5399	10.5400	10.5399	0.0001	10.5379	10.5380	10.5379	0.0001	0.0070
10	200	Concave 90°	Domeless	Small	10.5011	10.5010	10.5012	0.0001	10.5004	10.5004	10.5005	0.0001	10.5000	10.5002	10.5001	0.0001	0.0010
12	200	Concave 45°	Dome	Free	10.5140	10.5142	10.5142	0.0001	10.5080	10.5082	10.5080	0.0001	10.5067	10.5067	10.5067	0.0000	0.0074
13	200	Convex 45°	Dome	Free	10.5022	10.5022	10.5021	0.0001	10.4976	10.4976	10.4976	0.0000	10.4951	10.4953	10.4951	0.0001	0.0070
14	200	Concave 180°	Dome	Free	10.5176	10.5175	10.5176	0.0001	10.5132	10.5133	10.5133	0.0001	10.5127	10.5127	10.5126	0.0001	0.0049
15	200	Convex 180°	Dome	Free	10.5041	10.5042	10.5042	0.0001	10.5004	10.5000	10.5002	0.0002	10.4991	10.4991	10.4993	0.0001	0.0050
16	200	Concave 90°	Dome	Free	10.5163	10.5165	10.5163	0.0001	10.5159	10.5157	10.5160	0.0002	10.5154	10.5154	10.5153	0.0001	0.0010
17	300	Concave 45°	Trough	Top	10.5036	10.5035	10.5036	0.0001	10.4971	10.4970	10.4970	0.0001	10.4958	10.4959	10.4958	0.0001	0.0077
18	300	Convex 45°	Trough	Mid	10.4995	10.4995	10.4994	0.0001	10.4953	10.4955	10.4953	0.0001	10.4929	10.4930	10.4929	0.0001	0.0065
19	300	Concave 180°	Trough	Bottom	10.4991	10.4994	10.4993	0.0002	10.4951	10.4951	10.4953	0.0001	10.4937	10.4937	10.4939	0.0001	0.0055
20	300	Convex 180°	Trough	Mid	10.5199	10.5120	10.5197	0.0045	10.5159	10.5160	10.5159	0.0001	10.5141	10.5143	10.5141	0.0001	0.0030
21	300	Concave 90°	Trough	Top	10.5029	10.5027	10.5026	0.0002	10.5023	10.5022	10.5023	0.0001	10.5019	10.5020	10.5019	0.0001	0.0008
22	300	Concave 45°	Trough	Mid	10.5036	10.5033	10.5035	0.0002	10.4959	10.4959	10.4958	0.0001	10.4941	10.4943	10.4941	0.0001	0.0093
23	300	Convex 45°	Trough	Top	10.5256	10.5255	10.5256	0.0001	10.5189	10.5185	10.5188	0.0002	10.5176	10.5176	10.5177	0.0001	0.0079
24	300	Concave 180°	Trough	Mid	10.5113	10.5117	10.5116	0.0002	10.5050	10.5050	10.5053	0.0002	10.5043	10.5044	10.5041	0.0002	0.0073
25	300	Convex 180°	Trough	Bottom	10.5070	10.5071	10.5070	0.0001	10.4999	10.4996	10.4998	0.0002	10.4982	10.4983	10.4982	0.0001	0.0088
26	300	Concave 90°	Trough	Top	10.5050	10.5050	10.5051	0.0001	10.5042	10.5043	10.5041	0.0001	10.5043	10.5041	10.5044	0.0002	0.0008

Airfoil	Radial Position [mm]	Orientation	Machine	Fixture method	Pre				Stage 1				Stage 2				Weight Loss
					Weight [g]	Weight [g]	Weight [g]	SD	Weight [g]	Weight [g]	Weight [g]	SD	Weight [g]	Weight [g]	Weight [g]	SD	
1	300	Concave 45°	Domeless	Big	82.491	82.491	82.490	0.0006	82.170	82.170	82.170	0.0000	82.130	82.129	82.129	0.0006	0.3613
2	300	Convex 45°	Domeless	Big	82.464	82.465	82.465	0.0006	82.181	82.180	82.181	0.0006	82.134	82.135	82.134	0.0006	0.3303
3	300	Concave 180°	Domeless	Big	82.390	82.391	82.390	0.0006	82.173	82.173	82.173	0.0000	82.074	82.075	82.074	0.0006	0.3160
4	300	Convex 180°	Domeless	Big	82.406	82.406	82.407	0.0006	82.251	82.250	82.250	0.0006	82.134	82.133	82.135	0.0010	0.2723
5	300	Concave 90°	Domeless	Big	82.282	82.282	82.283	0.0006	82.196	82.196	82.196	0.0000	82.140	82.141	82.140	0.0006	0.1420
6	200	Concave 45°	Domeless	Small	82.344	82.344	82.344	0.0000	82.057	82.057	82.057	0.0000	81.981	81.981	81.981	0.0000	0.3630
7	200	Convex 45°	Domeless	Small	82.330	82.330	82.331	0.0006	82.036	82.036	82.036	0.0000	81.974	81.975	81.975	0.0006	0.3557
8	200	Concave 180°	Domeless	Small	82.304	82.305	82.304	0.0006	82.085	82.085	82.085	0.0000	82.036	82.036	82.036	0.0000	0.2683
9	200	Convex 180°	Domeless	Small	82.359	82.359	82.359	0.0000	82.159	82.159	82.159	0.0000	82.094	82.093	82.094	0.0006	0.2653
10	200	Concave 90°	Domeless	Small	82.278	82.278	82.278	0.0000	82.174	82.176	82.174	0.0012	82.169	82.170	82.169	0.0006	0.1087
12	200	Concave 45°	Dome	Free	82.285	82.286	82.285	0.0006	81.913	81.913	81.913	0.0000	81.844	81.843	81.844	0.0006	0.4417
13	200	Convex 45°	Dome	Free	82.260	82.261	82.260	0.0006	81.919	81.919	81.919	0.0000	81.850	81.851	81.851	0.0006	0.4097
14	200	Concave 180°	Dome	Free	82.264	82.264	82.264	0.0000	82.020	82.020	82.021	0.0006	81.993	81.992	81.993	0.0006	0.2713
15	200	Convex 180°	Dome	Free	82.282	82.281	82.281	0.0006	82.040	82.039	82.039	0.0006	82.020	82.019	82.019	0.0006	0.2620
16	200	Concave 90°	Dome	Free	82.222	82.223	82.222	0.0006	82.129	82.129	82.129	0.0000	82.101	82.102	82.101	0.0006	0.1210
17	300	Concave 45°	Trough	Top	82.225	82.225	82.225	0.0000	81.974	81.974	81.974	0.0000	81.891	81.891	81.891	0.0000	0.3340
18	300	Convex 45°	Trough	Mid	82.220	82.220	82.210	0.0058	81.993	81.993	81.994	0.0006	81.913	81.914	81.913	0.0006	0.3033
19	300	Concave 180°	Trough	Bottom	82.225	82.225	82.224	0.0006	82.051	82.053	82.051	0.0012	82.024	82.024	82.024	0.0000	0.2007
20	300	Convex 180°	Trough	Mid	82.266	82.266	82.266	0.0000	82.094	82.093	82.094	0.0006	82.055	82.054	82.055	0.0006	0.2113
21	300	Concave 90°	Trough	Top	82.289	82.290	82.289	0.0006	82.165	82.165	82.165	0.0000	82.159	82.159	82.160	0.0006	0.1300
22	300	Concave 45°	Trough	Mid	82.286	82.286	82.286	0.0000	82.000	82.000	82.001	0.0006	81.928	81.928	81.928	0.0000	0.3580
23	300	Convex 45°	Trough	Top	82.275	82.276	82.275	0.0006	82.061	82.062	82.061	0.0006	81.987	81.986	81.985	0.0010	0.2893
24	300	Concave 180°	Trough	Mid	82.261	82.260	82.261	0.0006	82.113	82.113	82.113	0.0000	82.082	82.081	82.081	0.0006	0.1793
25	300	Convex 180°	Trough	Bottom	82.224	82.224	82.224	0.0000	82.040	82.041	82.040	0.0006	82.014	82.015	82.014	0.0006	0.2097
26	300	Concave 90°	Trough	Top	82.285	82.286	82.284	0.0010	82.189	82.189	82.189	0.0000	82.179	82.178	82.179	0.0006	0.1063

Appendix C: **Theoretical scaling of domeless vibrofinishing**

To find a scaled domeless bowl to the Hashimoto and Johnson's mechanical vibration model [20], the total mass, *M* is required to be calculated. As the critical difference between dome and domeless bowl is the absence of the dome, a higher media volume can be placed in the domeless bowl. To understand how much media volume is added in replacement of the dome, an approximation of the volume of dome component of a dome bowl can be calculated. Note that the total mass will be converted to total weight for unit standardisation.

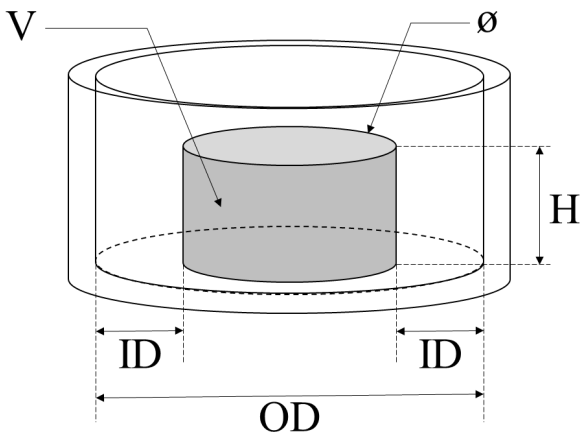

Figure A.0.1 Schematic Drawing of dome bowl with dimensions of the dome component

Dimensions are provided in the paper with the height of dome (H) at 185 mm, outer diameter (OD) at 533 mm, inner diameter (ID) at 191.25mm. Therefore, diameter of the dome can be calculated:

$$\emptyset = 533 - (191.25 \times 2) = 146.5\, mm \tag{A.0.1}$$

The volume of the dome can be therefore calculated:

$$V = \frac{\pi \cdot \emptyset^2 \cdot H}{4} = 3.12 \times 10^6\ mm^3 = 3.123\ litres \quad \text{(A.0.2)}$$

By converting and assuming a replacement of the dome with media, the volume of media of a domeless bowl can be calculated by adding the original volume of media for a dome bowl of 28.3 litres with the media addition, resulting in a media volume of 31.423 litres. By multiplying this value with the given media density of 1.43 g/cm^3 and converting to weight by multiplying by 9.81m/s^2, the weight of the media is calculated to 440.81 N.

The weight of the domeless bowl can be calculated by subtracting the total weight of the dome bowl, provided as 772.3 N, to the combined weight of the media and component. First, the given volume of the bowl, provided 28.3 litres, or 28.3 x 10^6 mm^3, can be multiplied by the media density of 1.43 g/cm^3 to give a total media mass of 40.47 kg. This is converted to 397 N by multiplying by 9.81m/s^2. Additionally, the mass of the component in the bowl can be calculated by multiplying the given volume of 3887.72 mm^3 with a referenced density of a hardened steel HRC62 of 7.85 g/cm^3 [27]. This gives a component weight of 299.39 N. Therefore, the weight of the domeless bowl can be calculated by subtracting the dome bowl weight to the combined weight of media and component:

$$\begin{aligned} Weight\ of\ domeless\ bowl\ body &= 772.3 - (397 + 299.39) \\ &= 75.91\ N \end{aligned} \quad \text{(A.0.3)}$$

Finally, the weight of the domeless bowl process, which includes the weight of the bowl, media and part can be summarised as 816.11 N.